ABSTRACT

Title of Dissertation:	UNDERSTANDING ENVIRONMENTAL FACTORS DRIVING WILDLAND FIRE IGNITIONS IN ALASKAN TUNDRA
	Jiaying He, Doctor of Philosophy, 2020
Dissertation directed by:	Professor, Tatiana V. Loboda, Department of Geographical Sciences

Wildland fire is a dominant disturbance agent that drives ecosystem change, climate forcing, and carbon cycle in the boreal forest and tundra ecosystems of the High Northern Latitudes (HNL). Tundra fires can exert a considerable influence on the local ecosystem functioning and contribute to climate change through biogeochemical and biogeophysical effects. However, the drivers and mechanisms of tundra fires are still poorly understood. Research on modeling contemporary fire occurrence in the tundra is also lacking. This dissertation addresses the overarching scientific question of "*What environmental factors and mechanisms drive wildfire ignition in Alaskan tundra?*" Environmental factors from multiple aspects are considered including fuel type and state, fire weather, topography, and ignition source. First, to understand the spatial distribution of fuel types in the tundra, multi-year satellite observations and field data were used to develop the first fractional coverage product of major fuel type components across the entire Alaskan tundra at

30 m resolution. Second, to account for the primary ignition source of fires in the HNL, an empirical-dynamical modeling framework was developed to predict the probability of cloud-to-ground (CG) lightning across Alaskan tundra, through the integration of Weather Research and Forecast (WRF) model and machine learning algorithm. Finally, environmental factors including fuel type distribution, fuel moisture state, WRF simulated ignition source and fire weather, and topographical features, were combined with empirical modeling methods to understand their roles in driving wildland fire ignitions across Alaskan tundra from 2001 to 2019. This work demonstrates the strong capability for accurate prediction of CG lightning and wildland fire probabilities, by incorporating dynamic weather models, empirical methods, and satellite observations in data-scarce regions like the HNL. The developed models present a novel component of fire danger modeling that can considerably strengthen the current capability to forecast fire occurrence and support operational fire management agencies in the HNL. In addition, the insights gained from this research will allow for more accurate representation of wildfire ignition probabilities in studies focused on assessing the impact of the projected climate change in HNL tundra which has largely absent in previous modeling efforts.

UNDERSTANDING ENVIRONMENTAL FACTORS DRIVING WILDLAND FIRE IGNITIONS IN ALASKAN TUNDRA

by

Jiaying He

Dissertation submitted to the Faculty of the Graduate School of the
University of Maryland, College Park, in partial fulfillment
of the requirements for the degree of
Doctor of Philosophy
2020

Advisory Committee:
Dr. Tatiana V. Loboda, Chair
Dr. Christopher Justice
Dr. Nancy French
Dr. Evan Ellicott
Dr. Rachel Pinker

Dedication

To my dear parents

For their unconditional love and support

To all women who contribute their life

To the development of Science, Technology, Engineering, and Math (STEM)

Acknowledgements

Writing acknowledgements is never an easy task for someone like me who is not good at expressing his or her feelings. After submitting my dissertation draft to my dear dissertation committee, I finally get a chance to calm down and to think about who and how I would like to thank. Looking back at my six years as a member of University of Maryland and Department of Geographical Sciences, it has been such a precious journey in my life to learn how to grow up, to think about who I want to be, and even to reshape my personality.

First and foremost, I would like to thank my advisor Dr. Tatiana Loboda for being such a great advisor, a scholar, and a role model as a female scientist. Thank you for all your support, guidance, and encouragement. Thank you for your trust and high standards that help me rebuild my confidence and push me to excel myself. Having you as my advisor is the luckiest thing that I have had during the past six years and encourages me to keep pursuing scientific research.

I am also very grateful for the mentorship and encouragement from all the members of my dissertation advisory committee. To Dr. Chris Justice, thank you for your scientific mind and forward thinking that inspire me to think like a scientist. To Dr. Nancy French, thank you for your kind help and solid knowledge that guide my dissertation work and thank you for being a great role model of female scientist for me. To Dr. Evan Ellicott, thank you for all your knowledge and encouragement that support me throughout this journey. To Dr. Rachel Pinker, thank you for agreeing to serve as my dean's representative.

Special thanks to my lovely lab mates Varada, Tony, Joanne, Amanda and Allison! Thank you for always being so supportive and helpful during the past four years. I feel very grateful for having your company through this journey. I would like to thank Liza Jenkins as well, for all your knowledge and help during the most exciting field trip I have ever had at Seward Peninsula, Alaska in 2017.

To Rachel Berndtson, thank you for your patience and kind help whenever I ran into problems and came to you for solutions. To Jack Ma, Jonathan Resop, Elle Lim and Kristen Bergery, thank you all for the best TA experiences I have ever had working with the MPGIS program. Also thanks to Varaprasad Bandaru for the great RA opportunity to work with and to learn from you.

To all my cohort and colleagues at Department of Geographical Sciences, it's a great opportunity to know and to work with all of you. Thank you for sharing the journey of grad school with me. Also special thanks to all the lab members of Room 2138 at Lefrak Hall. I really enjoy being a member of this lab because of you.

To all the instructors of the RecWell group fitness classes at UMD, thank you all for your energetic and fun classes that always reboot my brain after working for an entire day.

Last but not the least, I would like to express my thanks to my family and friends. Thank you for always being there for me.

Table of Contents

List of Tables

Chapter 2:

Chapter 3:

Chapter 4:

List of Figures

Chapter 1:

Chapter 2:

Chapter 3:

Chapter 4:

List of Abbreviations

ABoVE – Arctic-Boreal Vulnerability Experiment

ALDN – Alaskan Lightning Detection Network

ALFD – Alaskan Large Fire Database

ALFRESCO – Alaska Frame-based Ecosystem Code

AUC – Area Under Curve

BLM – Bureau of Land Management

BUI – Buildup Index

CAPE – Convective Available Potential Energy

CAVM – Circumpolar Arctic Vegetation Map

CFFBPS – Canadian Forest Fire Behavior Prediction System

CFFDRS – Canadian Forest Fire Danger Rating System

CFFWIS – Canadian Forest Fire Weather Index System

CG – Cloud-to-ground

DBSCAN – Density-Based Spatial Clustering of Applications with Noise

DC – Drought Code

DEM – Digital Elevation Model

DMC – Duff Moisture Code

DOE – Department of Energy

DOI – Department of Interior

DOY – Day of Year

FCCS – Fuel Characteristic Classification System

FFMC – Fine Fuel Moisture Code

FIRMS – Fire Information for Resource Management System

FLM – Fuel Loading Model

FWI – Fire Weather Index

GVMI – Global Vegetation Moisture Index

HNL – High Northern Latitudes

IfSAR – Interferometric Synthetic Aperture Radar

IQR – Interquartile Range

ISI – Initial Spread Index

MAE – Mean Absolute Error

MDA – Mean Decrease Accuracy

MODIS – Moderate Resolution Imaging Spectroradiometer

MSE – Mean Squared Error

NARR – North American Regional Reanalysis

NASA – National Aeronautics and Space Administration

NBR – Normalized Burn Ratio

NCEP – National Centers for Environmental Prediction

NDII – Normalized Difference Infrared Index

NDVI – Normalized Difference Vegetation Index

NDWI – Normalized Difference Water Index

NFDRS – National Forest Danger Rating System

NGEE – Next Generation Ecosystem Experiments

NWP – Numerical Weather Prediction

OLI – Operational Land Imager

OOB – Out-of-bag

ORNL DAAC – Oak Ridge National Laboratory Distributed Active Archive Center

PFT – Plant Functional Type

PLI – Parcel Lifted Index

QA – Quality Assessment

RAWS – Remote Automated Weather Stations

RF – Random Forest

RH – Relative Humidity

RMSE – Root Mean Squared Error

ROC – Receiver Operating Characteristics

TC – Tasseled Cap

UTC – Coordinated Universal Time

VHR – Very High Resolution

WRF – Weather Research and Forecast

Chapter 1: Introduction

1.1 Background and Motivation

Wildland fire is a dominant disturbance agent that drives ecosystem change, climate forcing and carbon cycle in the boreal forest and tundra ecosystems of the High Northern Latitudes (HNL; Bond-Lamberty et al., 2007; Sulla-Menashe et al., 2018). Satellite observations show that tundra fires are common throughout the pan-Arctic region (Figure 1.1; Masrur et al., 2018). The Alaskan tundra has also witnessed several severe fires or fire seasons in recent years, namely the 2010 fire season in the Noatak River valley and the 2015 fire season in Southwest Alaska (Figure 1.2). Although Alaskan tundra only occupies approximately 10% of the world's tundra area, it has contributed more than 50% of the global tundra burned area since 2001. Moreover, paleoecological data indicate that frequent burnings had occurred in Alaskan tundra under suitable climate and fuel scenarios (Higuera et al., 2011; Hu et al., 2015). Climate is now changing at a rapid rate in the Arctic (Larsen et al., 2014). As the only Arctic region in the United States, Alaska has experienced twice the warming rate of other areas in the US since the 1950s (Stewart et al., 2013). This warming is likely to drive an increase in fire activity and changes in fire regimes within the Alaskan tundra ecosystem in the future regardless of climate change mitigation strategies (French et al., 2015; Young et al., 2017).

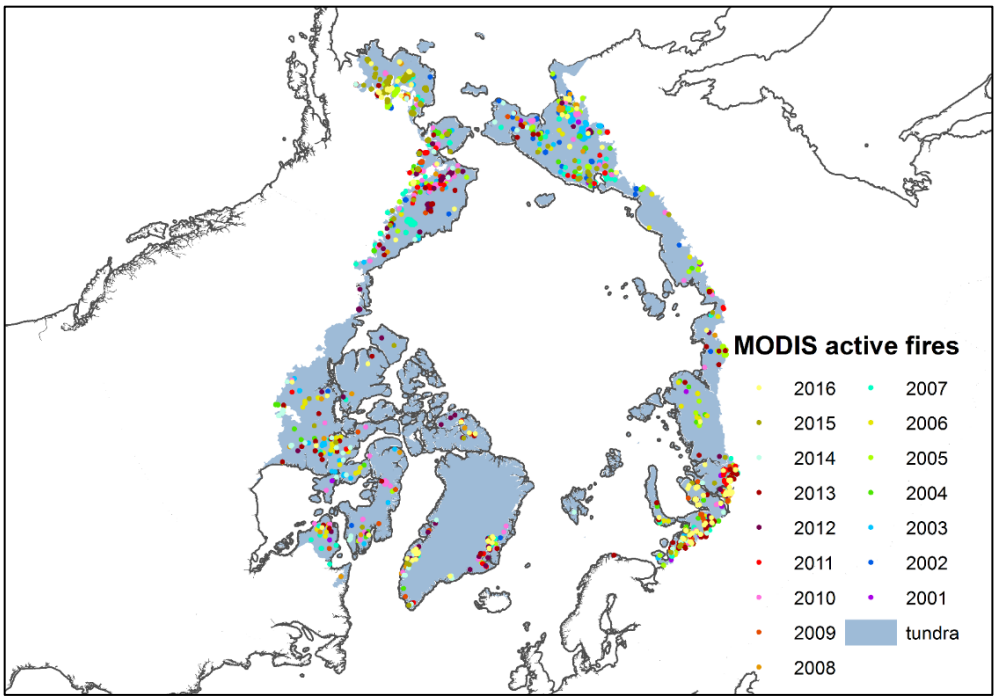

Figure 1.1. Active fires detected by Moderate Resolution Imaging Spectroradiometer (MODIS) sensors in the pan-Arctic tundra ecosystems from 2001 to 2016.

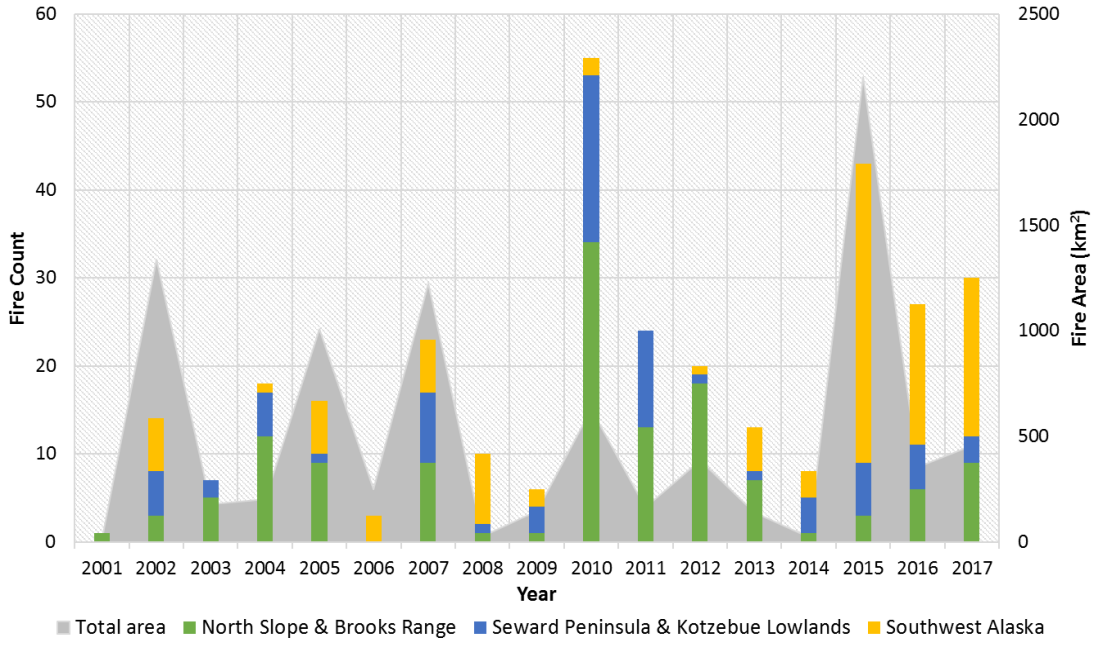

Figure 1.2. Fire count and burned area in different regions of Alaskan tundra from 2001 to 2017 according to Alaska Large Fire Database (ALFD).

Tundra fire acts as a catalyst for biogeochemical processes and releases large amounts of ancient carbon stored in the organic soil and widespread underlying permafrost, thus affecting both the regional and global carbon cycle (Jones et al., 2015; Mack et al., 2011). The extreme 2007 Anaktuvuk fire in Alaska burned an area of 1,039 km^2 and released approximately 2.1 Tg of carbon stocked in the organic soil and permafrost into the atmosphere (Mack et al., 2011). Fire-induced changes in surface albedo and post-fire vegetation compositions alter the surface radiative forcing with subsequent feedbacks into the climate system (French et al., 2016; Frost et al., 2020; McManus et al., 2012; Pearson et al., 2013). Climate change is regarded as the leading factor that alters ecosystem services and functions in the Arctic (Hinzman et al., 2005; Meredith et al., 2019; Post et al., 2009), however, the impact of climate change is likely to be strongly amplified by the rapid response of fire activities, which could eclipse the direct influences of climate change on the ecosystems (Flannigan et al., 2000).

Despite the importance of tundra fires, current research is primarily limited to the evaluation of post-fire impacts such as fire severity (Loboda et al., 2013), ecosystem responses (Bret-Harte et al., 2013), and carbon budget change (Mack et al., 2011) with comparatively little attention to modeling tundra fire occurrence. Previous studies have modeled historical or future tundra fire regimes with either empirical methods or ecosystem models, e.g. the Alaska Frame-Based Ecosystem Code (ALFRESCO; Higuera et al., 2011; Joly et al., 2012; Young et al., 2017). recently examined the climatic factors influencing tundra fire activities at a large spatial scale for the entire circumpolar region. However, research on modeling

contemporary fire occurrence is lacking in current English language peer-reviewed literature. Although numerous studies have modeled the interactions between environmental factors and wildfire occurrences in boreal forests, their results are not directly applicable to the tundra ecosystems due to their different ecosystem functioning and responses (French et al., 2015; Rocha et al., 2012). Studies of wildland fires have three major components: fire occurrence, fire spread and fire impacts. Considering the lack of efforts on understanding the driving mechanisms of wildland fire in the tundra and on modeling fire potential, this dissertation focuses on examining fire occurrence, and particularly how fire starts in the tundra

1.2 Environmental Factors Related to Wildfire Behavior

Wildfires are controlled by a variety of interacting factors (Pyne et al., 1996). Moritz et al. (2005) summarized the interactions between the influencing environmental factors and fire at multiple spatial and temporal scales (Figure 1.3). In particular, oxygen, heat and fuel are the three key components that support the combustion processes, which are typically known as the *Fire Fundamentals Triangle*. Beyond the combustion, fire behavior is a result of environmental conditions referred to as the *Fire Environment Triangle*, primarily including fuel, weather and topography. In the context of fire ecology, the life cycle of a wildland fire includes several stages: ignition, transition to spread, acceleration, and steady spread (Pyne et al., 1996). From the perspective of wildland fire behavior, the potential of fire occurrence refers to that of fire ignition. Although ignition source is not part of the *Fire Environment Triangle*, ignition source is a key factor that should be considered for understanding the fire ignition in addition to fuel, weather, and topography.

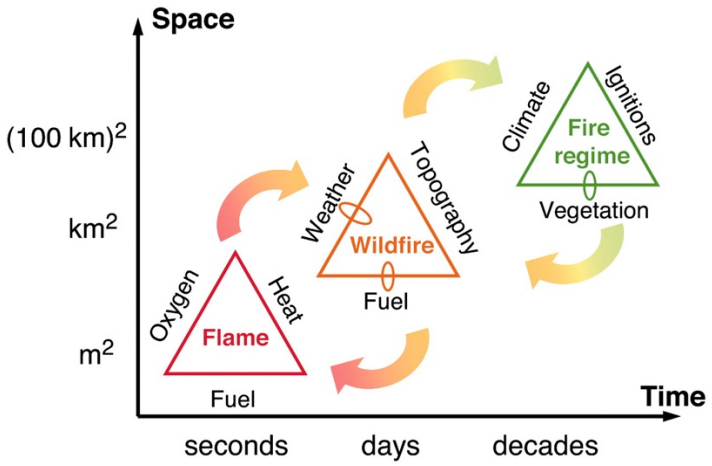

Figure 1.3. Factors controlling fires at different scales as an extension of the commonly used fire triangles. The left triangle represents the Fire Fundamentals Triangle and the middle one represents the Fire Environmental Triangle. This figure is from Moritz et al. (2005).

1.2.1 Ignition source

Wildfire ignition is primarily caused by cloud-to-ground (CG) lightning flashes and a variety of human factors including open flames, intentional and unintentional arson, equipment sparks, or power lines (Pyne et al., 1996). Majority of wildland fires in the remote and sparsely populated boreal forest and tundra ecosystems are ignited by lightning strikes (French et al., 2015; Veraverbeke et al., 2017). Current studies have diverging conclusions regarding the impact of climate change on global lightning activity in the future with some predicting an increase (Krause et al., 2014; Price & Rind, 1994) while others indicating a decrease (Finney et al., 2018; Murray, 2018). Therefore, understanding the factors and mechanisms driving lightning activity plays a vital role in understanding current and modeling future tundra fire potential.

Lightning is typically monitored using satellite- or ground-based systems for forecasting severe weather conditions and ensuring population safety (Nag et al., 2014). Satellite-based lightning monitoring primarily focuses on the tropical regions or examines the global patterns with geostationary satellites. Due to the limited coverage and coarse spatial resolution of satellite-based systems for the HNL, lightning monitoring in Alaska is primarily based on the ground-based Alaska Lightning Detection Network (ALDN) maintained by the Bureau of Land Management (BLM) since the 1980s (Fronterhouse, 2012). According to the ALDN observations, boreal forests of the Interior Alaska experience more frequent lightning strikes than the tundra (Dissing and Verbyla, 2003), which can be explained by the enhancement of local lightning storm development induced by air-mass thunderstorms and surface properties of the forests. The spatial distribution of lightning strikes throughout Alaska also varies seasonally and interannually. More than 90% of the lightning strikes in Alaska occur between June and August (Reap, 1991). Under relatively warm and dry conditions in the summer, Alaska experiences an increased quantity of lightning strikes induced by amplified convective activities, thus facilitating fire ignition potential (Peterson et al., 2010; Wendler et al., 2011). However, current studies of lightning mechanisms and related impacts on fires are limited to the boreal forests and are not readily transferable to the treeless tundra ecosystems where known CG lightning and the surface meteorology related to it differs substantially (Dissing and Verbyla, 2003).

1.2.2 Fire weather conditions

In addition to the weather processes that support lightning, weather elements such as air temperature, precipitation, and relative humidity play a dominant role in determining fire potential at the regional scale (Pyne et al., 1996). These elements that influence fire behavior are typically referred to as fire weather at an hourly or daily scale. Increased warming in the HNL regions is likely to lengthen the fire season and lead to an increase in burned area (Jolly et al., 2015). Specifically, temperature has been widely accepted as the most important factor that affects fire behavior primarily through an increase in evapotranspiration and associated decrease in surface moisture content (Flannigan et al., 2016; Williams et al., 2015). Additionally, dry conditions increase the probability of lighting-induced ignitions (Peterson et al., 2010) and enhance fuel flammability (Xiao and Zhuang, 2007) in the North American boreal forests.

Fire danger rating systems have been utilized around the world to quantify wildfire potential with numeric indices that guide fire management activities by integrating weather elements and other factors (Pyne et al., 1996). Two systems have been developed for North America from the early 20th century and updated multiple times since then, including the U.S. National Fire Danger Rating System (NFDRS) and the Canadian Forest Fire Danger Rating System (CFFDRS). Combining both hourly and daily weather observations, the latest 2016 version NFDRS produced four primary indices including Ignition Component (IC), Spread Component (SC), Energy Release Component (ERC), and Burning Index (BI) (Figure 1.4).

FWI System	Elements	NFDRS 2016
Daily Observations Required (4) (at Solar Noon) Temperature Relative Humidity Windspeed Rainfall **Hourly Observations for GFMC** Add Solar Radiation	**Weather Observations**	**Hourly Observations Required (120)** Temperature Relative Humidity Windspeed Rainfall Solar Radiation
	Intermediate Weather Outputs	Max/Min Temperature Max/Min Relative Humidity Precipitation Duration Daylength Vapor Pressure Deficit (VPD) Growing Season Index (GSI)
Fine Fuel Moisture Code (FFMC) – (5-16hr Timelag) Grass Fuel Moisture Code (GFMC) – (not part of Daily FWI)	**Fine Fuel Moisture**	1 hr Fuel Moisture 10 hr Fuel Moisture
Duff Moisture Code (DMC) – (15 day or 360 hour Timelag)	**Intermediate Fuel Moisture**	100 hr Fuel Moisture Live Herbaceous Fuel Moisture (LHM)
Drought Code (DMC) (53 day or 1272 hour Timelag)	**Drought Indicators**	1000 hr Fuel Moisture Live Woody Fuel Moisture (LWM) Keetch-Byrum Drought Index (KBDI)
Initial Spread Index (ISI) Buildup Index (BUI) Fire Weather Index (FWI)	**Fire Behavior Outputs**	Ignition Component (IC) Spread Component (SC) Energy Release Component (ERC) Burning Index (BI)

Figure 1.4. Comparison of CFFWIS (left) and NFDRS (right), source: National Wildfire Coordinate Group (https://www.nwcg.gov/publications/pms437/cffdrs/fire-weather-index-system).

Although originally introduced in 1925, the current CFFDRS has been developed since 1968 and widely applied throughout Canada since 1970 (Stocks et al., 1989). CFFDRS is comprised of two major sub-systems, including the Canadian Forest Fire Weather Index System (CFFWIS) and the Canadian Forest Fire Behavior Prediction System (CFFBPS). In particular, CFFWIS developed three fuel moisture codes and three fire behavior indices to describe the fuel moisture conditions and relative potential of fire behavior using consecutive daily observations of near-surface weather (Figure 1.4). Despite the similarities that NFDRS and CFFWIS share in both input and output data, these two systems are different in the specific requirements of

weather observations and assessment methods of fire danger (Pyne et al., 1996). Due to its simplicity in data preparation and calculation, the CFFWIS has been widely adopted by researchers and fire management teams worldwide in different ecosystems (Taylor and Alexander, 2006; Wang et al., 2017).

1.2.3 Surface fuels

Fuel type and state are critically important factors that control fire-environment interactions through altering fire characteristics and affecting ignition easiness. (Pyne et al., 1996). Fuel type represents properties of the fuel itself, such as fuel composition, continuity and loading. Fuel state is mainly related to moisture content primarily driven by the changing weather conditions at different temporal scales.

Fuel classification schemes, such as fuel models, inventory and photo guides, are commonly used to describe fuel type variability and organize fuel information. LANDFIRE, a program sponsored by U.S. Department of the Interior (DOI) and Department of Agricultural Forest Service (FS), has developed consistent surface fuel products throughout the US including Alaska and Hawaii, to characterize fuel composition and properties based on existing fuel classification systems. In Alaska, LANDFIRE provides products for the 13 Anderson Fire Behavior Fuel Model (FBFM13), 40 Scott and Burgan Fire Behavior Fuel Model (FBFM40), Canadian Forest Fire Danger Rating System (CFFDRS), Fuel Characteristic Classification System (FCCS), and Fuel Loading Model (FLM). These categorical classification datasets are developed with Landsat imagery using a rule-based approach that considers the limited availability of field data from the LANDFIRE reference

database and the difficulty of describing fuel conditions with generalized methods (Rollins, 2009).

The Alaskan tundra presents a very fine-scale mixture of shrub, herbaceous plants, moss and lichen components, which are inseparable even by very high resolution (VHR) images and thus is poorly represented by current categorical classifications at the Landsat scale. It is crucial to characterize the fractional representation of tundra fuel types to better understand the roles of individual component in driving tundra fire behavior.

The cumulative influences of previous and present fire weather conditions can further affect the dynamic fuel state characteristics including fuel moisture content and fuel temperature (Flannigan et al., 2016). Satellite-based measurements are widely used with physical or empirical models to assess fuel moisture levels at a large spatiotemporal scale (Yebra et al., 2013). Significant statistical relationships have been found between satellite-derived vegetation indices and fuel moisture content in different ecosystems (Yebra et al., 2008).

1.2.4 Topography

Variations in topographic features including elevation, slope steepness, aspect and land configuration also have the potential to affect wildfire behavior (Pyne et al., 1996). By controlling the exposure to sunlight and moisture pooling, topography can modify weather patterns and alter interactions of fuel and weather over time, therefore affecting fuel type and moisture content. Elevation above sea level can affect the fire environment by influencing climate conditions and fuel availability. With a direct impact on fire flame length and spread rate, slope is an important factor

affecting fire spread behavior. Representing the direction that a slope faces, aspect can affect fire behavior by altering the solar radiation amount and wind, therefore influencing fire weather and fuel conditions.

1.3 Fire modeling efforts

To understand the roles of these environmental factors on wildfire behaviors and further model the impacts of these factors on driving fire danger, two types of models have been developed in previous studies, including physical-based models that account for fire processes separately, and empirical models that utilize statistical methods to describe the patterns. Physical-based models that explicitly represent the wildfires processes are amongst the earliest attempts of fire occurrence modeling (Anderson, 2002; Anderson et al., 2000; Kourtz and Todd, 1991). Several major modules related to fire occurrence including lightning occurrence, fire ignition, fire smoldering and fire detection were described in these models. Subsequently, a series of equations based on experiments and assumptions were developed to incorporate the related environmental variables and to model the probability of fire occurrence.

In recent years, empirical models have been commonly adopted for modeling wildfire ignitions in studies across different ecosystems (Prestemon et al., 2013). For example, Liu et al. (2012), Yang et al. (2015), and Woo et al. (2017) predicted the forest fire risk using spatial point modeling methods. Generalized Linear Models have also been utilized for modeling fire occurrences in a variety of landscapes (Ager et al., 2018; Barbero et al., 2014; Vilar et al., 2016). Logistic regression and random forest (RF) based algorithms are also among the most popular methods for establishing the relationships between environmental factors and fire occurrences

with strong predictive capability (Guo et al., 2016; Keyser and Leroy Westerling, 2017; Van Beusekom et al., 2018; Vecín-Arias et al., 2016; Viedma et al., 2018; Wotton and Martell, 2005).

1.4 Research Questions

Considering the research gaps discussed above, this dissertation aims to address the overarching scientific question: *What factors and mechanisms drive wildland fire ignitions in Alaskan tundra biome?* This dissertation examines the impacts of surface fuel distribution, ignition sources, and other environmental factors on fire ignition probability by integrating field observations, remote sensing products, numerical weather forecasting model, and machine learning algorithm. To address the overarching scientific question, three integrated studies were conducted in this dissertation (Figure 1.4).

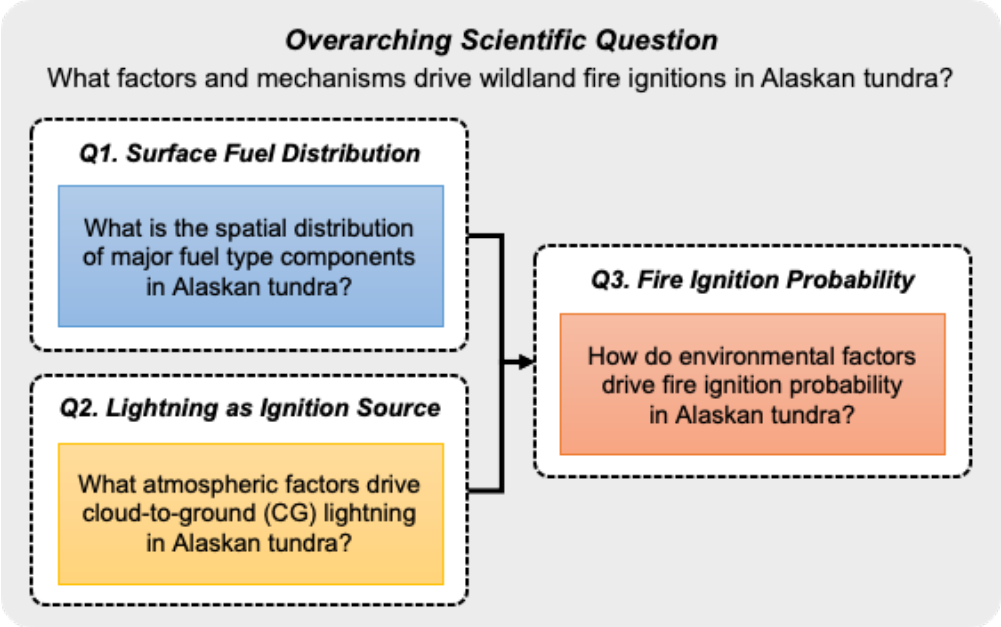

Figure 1.5. Framework of Research Questions and Objectives

Question 1: What are the spatial distribution patterns of major fuel types in Alaskan tundra?

This question examines the spatial distribution of major fuel type components in the shrub and graminoid dominated tundra in Alaska. This question focuses on developing a fractional cover product of the key tundra fuel components using field observations and Landsat 8 imagery at 30m resolution.

Question 2: What atmospheric factors and mechanisms drive CG lightning activity in Alaska tundra?

This question identified significant atmospheric and cloud properties that drive the distribution of CG lightning strikes in Alaskan tundra. This question is centered on developing an empirical-dynamical modeling framework for predicting CG lightning distribution combining a commonly used Numeric Weather Prediction (NWP) model, Weather Research and Forecast (WRF), and RF algorithm, to support fire monitoring and modeling effects in the tundra.

Question 3: How do environmental factors drive fire ignition probability in Alaskan tundra?

This question develops an empirical model for predicting wildfire ignition probability in the tundra using Moderate Resolution Imaging Spectroradiometer (MODIS) derived fire ignition locations and related environmental factors obtained through the integration of remote sensing products and WRF-generated weather conditions. Furthermore, this question explores the important environmental factors that drive wildfire ignitions in Alaskan tundra through these modeling efforts.

1.5 Dissertation Structure

Chapter 1 provides the overall background and motivation of this doctoral dissertation. It also introduces the major research questions and the organization of this study. The remainder of the dissertation is organized into three separate research chapters, a conclusion, supplementary materials and bibliography.

Chapter 2 focuses on addressing the research question 1 through the development of a fractional cover map product of major fuel type components, including woody (shrub), herbaceous (sedge and grass) and nonvascular (lichen and moss), in Alaskan tundra. I used Landsat 8 Operational Land Imager (OLI) surface reflectance data collected from 2013 to 2018 to develop seasonal mosaics of surface reflectance and spectral indices across the entire tundra in Alaskan. I then developed the fractional cover maps circa 2015 with field observations from three field trips to the tundra and the seasonal mosaics. This product has shown strong capability of capturing both detailed distribution of vegetation fuel components and describing the general spatial patterns of vegetation communities across the ecoregions in Alaskan tundra. This work has been peer reviewed and published in Remote Sensing of Environment (He et al., 2019). The data product I developed has been archived on the Oak Ridge National Laboratory Distributed Active Archive Center (ORNL DAAC; He et al., 2020).

Chapter 3 addresses the research question 2. This chapter develops an empirical-dynamical framework to model the CG lightning probability across Alaskan tundra based on WRF simulation and RF algorithm. I first conducted a sensitivity analysis to identify the optimal parameterization setting combination for

WRF simulation in the study area. Then four types of atmospheric variables were extracted from WRF simulation results to train an empirical model using RF algorithm, with CG lightning observations from the ALDN.

Chapter 4 corresponds to the research question 3 and discusses the results of modeling fire ignition probability in Alaskan tundra from 2001 to 2019 with a variety of related environmental factors, based on the results from Chapters 2 and 3. In this chapter, I prepared environmental factors for the tundra using WRF simulated weather variables and remote sensing products. CG lightning probability, near surface weather variables and CFFWIS were obtained based on WRF simulations using the method developed in Chapter 3, due to the lack of weather stations in the remote tundra. Fuel type and fuel state were obtained from Landsat-based product from Chapter 2 and MODIS surface reflectance data. I was then able to identify the key factors driving tundra fire ignitions in Alaska through modeling efforts with both RF and logistic regression algorithms.

Chapter 5 presents the primary conclusions of this doctoral dissertation. This chapter first summarizes the major research findings from Chapters 2 – 4. It then discusses the overall contribution of this dissertation to the broader Arctic scientific research and the operational fire management efforts in the HNL. Future insights of this research are also discussed in this chapter.

Chapter 2: Mapping Fractional Cover of Major Fuel Type Components across Alaskan Tundra[1]

2.1 Summary

Wildland fire is common and widespread in Alaskan tundra. Tundra fires exert considerable influence on local ecosystem functioning and contribute to climate change through biogeochemical (e.g. carbon cycle) and biogeophysical (e.g. albedo) effects. These treeless landscapes are characterized by a high degree of variation in fuel loading at scales much finer than moderate (30 m) satellite observations. However, because of the remoteness of the tundra and its lower contribution to carbon release compared to boreal forests, most frequently tundra fuels are poorly characterized, limiting the effective development of tundra-specific fire occurrence and behavior models. This study presents an approach to mapping the fractional coverages of major fuel type components in Alaskan tundra circa 2015 combining field data and Landsat 8 Operational Land Imager (OLI) observations. I adopt a multi-step method based on random forest (RF) algorithm to estimate the fractional vegetation cover of woody, herbaceous, and nonvascular components at subpixel level. I demonstrate the strong capability of exploiting multi-seasonal spectral information to identify these component types, with R-squared values around 0.9 and root mean squared errors below 10% for predicting their fractional cover. The

[1] This chapter has been published in Remote Sensing of Environment as He, J., Loboda, T. V, Jenkins, L., Chen, D., 2019. Mapping fractional cover of major fuel type components across Alaskan tundra. Remote Sensing of Environment, 232, 111324. The output maps of this chapter have been documented on Oak Ridge National Laboratory Distributed Active Archive Center (ORNL DAAC) as He, J., T.V. Loboda, L. Jenkins, and D. Chen. 2019. ABoVE: Distribution Maps of Wildland Fire Fuel Components across Alaskan Tundra, 2015. ORNL DAAC, Oak Ridge, Tennessee, USA.

mapping products depict the spatial distribution of woody, herbaceous, and nonvascular components at subpixel resolution across Alaskan tundra, which can function as a critical input for studying wildland fire risk and behavior in the tundra. The distributions of these fuel components align well with climate-based tundra ecoregions although climate variables are not included in my models.

2.2 Introduction

Wildland fire is common across tundra, the coldest vegetated land ecosystem on Earth. Active fire products derived from satellite data identify a widespread distribution of fire across the pan-Arctic tundra (Masrur et al., 2018). Out of the 10,260 km^2 global burned area in the tundra between 2001 and 2015, 54% was concentrated in Alaska as estimated by satellite-based burned area data (Loboda et al., 2017). Paleoecological and historical records also reveal frequent fire occurrence in Alaskan tundra (French et al., 2015; Higuera et al., 2011).

As a major disturbance in the tundra, wildfire exerts strong influence on the ecosystem state and functioning, including deepening of the active layer (Jones et al., 2015), release of ancient carbon to the atmosphere (Mack et al., 2011), decrease of land surface albedo (French et al., 2016) and shift in vegetation communities (Racine et al., 2004). These impacts further contribute to climate change through the alteration of surface energy budget and global carbon cycle (French et al., 2016; Mack et al., 2011; Pearson et al., 2013). Rapid climate warming in the Arctic observed during recent decades and projected under various climate change scenarios is likely to increase tundra fire occurrence in future (French et al., 2015; Young et al., 2017).

Despite its importance for global biogeochemical and biogeophysical processes, tundra fire receives much less attention compared to fire in other ecosystems. Although the number of studies on tundra fire has grown considerably in recent years, they mainly focus on quantifying post-fire impacts (French et al., 2016; Loboda et al., 2013) or examining fire regimes (French et al., 2015; Rocha et al., 2012). Critical for accurate monitoring of fire potential and for assessing its ecological and climatic impacts, in-depth knowledge of fire ecology and improved modeling capability of fire occurrence are still lacking for the tundra. Current approaches primarily developed upon boreal forest fire studies are thus insufficient to establish improved modeling and predictive capability to assess the present and future tundra fire potential.

Wildfire occurrence is controlled through the interaction of fuel, weather, and topography (Pyne et al., 1996). Effective modeling of fire occurrence requires accurate characterization of these environmental factors. This is, however, difficult for the tundra under current efforts due to the lack of in situ data for all three factors. Compared to other ecosystems, very limited fuel inventory plots have been visited in Alaskan tundra because of its remoteness. Existing fuel type products provided by LANDFIRE (https://landfire.gov) for Alaskan tundra (Table 2.1) are primarily developed based on the generic fuel classification schemes designed for other ecosystems. In particular, 13 Anderson Fire Behavior Fuel Model (FBFM13), 40 Scott and Burgan Fire Behavior Fuel Model (FBFM40), and Canadian Forest Fire Danger Rating System (CFFDRS) include logging slash in their schemes and thus cannot describe the surface fuel compositions in the tundra. Limited fire weather

stations and little to none geodetic surveys within Alaskan tundra also lead to the lack of accurate weather and topographical measurements. Primarily built upon remotely sensed observations, models and interpolations, existing strategies and datasets developed for wildfire monitoring thus simply provide a generic estimation of the tundra environment in Alaska.

Table 2.1. LANDFIRE fuel products and their major fuel strata or types available for Alaskan tundra

Fuel classification system	Major fuel strata or types
13 Anderson Fire Behavior Fuel Model (FBFM13; Anderson, 1982)	Grass, shrub, timber, logging slash
40 Scott and Burgan Fire Behavior Fuel Model (FBFM40; Scott & Burgan, 2005)	Nonburnable, grass, grass-shrub, shrub, timber-understory, timber litter, slash-blowdown
Canadian Forest Fire Danger Rating System (CFFDRS; Hirsch, 1996)	Coniferous, deciduous, mixedwood, slash, open
Fuel Characteristic Classification System (FCCS; Ottmar et al., 2007)	Canopy, shrub, nonwoody fuels, woody fuels, litter-lichen-moss, ground fuels

Whereas, tundra environment varies at a very fine spatial scale with extremely high local heterogeneity (Davidson et al., 2016; Frost et al., 2014; Lara et al., 2018; McManus et al., 2012), which makes existing products poorly suited for capturing its detailed spatial variability. Specifically, Alaskan tundra presents a highly variable and mixed combination of burnable vegetation materials, including shrubs, herbaceous plants, mosses and lichens. These fuel type components can affect fire occurrence and behavior in multiple ways (Innes, 2013; Rocha et al., 2012). First, fuel flammability varies by plant types in Alaskan tundra (Sylvester and Wein, 1981). Live leaves from shrub species tend to have higher fire-potential ratings than herbaceous plants. Second, the variability of post-fire fuel recovery and accumulation rates among

vegetation types can lead to different fire frequency levels across the tundra (Innes, 2013). Tundra regions dominated by grasses or sedges tend to burn more frequently than those with shrubs or mosses do because of their faster recovery rates. Third, tundra vegetation composition also impacts burned area extent (Rocha et al., 2012). For example, larger burned areas are more frequently found within moist shrub and tussock tundra compared to non-acidic tundra. Thus, identifying the detailed composition and distribution of fuel type components is critical for understanding tundra fire occurrence and behavior.

However, the fine-scale fuel components in the tundra can only be separated at centimeter-level resolution with drone data (Figure 2.1) and are not directly classifiable even in very high resolution (VHR; 1–5 m) imagery. Categorical LANDFIRE products developed at 30-m resolution poorly capture the actual fuel distribution in the tundra. Recent efforts, although limited, have been conducted to characterize the fractional vegetation properties at subpixel level for Alaskan tundra with Landsat imagery. For example, Macander et al., (2017) developed fractional coverage maps of plant functional types (PFTs) across the North Slope region of Alaska. Berner et al. (2018) also mapped the fractional dominance and aboveground biomass (AGB) of shrubs on the North Slope. However, these products are not directly transferable to fuel classification schemes in the tundra because of the different vegetation cover definitions adopted. They also fail to capture the information of other tundra regions like Seward Peninsular and Noatak, which have more frequent and intense fire activities than the North Slope based on historical records (French et al., 2015; Rocha et al., 2012).

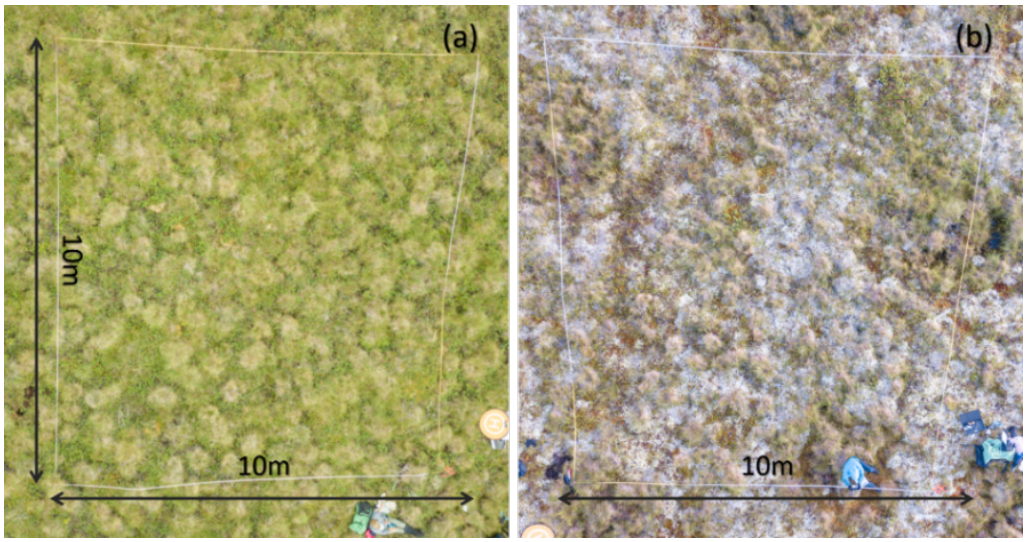

Figure 2.1. Examples of highly mixed fuel type components in Alaskan tundra: (a) shrub and graminoid tussocks; (b) grass, lichen and moss.

While fractional cover products for tundra are only at their early stages of emergence, a variety of approaches has been developed to unmix land cover fractions with multi-source remote sensing data across different (most frequently tree dominated) ecosystems. Supervised regression algorithms with multi-temporal spectral metrics are among the most commonly adopted methods for fractional cover mapping (Hansen et al., 2013; Olthof and Fraser, 2007; Selkowitz, 2010). RF regression, an ensemble learning method based on decision tree regression, has been found to have strong capability in distinguishing vegetation fractions (Gessner et al., 2013; Liu et al., 2017; Marino et al., 2016). A second type of algorithms employs spectral mixture analysis to decompose sub-pixel fractional coverages (Guan et al., 2012; Ma et al., 2015; Mu et al., 2018; Somers et al., 2011). They primarily rely on spectral indices to determine the fractions of endmembers. However, the variability among endmembers is typically ignored in the modeling procedure (Somers et al., 2011). A third type of geometric-optical models has also been developed to derive

vegetation fractions with multi-angular remote sensing data (Chopping et al., 2008), though their applications are limited by the spatial data coverage.

The Arctic-Boreal Vulnerability Experiment (ABoVE) proposed by the National Aeronautics and Space Administration (NASA) has provided a new opportunity for conducting in-depth research on wildland fire in the tundra. Through the support of field campaigns by this program, researchers have been able to enlarge the spatial coverage and environmental conditions of field observations. Coupling with remote sensing datasets and existing algorithms, these field datasets make it possible to develop broad-scale mapping products for the tundra. In this study, I present an RF-based approach to mapping the fractional distributions of wildland fuel components in Alaskan tundra using multi-spectral and multi-temporal Landsat data circa 2015 and a suite of field observations collected across a large span of tussock and shrub tundra sites. Specifically, I focus on three fire-carrying fuel type components for the shrub or graminoid dominated tundra in the study area: (1) woody (shrub) component, (2) herbaceous (primarily sedge and grass) component, and (3) nonvascular (lichen and moss) component, and further develop separate maps for describing their fractional coverages. I determine these components in a qualitative way considering their differences in vegetation genera, fuel characteristics and spectral properties. This scheme also corresponds to fuel strata in the Fuel Characteristic Classification System (FCCS) and major fuel components in other existing systems (Table 2.1).

2.3 Study Area

A commonly used dataset, the Circumpolar Arctic Vegetation Map (CAVM; Walker et al., 2005; Figure 2.2), was used to determine the study area of Alaskan tundra (Beck et al., 2011; Bhatt et al., 2013; French et al., 2015; Raynolds et al., 2008). Burning in Alaskan tundra is primarily supported by surface vegetation fuels, including evergreen or deciduous shrubs, herbaceous species (sedges and grasses), mosses and lichens (Hu et al., 2015; Rocha et al., 2012). Dry sites in the tundra tend to be dominated by dwarf shrubs with some grasses, mosses, and lichens, while wet sites have more sedges and mosses (Sylvester and Wein, 1981).

Alaskan tundra shares similar vegetation communities and species across ecoregions (Alaska Department of Fish and Game, 2006; Viereck et al., 1992). The Unified Ecoregions of Alaska identifies four ecoregion groups and eleven ecoregion units within Alaskan tundra based on their climate, vegetation, geology, and topography (Nowacki et al., 2003; Figure 2.2). With a dry, polar climate, the Arctic Tundra ecoregion group is dominated by shrub and sedge tundra underlain by continuous permafrost. The Bering Tundra group shows a moist polar or maritime climate with principally Dryas-lichen and moist sedge-tussock tundra. Bering Taiga group, having a moist polar climate with relatively thin permafrost, is generally covered by Dryas-lichen, sedge-shrub tundra and mixed forests. Dominated by a dry continental climate, the Intermontane Boreal group are primarily covered by shrublands and forests.

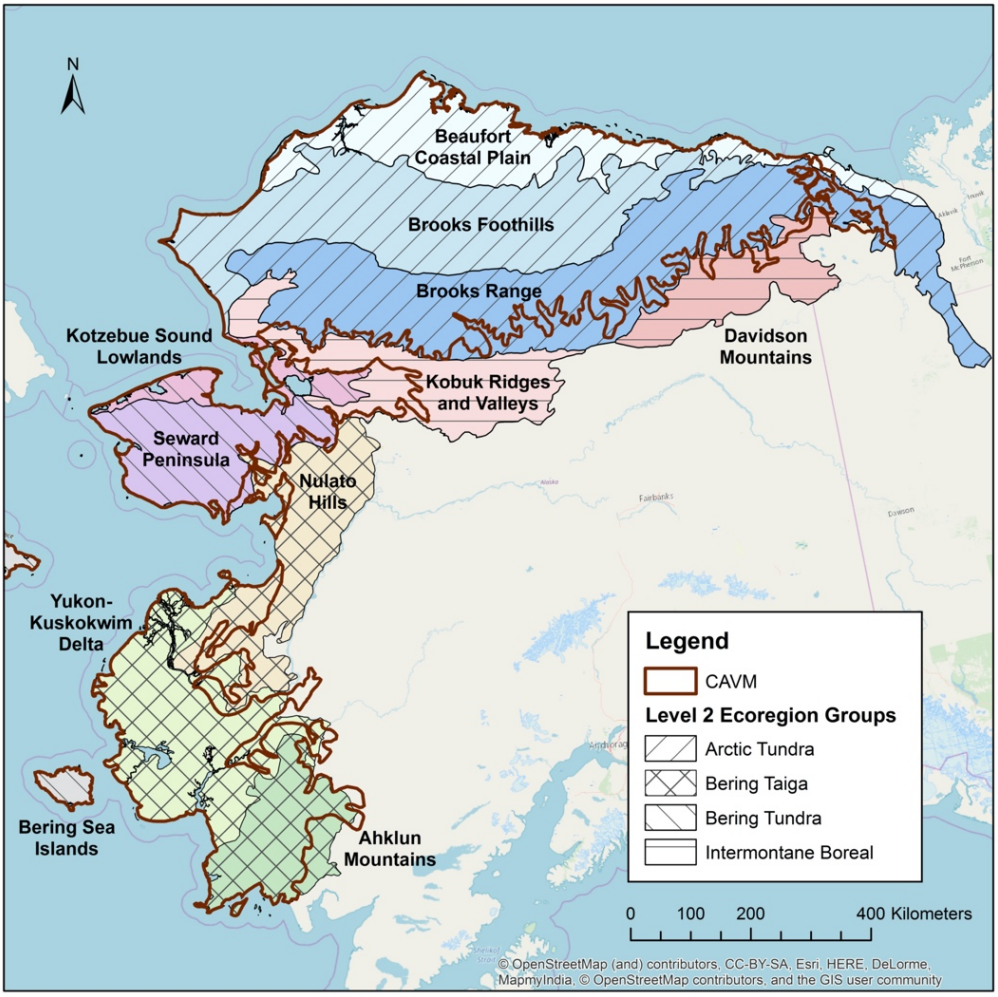

Figure 2.2. Alaskan tundra region defined by CAVM and corresponding ecoregions identified by the Unified Ecoregions of Alaska: 2001. Each color represents one ecoregion unit. Ecoregion units within the same Level 2 ecoregion groups are separated by different line patterns.

2.4 Data and Methods

The variability of the tundra vegetation types in surface reflectance and phenology makes it possible to capture the subpixel compositions using multi-spectral and multi-temporal remote sensing data. Dwarf shrub, sedge, and moss/lichen mix show distinguishable spectra according to the ground-based hyperspectral profiles

measured in the North Slope (Buchhorn et al., 2013; Davidson et al., 2016). Both field observations and satellite-derived spectral indices also identify considerable variations in the phenology patterns of tundra vegetation species during their short growing seasons (Beamish et al., 2017; Shaver and Kummerow, 1991; Stow et al., 1993). For example, graminoid species such as tussock cottongrass (*Eriphorum vaginatum)* and Bigelow's sedge (*Carex bigelowii*) tend to have an earlier onset of leaf expansion compared to shrub species like tealeaf willow (*Salix pulchra*) and dwarf birch (*Betula nana*; Shaver and Kummerow, 1991). By summarizing the fuel properties, spectral characteristics and phenology patterns of these vegetation types described above, I identified the following components of surface fuel types in Alaskan tundra for large-scale mapping in this study: (1) woody (shrub), (2) herbaceous (primarily sedge and grass), and (3) nonvascular (lichen and moss).

I then designed a four-step method to map the spatial distributions of these fuel components (Figure 2.3): (1) developing seasonal composites of spectral bands and indices with multi-temporal Landsat imagery for the entire Alaskan tundra; (2) generating a “tundra vegetation mask” to identify the shrub or graminoid dominated tundra with land cover classification; (3) RF modeling of fractional fuel component cover; (4) mapping fractional cover of major fuel type components across the shrub or graminoid dominated tundra in Alaska.

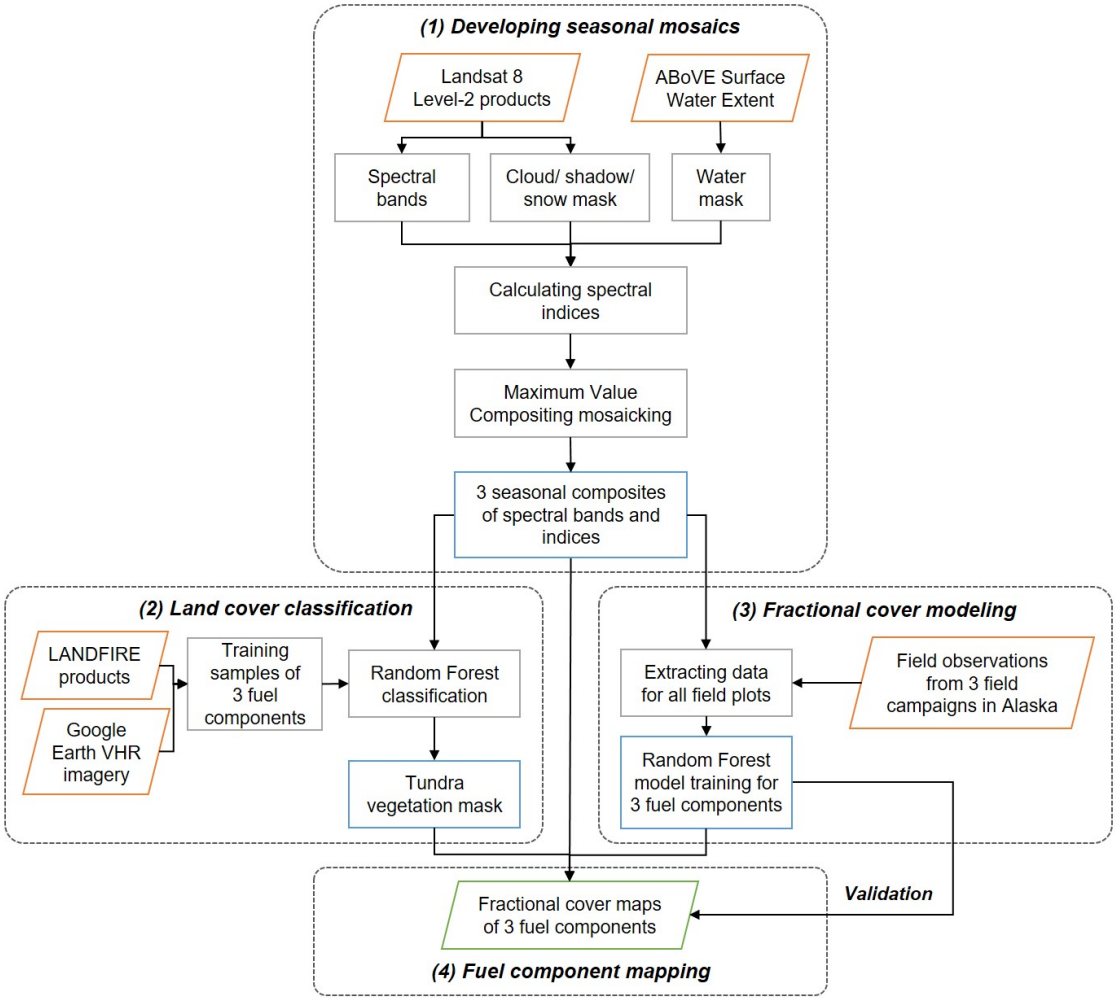

Figure 2.3. Flowchart of fractional fuel component mapping.

2.4.1 Data Sources

Landsat observations

Landsat 8 OLI imagery acquired from 2013 to 2017 was used to develop spatially continuous mosaics of Alaskan tundra. I downloaded the Level-2 surface reflectance data generated with Landsat 8 Surface Reflectance Code (LaSRC; Vermote et al., 2016) from the U.S. Geological Survey Earth Resources Observation and Science Center (Table 2.2). Since the growing seasons of tundra vegetation generally start from late-April or May and end in October, for each year, I

downloaded images acquired during late-April through October with land cloud coverage smaller than 70%, as estimated by the product metadata. Additionally, I excluded images with 80 – 90% snow coverage over vegetated land surface in late April, May and October based on my visual interpretation during the data download. In total, I obtained and processed 1837 Landsat 8 scenes covering 113 Worldwide Reference System-2 (WRS2) path/rows as summarized in Table 2.2.

Table 2.2. Summary of Landsat 8 OLI tiles processed in this study. WRS2 path/row overlaps exist between different regions.

Major regions	**WRS2 path range**	**WRS2 row range**	**Total number of path/rows**	**Total number of scenes**
North Slope and Noatak	64 ~ 85	10 ~ 13	70	932
Seward Peninsula	75 ~ 84	13 ~ 15	25	358
Southwest Alaska	73 ~ 80	15 ~ 19	29	752

Field observations

I collected fractional cover observations of the three fuel components from 222 10×10 m plots during three field campaigns in the tussock and shrub tundra of Alaska (Figure 2.4): 2012 campaign in the North Slope (NASA Terrestrial Ecology Grant NNX10AF41G), 2016 campaign in the Noatak River National Preserve and 2017 campaign in the Seward Peninsula (NASA Terrestrial Ecology Grant NNX15AT79A). Fractional coverages of fuel components within each plot were determined using ocular assessment. All three campaigns were conducted during late-July to mid-August. Considering the limited amount of field sites that I can visit during one single field trip, I combined field data from all three campaigns in this

study to provide a robust sample collection for driving an ecosystem-wide mapping method.

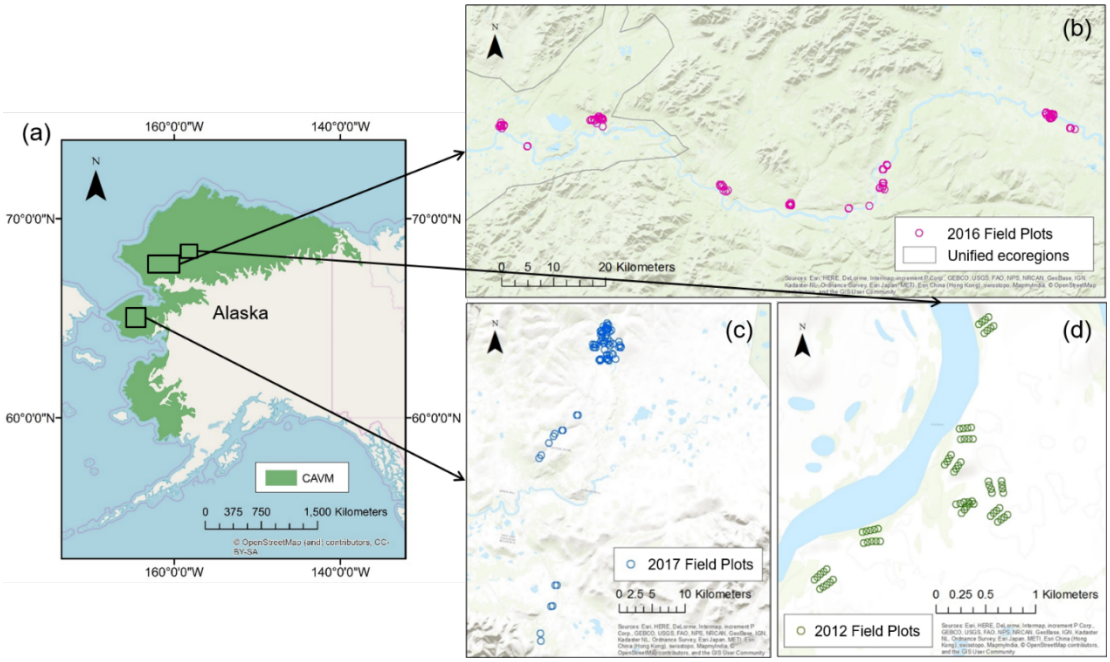

Figure 2.4. Alaskan tundra region as defined by CAVM (a) and three field campaign sites: (b) 2016 field plots in Noatak River National Preserve, (c) 2017 field plots in Seward Peninsula, (d) 2012 field plots in North Slope.

Field plots were established following a generally accepted scheme (Dyrness and Norum, 1983; Viereck, 1979). During each campaign, the data were collected within recovering burns as well as within areas that have not been identified as burned by either management records or satellite observations. This data collection design ensured that field data observations sampled a broad range of fire history and topographical features with varying compositions of woody, herbaceous, and nonvascular vegetation cover. The 2016 and 2017 data collection campaigns also ensured that a variety of drainage conditions was incorporated into the stratified sampling scheme. Specifically I identified four drainage categories based on slope

and flow accumulation using a method proposed by Kasischke and Hoy (2012). I then randomly selected South-East corner point for the 10×10m plots considering these factors prior to field visits. Although assessment of fractional cover during the 2012 field visit was conducted using the similar protocol, the site set up was more systematic in order to support a proper characterization of field sites for radar observations. In this case, corner points of 10×10 m plots were set up in two parallel transect lines 100m apart within an area of visibly uniform conditions following a previously established field protocol in existing studies (Bourgeau-Chavez et al., 2013; Bourgeau-Chavez et al., 2007).

Auxiliary data

To assist the development of seasonal composites, I utilized the 16-day Moderate Resolution Imaging Spectroradiometer (MODIS) Vegetation Indices product (MOD13Q1 Version 6) available on Google Earth Engine from 2013 to 2017 to examine the phenology of tundra vegetation and to determine the growing season periods for Landsat data collection and processing. The Normalized Difference Vegetation Index (NDVI) data layer in MOD13Q1 was used for deriving phenology trends.

Although the quality assessment (QA) band provided by the Level-2 LaSRC product identifies water pixels for each scene, I adopted the 30-m ABoVE Surface Water Extent data (Carroll et al., 2016) centered in 2011 to identify the representative extent of water bodies across the study area for spatial and temporal consistency. Using Landsat imagery centered on 1991, 2001 and 2011, this product maps the

distribution of surface water across the boreal and tundra regions in North America in these epochs.

To develop the tundra vegetation mask in step 3, I utilized a set of 30-m LANDFIRE products and VHR imagery freely available on Google Earth to assist the sampling of training and validation datasets for land cover classification. I acquired the FCCS, CFFDRS and FBFM40 products for Alaska (Table 2.1) in the latest available version 1.4.0, which incorporates Landsat imagery through 2014. VHR time series imagery provided by Google Earth was also accessed to help determine training and validation data through visual interpretation.

2.4.2 Developing seasonal composites of spectral bands and indices

First, I developed continuous composites of surface reflectance bands and spectral indices for pre-growing (late-April to early-June), peak-growing (mid-July to mid-August) and post-growing season (end-August to end-September). Since the specific timing of growing events varies by year and latitude, I extracted vegetation phenology patterns using NDVI data from MOD13Q1 to determine the specific dates of three growing seasons. I particularly examined four graminoid or shrub tundra regions as identified by CAVM across Alaska from north to south and compared the NDVI profiles of ten randomly sampled pixels in each region (Figure 2.5). According to the vegetation growing patterns shown from the profiles, I assigned the Landsat data acquired from April 21 to June 10 as the pre-growing season, the data acquired from July 1 to August 20 as the peak-growing season, and the data acquired from August 30 to September 30 as the post-growing season.

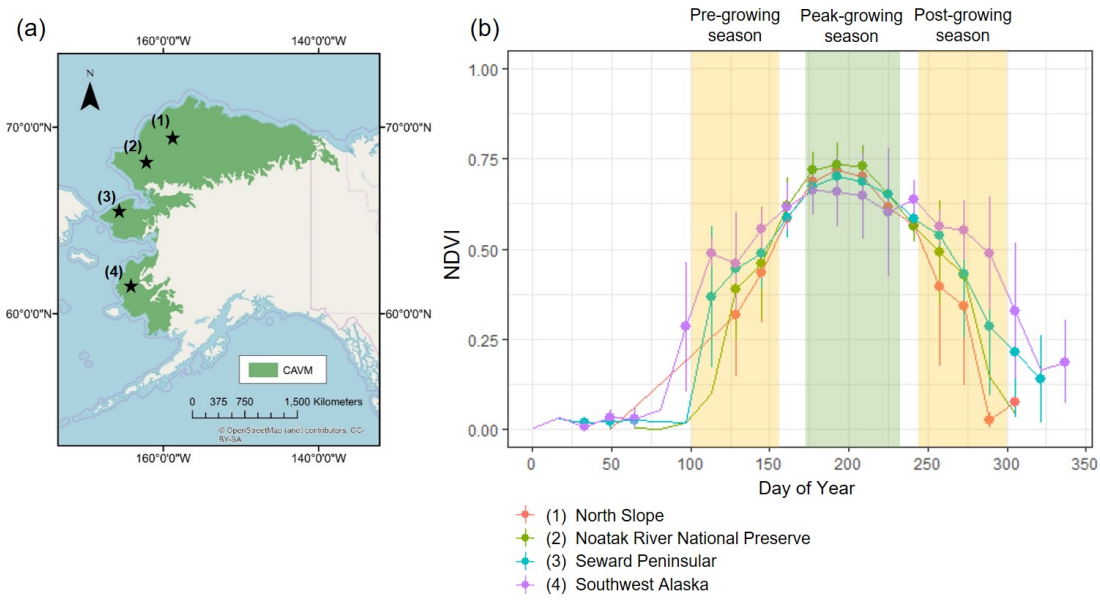

Figure 2.5. Averaged NDVI profiles extracted from MODIS product (MOD13Q1) on Google Earth Engine in four regions across Alaskan tundra (a). Ten pixels were randomly selected and plotted for each region as an example (b): (1) North Slope, (2) Noatak River National Preserve, (3) Seward Peninsula, (4) Southwest Alaska.

I then downloaded and organized the Landsat 8 data by growing seasons and extracted all surface reflectance and QA bands. Four ratio-based spectral indices and three Tasseled Cap (TC) components (Brightness, Greenness, and Wetness; Baig et al., 2014) were calculated for each scene to capture the detailed variability of vegetation spectral characteristics (Table 2.3). Particularly, I considered four ratio-based indices here including NDVI (Tucker, 1979), Normalized Burn Ratio (NBR; García and Caselles, 1991), Normalized Difference Water Index with near-infrared (NIR) and shortwave-infrared (SWIR) bands (NDWI1; Gao, 1996), and Normalized Difference Water Index with green and NIR bands (NDWI2; McFeeters, 1996).

Table 2.3. Landsat 8 spectral metrics used for developing seasonal composites.

Categories	Properties	Details
Surface Reflectance	Band 2	Blue: 0.45 – 0.51 μm
	Band 3	Green: 0.53 – 0.59 μm
	Band 4	Red: 0.64 – 0.67 μm
	Band 5	NIR: 0.85 – 0.88 μm
	Band 6	SWIR1: 1.57 – 1.65 μm
	Band 7	SWIR2: 2.11 – 2.29 μm
Spectral Indices	NDVI	$(\rho_{NIR} - \rho_{Red})/(\rho_{NIR} + \rho_{Red})$
	NBR	$(\rho_{NIR} - \rho_{SWIR2})/(\rho_{NIR} + \rho_{SWIR2})$
	NDWI1	$(\rho_{NIR} - \rho_{SWIR1})/(\rho_{NIR} + \rho_{SWIR1})$
	NDWI2	$(\rho_{Green} - \rho_{NIR})/(\rho_{Green} + \rho_{NIR})$
Tasseled Cap Components	TC Brightness (TCB)	$0.3029\rho_{Blue} + 0.2786\rho_{Green} + 0.4733\rho_{Red} + 0.5599\rho_{NIR} + 0.508\rho_{SWIR1} + 0.1872\rho_{SWIR2}$
	TC Greenness (TCG)	$-0.2941\rho_{Blue} - 0.243\rho_{Green} - 0.5424\rho_{Red} + 0.7276\rho_{NIR} + 0.0713\rho_{SWIR1} - 0.1608\rho_{SWIR2}$
	TC Wetness (TCW)	$0.1511\rho_{Blue} + 0.1973\rho_{Green} + 0.3283\rho_{Red} + 0.3407\rho_{NIR} - 0.7117\rho_{SWIR1} - 0.4559\rho_{SWIR2}$

Since Maximum Value Compositing (MVC) approach is effective in minimizing the impacts of cloud contamination, off-nadir viewing, aerosol and water vapor, I adopted this widely used method for developing seasonal mosaics across Alaskan tundra (Holben, 1986; Potapov et al., 2008; Roy et al., 2010; Stow et al., 2004). Before mosaicking, I masked out the cloud, cloud shadow, and snow pixels detected by the CFMask algorithm (Zhu et al., 2015). I further conducted morphological dilation for the masked pixels using a disk-shaped structuring element with five as the radius to remove the undetected cloud and shadow pixels. Although cloud/shadow pixels are generally thought to have lower NDVI than clear-sky pixels, pixels along the cloud/shadow edges mixed by shadow and vegetation signals could have higher NDVI than the clear-sky ones (Figure 2.6). Since the dilated mask could

still omit these edge pixels with high NDVI values that can affect MVC results, I filtered them out using the following criteria based on empirical values identified in the study area:

$$\rho_{NIR} < 0.2 \; and \; NDVI > 0.6,$$

where ρ_{NIR} represents the surface reflectance of NIR band. For each growing season, I identified the Landsat pixels with the maximum NDVI and then generated the mosaics for each band using the values from these pixels. The three output mosaics each include six spectral bands and seven indices as listed in Table 2.3. They then served as the input data for the following steps.

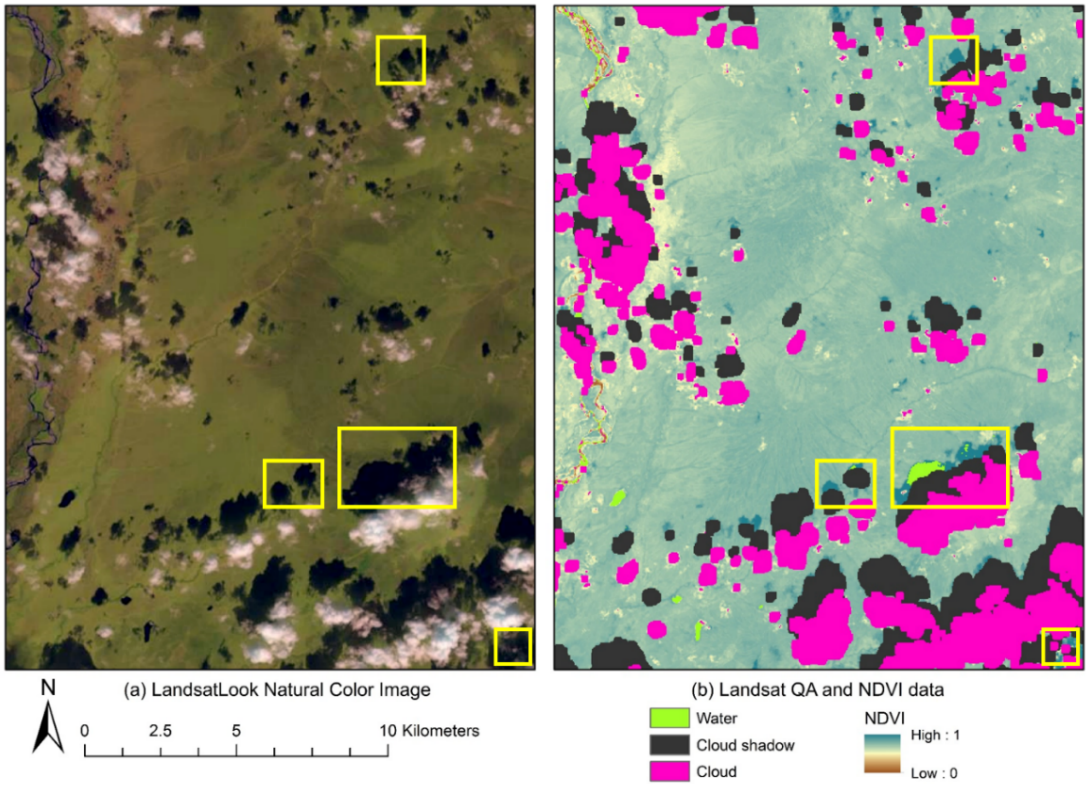

Figure 2.6. Unmasked cloud shadow pixels with high NDVI values from a Landsat 8 scene (Landsat Scene Identifier: LC80690122017228LGN00). Examples are

highlighted in yellow rectangles: (a) LandsatLook natural color image, (b) NDVI and cloud/shadow/water mask identified by level-2 QA data from the same Landsat scene.

2.4.3 Generating a tundra vegetation mask for shrub or graminoid dominated tundra

Since CAVM simply defines an approximate tundra boundary based on 1-km Advanced Very Higher Resolution Radiometer (AVHRR) data (Walker et al., 2005), I further developed a "tundra vegetation mask" layer to refine the shrub or graminoid dominated tundra region using RF classification. I have removed water body pixels in the previous step using the nominal water mask (Carroll et al., 2016). Here I identified three land cover classes including (1) tall shrub or tree, (2) built-up or barren land, (3) shrub or graminoid dominated tundra.

I first used the three acquired LANDFIRE products (CFFDRS, FBFM40 and FCCS) to define the general regions of the three classes based on their classification codes (Table 2.4). I then examined the random points by visually interpreting the moderate resolution and VHR time series imagery available on Google Earth based on expert knowledge. Points that are not representative of the classes they are supposed to represent were removed from the sampling dataset. For each class, I extracted the intersections of each product as its boundary for generating stratified sample points by area. In total, I acquired 436 points for the tall shrub or tree, 1176 points for the built-up or barren land, and 5238 points for shrub and graminoid tundra.

Table 2.4. Land cover classes and corresponding classification codes from LANDFIRE products.

Land cover classes	LANDFIRE products	Fuel class or identification code
Tall shrub or tree	FCCS	85, 87, 88, 89, 92, 93, 94, 101, 103, 105, 322, 332
	CFFDRS	C1, C2, C3, C4, C5, C6, C7
Built-up or barren land	FCCS	0
	CFFDRS	NB1, NB9
	FBFM40	NB1, NB9
Shrub or graminoid dominated tundra	FCCS	95, 97, 98, 99, 100, 318, 323, 324, 326, 327, 330, 331, 333, 334, 336, 337, 338, 339, 601, 602, 603, 604, 610, 611, 614, 615, 616, 617, 620, 623, 624, 625, 627, 629, 630, 632, 635, 637, 638
	CFFDRS	D1, S2, S3, O1A, M1, M2A, M2B, M2C, M3

I used all bands from the seasonal mosaics as the input features for training and mapping the tundra vegetation mask. For each class, I randomly selected 70% of the sampled points for training the RF classification algorithm and reserved the remaining 30% for assessing the classification accuracy. I also reported the overall out-of-bag (OOB) error rate to estimate the classifier error based on the training data. Specifically, the OOB error rate is generated by estimating the ratio of misclassification among all bootstrap iterations (Breiman, 2001).

2.4.4 RF modeling of fractional cover

Before modeling, I compared my designed sampling plots with full fire records, including both MODIS Active Fire Product and Alaska Large Fire Database, to make sure the plots were not impacted by fire and thus representative of undisturbed conditions since the time of the measurement. To predict the fractional cover of surface fuel components at the large scale, I trained individual RF regression models for the three components separately with the field observations and seasonal

composites developed in Section 2.4.2. In particular, the spectral properties from the three growing seasons, including all six surface reflectance bands, four ratio-based spectral indices, and three TC components, were used as the input parameters to train the RF models for estimating fractional cover. For each RF regression model, I set the number of input variables at each split to 14, the number of trees to grow as 500, and the node size to 5.

To assess the modeling accuracy, I not only examined the internal metrics provided by the RF regression algorithm, but also conducted cross-validation with our field observations. Specifically, I assessed the internal metrics including OOB, percent of variance explained, mean squared error (MSE) and root mean squared error (RMSE). For the cross-validation, I reserved 70% field data for model training and kept the remaining 30% for validation using a stratified random sampling strategy. I then reported the RMSE and R-squared values between the observed and estimated fraction values with the 30% validation dataset. For each fuel type component, I ran RF regression multiple times and selected an optimal one as the final model for estimating fractional cover.

I also assessed the importance of predictors in determining the fractional cover in each model. Although Mean Decrease Gini and Mean Decrease Accuracy (MDA; Breiman, 2001) are the most commonly used indicators to assess the contributions of independent variables, there is an on-going debate about their comparative robustness (Louppe et al., 2013). Here I chose to report the MDA, which evaluates the variable importance by estimating the mean decreased MSE with permutated variable values.

2.4.5 Fuel type component mapping

In the final step, I combined the results generated from the previous sections to develop fractional cover maps for the three fuel components. Only shrub or graminoid dominated tundra pixels identified by the "tundra vegetation mask" in Section 2.4.3 were subsequently used for mapping. I used the RF regression models developed in Section 2.4.4 to estimate the fractional cover of fuel components in Alaskan tundra. In addition to the statistical metrics adopted for assessing the RF modeling accuracy in Section 2.4.4, I further assessed the mapping results through comparisons with existing data products at similar spatial scales considering the limited coverage of our field observations.

I first examined the distribution of fuel component fractions against the ecoregions based on the expert knowledge. The variability of climatic and topographic conditions across ecoregions in the tundra affects the actual distribution of the burnable vegetation materials. Here I utilized the Unified Ecoregions of Alaska (Nowacki et al., 2003) product to define the ecoregions within the tundra (Figure 2.2). For each fuel component, I generated boxplots to summarize the fraction distributions within the two Level 1 ecoregion groups ("Boreal" and "Polar"). Since most ecoregions in Alaskan tundra are elements of the "Polar" group, I further examined the distributions of each ecoregion units within the "Polar" Level 1 group.

I then compared my results with existing vegetation cover products developed for the North Slope of Alaska to examine the differences caused by fractional cover definitions, field sampling strategies, and modeling methods. Although no fractional fuel type products have been developed, Beck et al. (2011) mapped the shrub cover of

deciduous species circa 2000 and Macander et al. (2017) quantified the fractional distributions of 16 PFTs across the North Slope of Alaska. I examined these products against the field observations. I also compared the overall results between the output maps and these two products with randomly selected sample points in the overlapping regions of all products. Since the definition of PFTs is not directly transferable to my fuel component scheme, here I used the "Total shrub" of PFT to compare with the woody component, the "Total herbaceous" of PFT to compare with the herbaceous component, and the "Total nonvascular plants" to compare with the nonvascular component. Although Berner et al. (2018) also mapped the dominance of shrub in the North Slope, they defined the shrub dominance differently as the percentage of shrub AGB over the total plant AGB and thus was not considered for comparison.

2.5 Results

2.5.1 Accuracy assessment of tundra vegetation mask

Both internal metrics from the RF algorithm and accuracy assessment were used to evaluate the performance of the tundra vegetation mask. The RF algorithm showed an overall OOB error rate of 2.21%. I then generated the confusion matrix using the reserved 30% data to validate the classification result (Table 2.5). The overall classification accuracy reaches 97.91%, although the producer's accuracy and user's accuracy vary among each land cover class. The class of tall shrub or tree receives the lowest producer's accuracy (77.86%) and user's accuracy (90.27%), while the other two classes have consistently high accuracy values. Across the 494,971.4

km^2 Alaskan tundra as estimated by CAVM, I identified 380,755.2 km^2 as shrub or graminoid dominated tundra.

Table 2.5. Confusion matrix of land cover classification for developing tundra vegetation mask.

		Reference				
		Tall shrub/ tree	**Built-up/ barren**	**Tundra**	**Total**	**User's accuracy**
Map	**Tall shrub/ tree**	102	0	11	113	90.27%
	Built-up/ barren	0	351	1	352	99.72%
	Tundra	29	2	1560	1591	98.05%
	Total	131	353	1572	2056	1
	Producer's accuracy	77.86%	99.43%	99.24%	1	Overall Accuracy: 97.91%

2.5.2 Accuracy assessment of fractional cover estimation

To assess the modeling results, I first examined the internal metrics generated from RF regression (Table 2.6). The RF models developed for all three fuel components perform well in explaining the percent of the variance, with 79.83%, 80.76%, and 80.02% for the woody (shrub), herbaceous (sedge and grass), and nonvascular (lichen and moss) components respectively. They also report high predictive power for fractional cover mapping with low MSE and RMSE values. The woody, herbaceous and nonvascular models show MSE values of 0.008852, 0.008117 and 0.007234, and RMSE values of 9.41%, 9.01%, and 8.51%, respectively.

Table 2.6. Statistical summary of three RF regression models.

Fuel component	**% variance**	**MSE**	**RMSE**
Woody component	79.83	0.008852	9.41%
Herbaceous component	80.76	0.008117	9.01%
Nonvascular component	80.02	0.007234	8.51%

I then evaluated the predicted fractional cover using the reserved 30% field samples. The comparisons between the modeled and observed values show strong agreement for the three fuel components (Figure 2.7). The RSME values for the validation samples are within 2% of those generated from the internal model statistics with 8.04%, 9.57%, and 10.11% for woody, herbaceous and nonvascular components, respectively. The R-squared values between observations and estimations for the validation data are approximately 0.95 for all fuel components, with 0.9717, 0.9633, and 0.9395 for the woody, herbaceous and non- vascular components respectively.

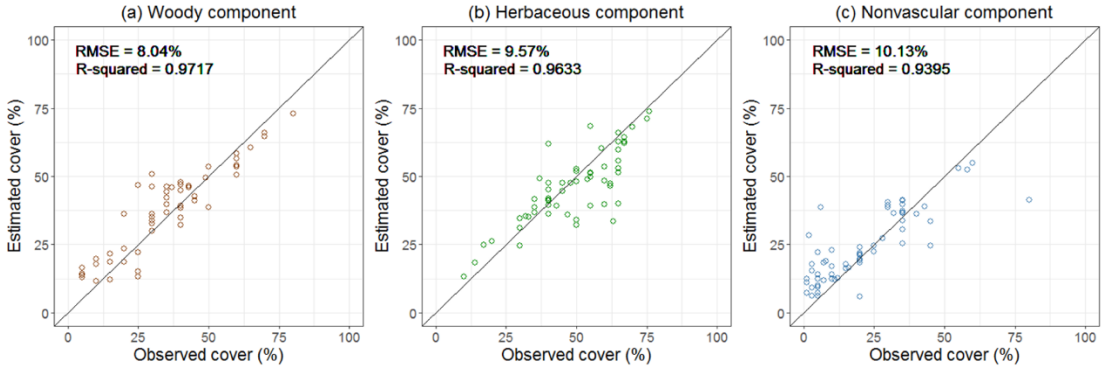

Figure 2.7. Scatter plots comparing estimated and observed fractional cover using the validation data for (a) woody, (b) herbaceous, and (c) nonvascular components. RMSE and R-squared values between the estimations and observations are reported in the scatter plot of each component. RSMEs are within 2% of those from the internal model statistics. R-squared values reach 0.95 for all components.

Spectral bands and indices during pre- and peak-growing seasons play the most important role in determining the fractional cover of woody and herbaceous components in Alaskan tundra (Figure 2.8 a-b), while spectral indices during post-growing seasons contribute most to the cover estimation of nonvascular component (Figure 2.8 c). For the woody component, the spectral reflectance of the red band

during the peak-growing season shows the highest MDA value of 14.73% in the RF regression model, followed by that of the blue band during the pre-growing season (13.53%) and NDVI during the peak-growing season (11.78%). For the herbaceous component, the spectral reflectance of the red band during the pre-growing season shows the highest MDA value of 16.66%, followed by NBR during the peak-growing season (15.79%) and the spectral reflectance of the green band during the pre-growing season (13.83%). As for the nonvascular component, NBR during the post-growing season is the most important independent variable in the regression model with an MDA value of 19.15%. NDWI2 and NDVI during the post-growing season also show high MDA values (13.77% and 11.75% respectively) in determining the fractional cover. Although RF regression can alleviate the multicollinearity issue through bootstrap aggregation, biases in variable importance can still exist among correlated features.

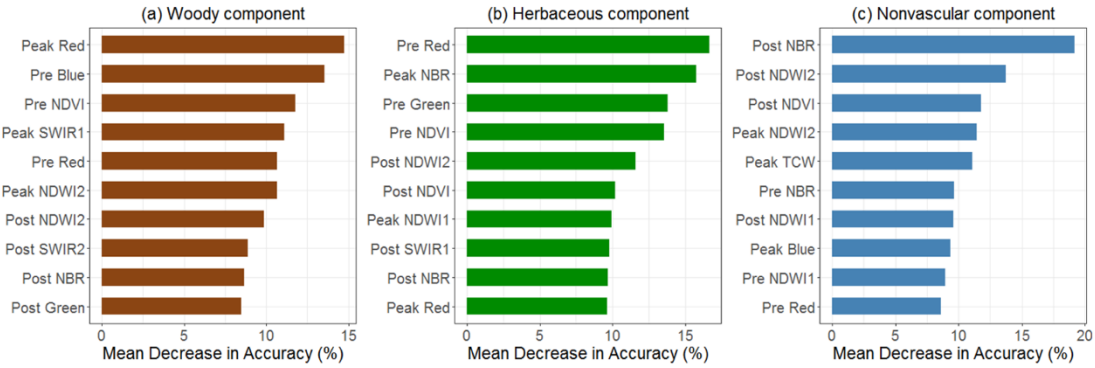

Figure 2.8. Top 10 important independent variables and their MDA values from RF regression models for (a) woody, (b) herbaceous and (c) nonvascular components. Spectral bands and indices during pre- and peak-growing seasons play the most important role in determining the fractional cover of woody and herbaceous

components (a-b), while spectral indices in the post-growing seasons contribute most to the cover estimation of nonvascular component (c).

2.5.3 Fractional cover of major fuel type components across Alaskan tundra

The fractional distributions of three fuel components were mapped across the shrub and graminoid tundra in Alaska circa 2015 (Figure 2.9). From the south to the north of Alaska, shrub cover shows a slightly decreasing trend as the temperature falls (Figure 2.9 a). The Southwest Alaska shows a larger portion of the area with high shrub fraction compared to the North Slope and the Seward Peninsula. For the North Slope and the Seward Peninsula, shrub cover is higher along the rivers (Figure 2.9). The herbaceous component of sedge and grass is dominant and widely distributed across the entire study area (Figure 2.9 b). In particular, the central North Slope has a high fractional cover of sedge and grass. As can be expected, the nonvascular component is highly concentrated in the northern part of the North Slope (Figure 2.9 c). From the north to the south across the entire tundra region, a general decreasing trend in the distribution of lichen and moss is clearly observed.

A closer examination of my mapping results in the Noatak River National Preserve shows an increase in the shrub fraction along the drainages (Figure 2.10 b), while other regions have higher coverages of the herbaceous fuels including sedge and grass (Figure 2.10 c). The amount of the nonvascular component is generally low in this example and is most frequently observed in high concentrations only close to the barren land along the river or the mountains (Figure 2.10 d).

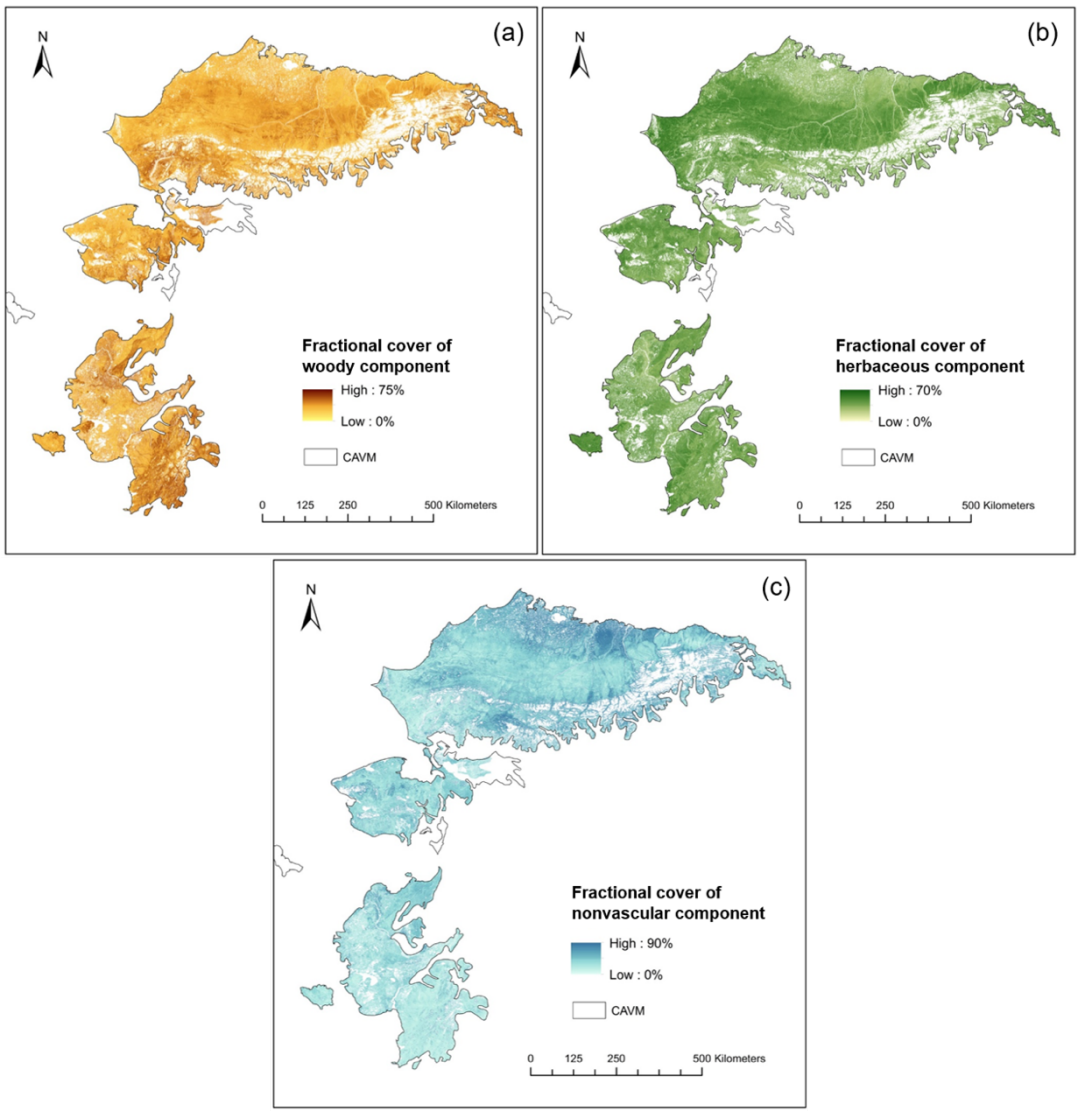

Figure 2.9. Fractional cover of three major fuel type components across Alaskan tundra: (a) woody, (b) herbaceous, and (c) nonvascular components.

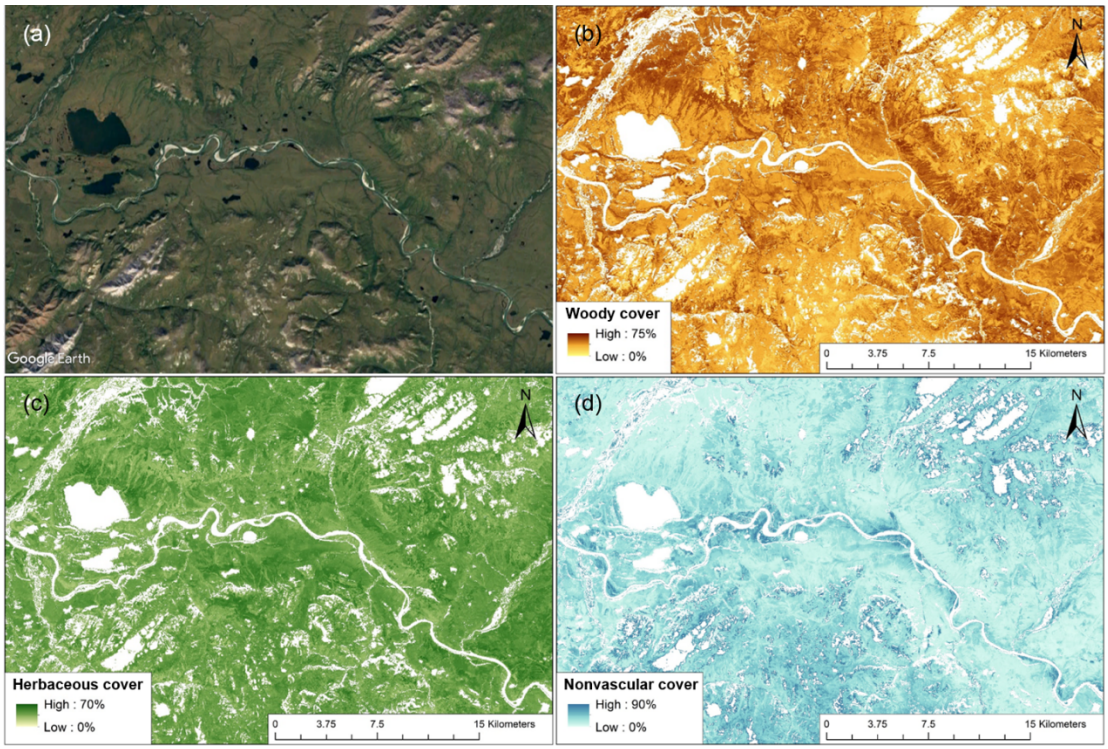

Figure 2.10. Examples of fractional cover distributions in a tundra region near Lake Narvakrak in the Noatak River National Preserve: (a) VHR image from Google Earth; (b) woody component; (b) herbaceous component; (d) nonvascular component.

I then summarized the spatial distributions of fractional fuel cover by the unified ecoregions in Alaskan tundra to examine their patterns. As expected, the comparison between the two Level 1 schemes (Boreal and Polar) shows a higher coverage of the woody component within the "Boreal" scheme (Figure 2.11 a). The "Boreal" scheme has a mean shrub coverage of 37.96% while that of the "Polar" scheme has a lower mean value of 31.57%. The "Boreal" scheme has an interquartile range (IQR) of 33.23% to 43.47%, while the IQR of "Polar" ranges from 24.23% to 37.82%. Since the "Polar" scheme includes three Level 2 groups and nine ecoregion units, I further examined the distribution of shrub coverage within this scheme. From

north to south, the shrub coverage increases gradually among all the Level 2 groups and the ecoregion units (Figure 2.11 b). The woody component cover of units in "Arctic Tundra" and "Bering Tundra" is comparable but lower than that in the "Bering Taiga" in general. Specifically, the "Beaufort Coastal Plain" located in the northernmost part of Alaska has the lowest shrub cover on average of 27.61%, while the southernmost "Ahklun Mountains" unit has the highest mean cover of 39.04%.

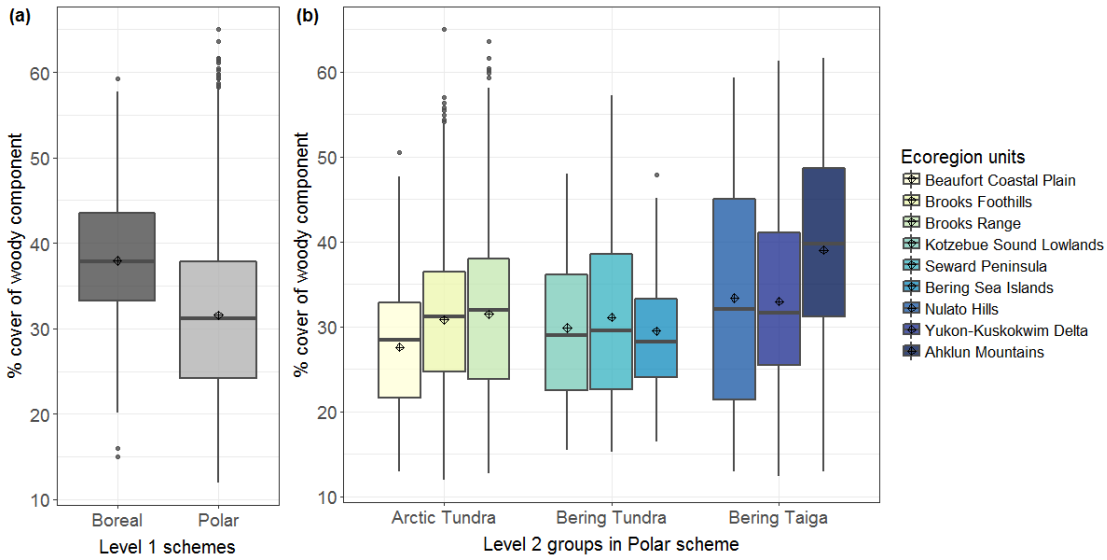

Figure 2.11. Boxplots of woody component cover against ecoregions in Alaskan tundra: (a) woody component cover by Level 1 scheme; (b) woody component cover by Level 2 ecoregion groups in the "Polar" scheme (ecoregion units are colored from light yellow to dark blue based on the latitude from north to south). Shrub coverage increases gradually among all the Level 2 groups and the ecoregion units, from north to south (b).

For the herbaceous component (sedge and grass), the comparison between the two Level 1 schemes (Boreal and Polar) suggests no obvious differences (Figure 2.12 a). The "Boreal" scheme shows a mean herbaceous coverage of 38.76% while that of

the “Polar” scheme has a higher value of 39.58%. The IQR of “Boreal” and “Polar” schemes are about 33.77% – 43.23% and 33.28% – 45.68% respectively. The mean fractional cover values of all Level 2 groups are also comparable in general, with values of about 38% to 40%. The sedge/grass distribution of units within the “Bering Taiga” group is consistent (Figure 2.12 b). However, the “Brooks Foothills” in “Arctic Tundra” and the “Bering Sea Islands” in “Bering Tundra” tend to have a higher herbaceous cover than other units within groups do.

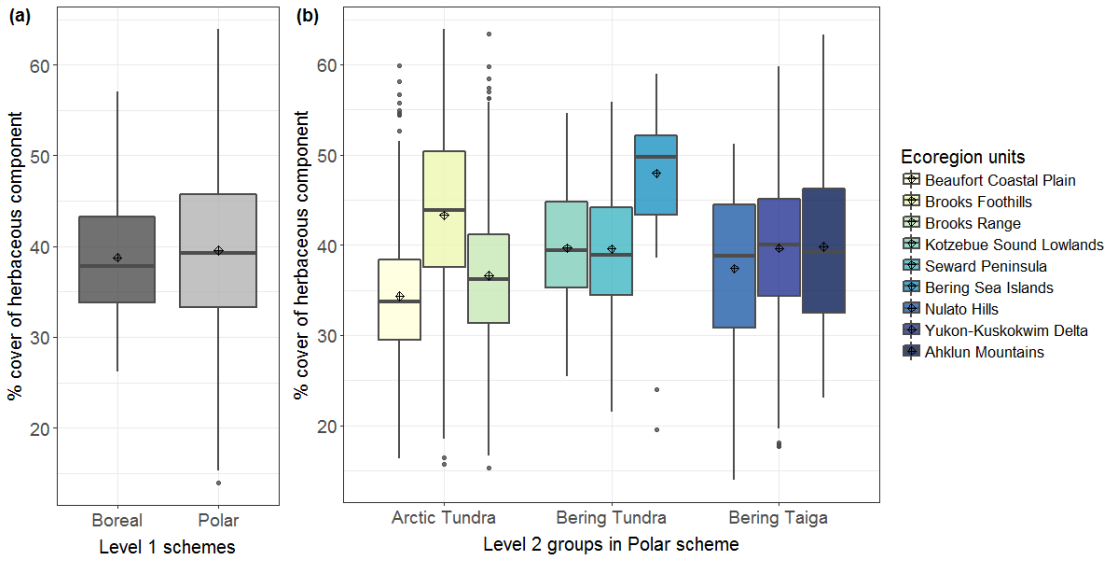

Figure 2.12. Boxplots of herbaceous component cover against ecoregions in Alaskan tundra: (a) herbaceous component cover by Level 1 scheme; (b) herbaceous component cover by Level 2 ecoregion groups in the “Polar” scheme (ecoregion units are colored from light yellow to dark blue based on the latitude from north to south). Herbaceous cover values among Level 2 groups are generally comparable, with relative higher values in the “Brooks Foothills” and “Bering Sea Islands” units (b).

For the nonvascular (lichen and moss) component, the comparison between the Level 1 schemes shows a higher cover of nonvascular vegetation within the "Polar" scheme (Figure 2.13 a). The "Boreal" scheme shows an average coverage of 33.95% while that of the "Polar" scheme has a higher value of 41.32%. The "Boreal" scheme has an IQR of 15.24% to 40.11%, while that of the "Polar" scheme ranges from 23.41% to 56.99%. From north to south, the lichen/moss cover shows a slightly decreasing trend among the Level 2 groups and the ecoregion units (Figure 2.13 b). The mean values of lichen/moss cover in the "Arctic Tundra", "Bering Tundra" and "Bering Taiga" are about 47.14%, 36.90%, and 30.04% respectively. Specifically, the "Beaufort Coastal Plain" and "Brooks Range" show the highest lichen/moss covers compared to other units. Within the "Bering Tundra" and "Bering Taiga" groups, the nonvascular fractional cover also decreases gradually as the latitudes become lower.

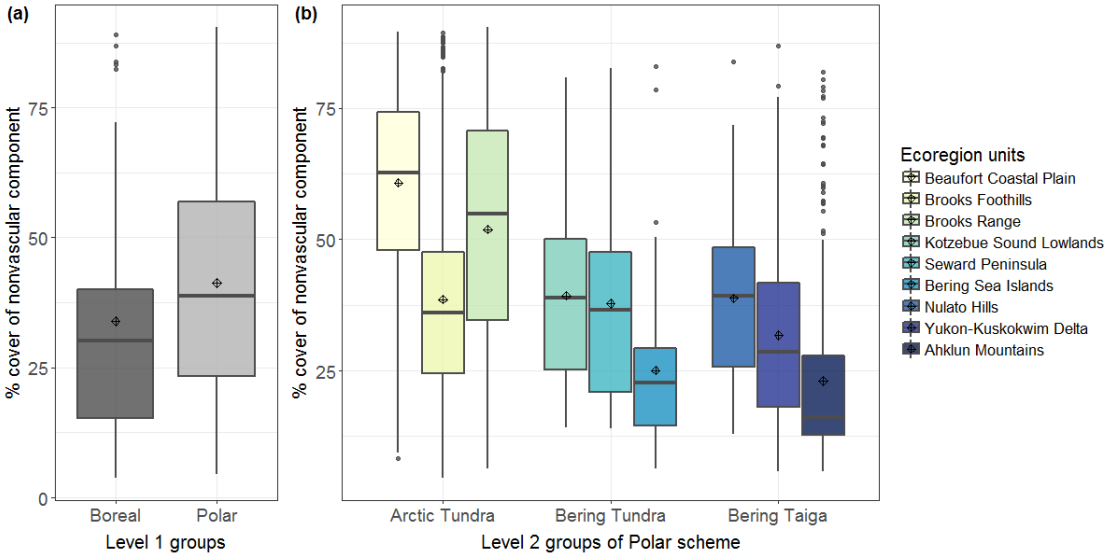

Figure 2.13. Boxplots of nonvascular component cover against ecoregions in Alaskan tundra: (a) nonvascular component cover by Level 1 scheme; (b) nonvascular component cover by Level 2 ecoregion groups in the "Polar" scheme (ecoregion

units are colored from light yellow to dark blue based on the latitude from north to south). Nonvascular coverage shows a decreasing trend among the Level 2 groups and the ecoregion units from north to south (b).

I further compared my outputs with existing fractional vegetation cover products developed for the tundra. A scatter plot comparison between our field observations and the shrub cover circa 2000 (Beck et al., 2011) suggests that the 2000 shrub cover product overestimates the actual fractional cover of shrub in the North Slope (Figure 2.14 a). Compared to the field observations of fractional cover collected in the North Slope, the PFT maps circa 2015 (Macander et al., 2017) show an overestimation of shrub cover and an underestimation of lichen/moss cover, while the fractional cover values of herbaceous species (sedge/ grass) are relatively comparable (Figure 2.14 b).

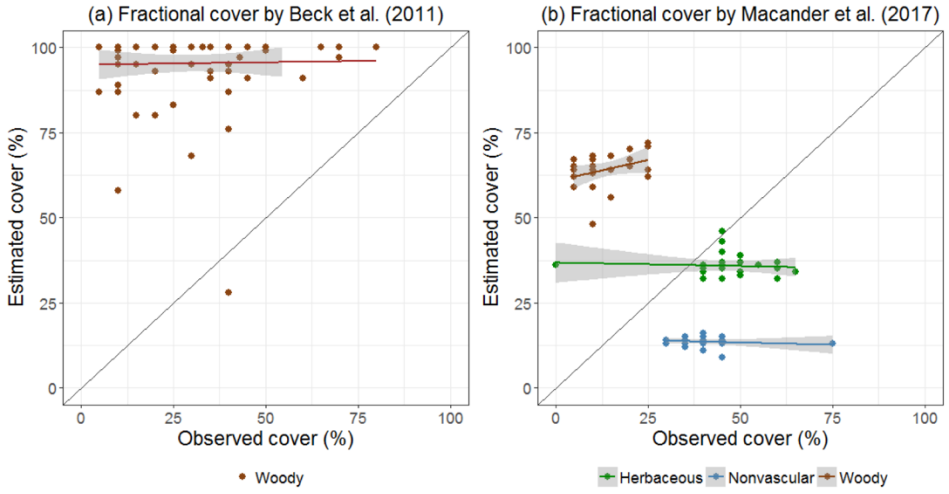

Figure 2.14. Scatter plots comparing our field observations and estimations from other products: (a) 2000 shrub cover (Beck et al., 2011); (b) PFT products (Macander et al., 2017). Compared to our field observations, the PFT product (Macander et al., 2017) tends to overestimate the shrub cover, but underestimate the

lichen/moss cover. The fractional cover of herbaceous species (sedge/grass) is relatively comparable.

The comparison between my maps and the existing products using approximately 20,000 randomly selected pixels in the North Slope (Figure 2.15) indicates similar patterns to those observed in comparing other products to field data directly. Fractional cover values of woody component (shrub) in both products are higher than the estimations in my results (Figure 2.15 a–b). Specifically, the majority of values were identified as 100% or 0% in Beck et al. (2011) in the North Slope. The fractional cover values of herbaceous species (sedge/grass) are comparable between the result and the product developed by Macander et al. (2017), ranging from about 20% to 75% (Figure 2.15 c). However, the coverage values of nonvascular component (lichen/moss) are much higher in my result when compared to those in the PFT product (Figure 2.15 d). The PFT product suggests that the nonvascular species including lichen and moss have a general coverage of 0% – 25% in the North Slope, while my result indicates that lichen/moss can cover from 0% to 80%, mostly concentrated between 10% and 50% (Figure 2.15 d).

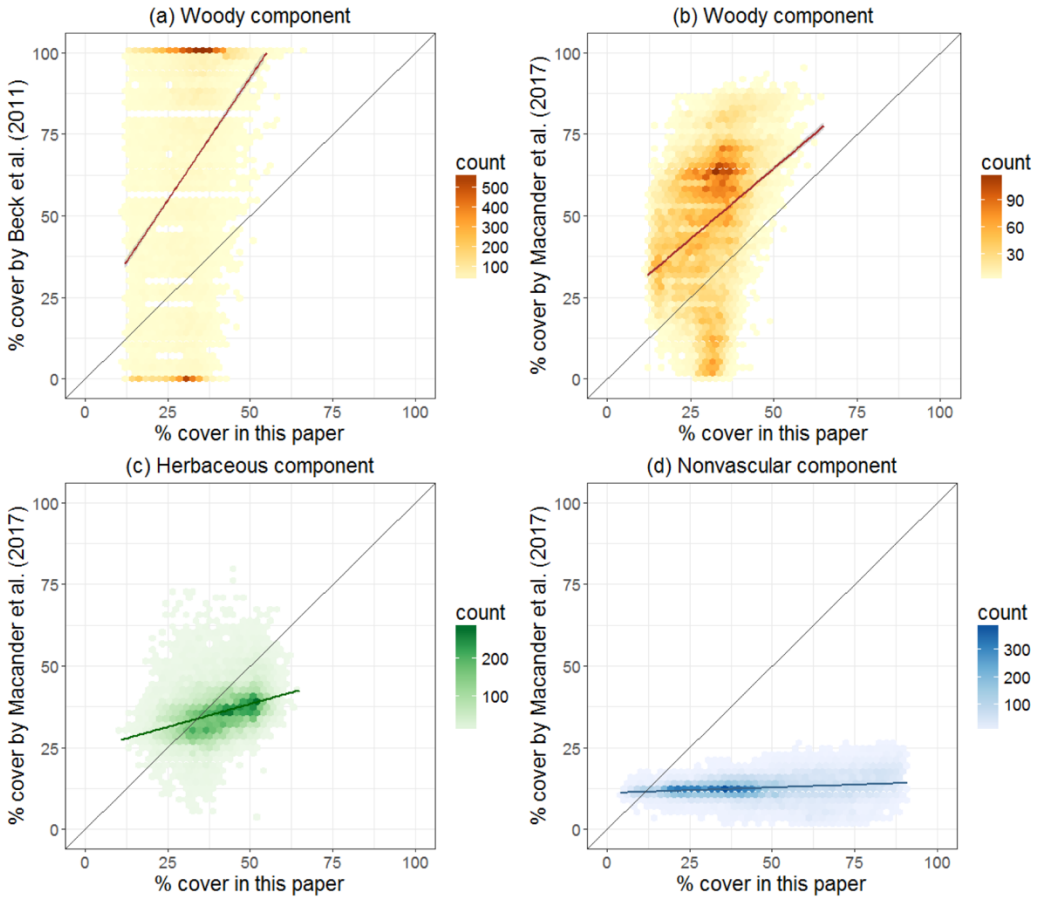

Figure 2.15. Density plots comparing my results and estimations from existing products: (a) woody component cover circa 2000 by Beck et al. (2011); (b) woody component cover circa 2015 by Macander et al. (2017); (c) herbaceous component cover circa 2015 by Macander et al. (2017); (d) nonvascular component cover circa 2015 by Macander et al. (2017). Fractional cover values of woody component in both products are higher than the estimations in my results. Nonvascular component tends to have much higher coverage than in the PFT product.

2.6 Discussions

Woody species in Alaskan tundra usually have higher surface reflectance in the NIR to SWIR spectrum but lower reflectance in the visible spectral regions

compared to herbaceous species such as sedge and grass (Buchhorn et al., 2013; Strauss et al., 2012). Previous studies have demonstrated the importance of multi-spectral bands and NDVI in estimating the fractional coverage of shrub (Kushida et al., 2009; Selkowitz, 2010; Vierling et al., 1997). Multi-seasonal information and middle-infrared portion of the spectrum also contribute strongly to the accuracy of shrub cover prediction (Selkowitz, 2010). Both woody and herbaceous models demonstrate the importance of pre-growing season spectral information in distinguishing the woody and herbaceous components. This can be explained by their different phenological stages (Shaver and Kummerow, 1991). The in-situ measurements of surface reflectance have shown that the lichen/moss component has different spectrum patterns when compared to woody or herbaceous species (Buchhorn et al., 2013; Huemmrich et al., 2013; Strauss et al., 2012). My modeling result suggests that spectral indices integrating these bands in the post-growing season are effective in separating lichen/moss from woody and herbaceous components. This is likely to be driven by the exposure of spectral signals by lichen/moss due to the senescence of vascular species in the tundra during September.

In addition to spectral bands provided by 30-m Landsat imagery, existing research has suggested that higher spatial resolution and red-edge (RE) spectral bands have the potential to improve fractional vegetation mapping efforts in the tundra (Davidson et al., 2016; Selkowitz, 2010; Stow et al., 1993). The launch of Sentinel-2 Multi- Spectral Instrument incorporating three RE bands provides the opportunity to improve the estimation accuracy of surface vegetation distribution at a broad spatial scale.

Developed only using spectral signatures, my mapping results also show effectiveness in representing the fuel component distribution across ecoregions with different bioclimatic conditions. The "Boreal" ecoregion scheme shows a higher cover of the woody component but a lower cover of the nonvascular component than the "Polar" ecoregion scheme in general. Mostly located in interior Alaska with a dry continental climate, ecoregions in the "Boreal" scheme tend to be dominated by shrubs and even boreal forests in these mountainous regions. Within the "Polar" scheme, the fractional cover of fuel components identified in this study also corresponds to the bioclimatic environment based on expert knowledge (Gallant et al., 1995; Nowacki et al., 2003). The low fractional cover values of the woody component in the Beaufort Coastal Plain and Brooks Foothills ecoregions are likely to be driven by their polar climate and poor soil drainage conditions. With higher summer temperature and more annual precipitation then other tundra areas, ecoregions as part of the "Bering Taiga" group (Nulato Hills, Yukon-Kuskokwim Delta and Ahklun Mountains) are covered with more woody fuels such as dwarf or tall scrub communities with wet graminoid species dominating in some regions, which is also evident in my maps.

Although the accuracy assessment shows strong predictive capability for fractional fuel mapping in Alaskan tundra, uncertainties still exist in the modeling and mapping results due to the limited spatial coverage of field observations, partially caused by the difficulty of obtaining field observations in the tundra. Regions with no available field data such as the Southwest Alaska and the northern North Slope could have higher uncertainties in my fractional cover maps. The mismatch of spatial

resolutions between the 10×10 m field plots and the 30×30 m Landsat 8 pixels could also introduce errors in the modeling and validation processes. During field campaigns, we have made our efforts on establishing sample plots in areas with visibly homogeneous distributions of vegetation species. However, it is possible that the actual vegetation coverages across one Landsat pixel may not be fully represented by the smaller than pixel field plots. Since the impacts of sample plot size on modeling and validation of fractional coverages is still unknown, future studies can elaborate on this and provide insights.

In addition, the results largely rely on the quality of the seasonal mosaics developed across the entire study area. First, maintaining the spatial consistency of these mosaics in Alaskan tundra is hindered by the pervasive cloud coverage and incomplete masking of cloud and cloud shadow pixels in the Landsat data. Although the CFMask algorithm delineates the major regions of cloud and shadow, it fails to identify all cloud- and shadow-impacted pixels. Second, matching multiple phenological stages of vegetation across different regions is challenging because of the differences in illumination properties and vegetation growing states under different climatic conditions (Muller et al., 1999; Selkowitz, 2010). Therefore, in order to maintain spatially and temporally consistent mosaics, I adopted the MVC method based on NDVI values with carefully defined growing periods using multi-year Landsat imagery.

It is also worth mentioning that the mismatches between my results and existing products can be caused by the differences in the cover definition and field sampling strategy. Beck et al. (2011) defined two shrub types – tall (> 1 m) and short

– and mapped the total and tall shrub coverages. Here I chose the total shrub cover for comparison, which can explain why my estimates are lower. Macander et al. (2017) developed the fractional distribution maps of detailed PFTs. I used their integrated coverages of total shrubs, total herbaceous and top nonvascular plants for comparison, which can lead to the differences in my result comparisons. In addition, instead of collecting field measurements, Beck et al. (2011) extracted sample data by aggregating classified pixels from VHR imagery for training their regression algorithm, which could lead to the overestimation the actual shrub coverage in their mapping output. Moreover, Macander et al. (2017) collected field data from sites widely distributed across the North Slope, while our field data had no coverage within the Beaufort Coastal Plain ecoregion and only limited sites in the Brooks Foothills. This could explain the differences in the estimated cover of the nonvascular component in those regions between my result and that of Macander et al. (2017).

2.7 Conclusions

In this study, I deliver the first fractional cover maps of major fuel type components across Alaskan tundra circa 2015. I map the spatial distributions of woody, herbaceous and nonvascular components in this highly heterogeneous landscape. Although our field observations are comparatively limited in quantity and spatial coverage, the findings are broadly consistent with expected distribution according to bioclimatological conditions.

I present a method of using multi-spectral and multi-seasonal observations in the differentiation of fuel components. The results show that this combination offers strong predictability from moderate resolution data and thus is critical for mapping

efforts at a broad spatial scale. This method can be adopted in monitoring other vegetation properties such as vegetation dominance and biomass.

In addition, the long-term archive of moderate resolution data in Alaska offers an opportunity to examine the fuel composition change in Alaskan tundra as a result of both climate change and fire occurrence. The outputs and spectral indicators identified in this paper can assist long-term monitoring of fuel type components in the tundra. These fuel maps and their periodic updates can create a strong basis for enhancing modeling capabilities for both assessing fire behavior and post-fire ecological impacts.

Chapter 3: Modeling cloud-to-ground lightning probability in Alaskan tundra through the integration of Weather Research and Forecast (WRF) model and machine learning method[2]

3.1 Summary

Wildland fires exert substantial impacts on tundra ecosystems ranging from biogeochemical impact on climate system to habitat suitability for various species. Lightning is the primary ignition source of wildfires and it is critical to understand mechanisms and factors driving cloud-to-ground (CG) lightning strikes in this cold treeless environment to support operational forecasting and future modeling of fire activity. The existing CG lightning studies primarily focus on Alaskan and Canadian boreal forests where land-atmospheric interactions are different and, thus, not likely to be representative of tundra conditions. In this study, I designed an empirical-dynamical method integrating Weather Research and Forecast (WRF) simulation and machine learning algorithm to model the probability of CG lightning strikes across Alaskan tundra between 2001 and 2017. This study recommended using Thompson 2-moment and Mellor-Yamada-Janjic (MYJ) schemes as microphysics and planetary boundary layer parameterizations for WRF simulations in the tundra. The modeling and forecasting test results have shown strong capability of predicting CG lightning probability in Alaskan tundra, with Area Under the Curve (AUC) values above 0.9. I found that parcel lifted index (PLI) and vertical profiles of atmospheric variables, including geopotential height, dew point temperature, relative humidity (RH) and

[2] This chapter is under review in Environmental Research Letters, the special issue of "Resiliency and Vulnerability of Arctic and Boreal Ecosystems to Environmental Change: Advances and Outcomes of ABoVE (the Arctic Boreal Vulnerability Experiment)".

velocity speed, important in predicting lightning occurrence, suggesting the key role of convection in lightning formation in the tundra. This method can be applied to data-scarce regions and support future studies of fire potential in the High Northern Latitudes (HNL).

3.2 Introduction

Wildfire is a primary disturbance across boreal forest and tundra ecosystems in the pan-Arctic region (Bond-Lamberty et al., 2007; French et al., 2015; Goetz et al., 2005). Although much more rare and generally less severe than boreal fires, tundra fires can alter ecosystem functioning through biogeophysical and biogeochemical processes and drive environmental changes in carbon cycling and energy budget (Bret-Harte et al., 2013; French et al., 2016; Jones et al., 2015; Mack et al., 2011; Pearson et al., 2013). Specifically, they release large stores of carbon generally locked in organic soil and permafrost: for example, the 2007 Anaktuvuk River fire on the North Slope of Alaska burned 1,039 km^2 and released ~2.1 Tg carbon into the atmosphere (Mack et al., 2011). Although most tundra fires are not nearly as severe as the Anaktuvuk River fire event, they are common, particularly in Alaska. Alaskan tundra burns more than any other tundra regions worldwide, accounting for 54% of the 10,260 km^2 burned area in the tundra worldwide between 2001 and 2015, as estimated by satellite observations (He et al., 2019). With very short growing periods in the HNL, post-fire recovery for critical components of tundra ecosystem, e.g. lichen, can last for several decades, which is comparable to recovery rate of the boreal forests (Jandt et al., 2008; Racine et al., 1987). As a result,

tundra fires impact long-term winter forage availability for caribou and subsequently influence the subsistence resources of local communities (Gustine et al., 2014).

Fires in the remote and generally inaccessible HNL are primarily ignited by CG lightning (French et al., 2015; Veraverbeke et al., 2017). Future climate projections indicate potential increase of CG lightning under warming conditions (Price and Rind, 1994a; Romps et al., 2014), which will subsequently lead to more fire occurrence and larger burned area in both boreal forest and tundra ecosystems (French et al., 2015; Krause et al., 2014; Veraverbeke et al., 2017; Wotton et al., 2010). Numerous studies have examined characteristics (Dissing and Verbyla 2003; Kochtubajda et al. 2019; Reap 1991; Farukh et al. 2011), explored driving factors and developed predictive models (Blouin et al., 2016; Burrows, 2008; Burrows et al., 2005) for CG lightning activity in Alaskan and Canadian boreal forests. However, considerably less is known about factors driving CG lightning for the treeless tundra. The substantial differences in surface layer conditions between tree-dominated and treeless landscapes (Beringer et al., 2005; Dissing and Verbyla, 2003; Rivas Soriano et al., 2019; Van Heerwaarden and Teuling, 2014) imply that understanding of lightning processes in the boreal forests is not necessarily readily transferable to the tundra. Therefore, tundra-focused studies are critical for enhancing the modeling capability of lightning and fire potential and assisting wildfire management efforts in future.

Typically, lightning formation is associated with atmospheric convection in cumulonimbus clouds (Anderson, 1992). Lightning flashes are generated through the buildup, separation, and transfer procedures of electric charges between cloud

particles (Saunders, 2008; Yair, 2008). The occurrence and intensity of lightning activity are generally related to factors such as convective cloud development, cloud structure, and hydrometeor attributes (Baker et al., 1999; Buiat et al., 2017; Price and Rind, 1994b). However, explicit simulation and prediction of the electrification processes can be computationally expensive (Zepka et al., 2014). Further efforts are also required to comprehensively understand the detailed microphysical procedures contributing to charge accumulation (Rakov and Uman, 2003; Saunders, 2008). CG lightning modeling thus primarily rely on developing its relationships with observed or model-resolved parameters related to convective activities and cloud microphysical properties.

Classificatory schemes or simple regression methods developed with convective indices or weather conditions from observations or weather model outputs were among the early attempts for lightning modeling (Anderson, 1991; Andersson et al., 1989; Fuquay, 1980; Reap and Foster, 1979; Reap and MacGorman, 1989; Sly, 1965). With the development of General Circulation Models (GCMs) and Numerical Weather Prediction (NWP) models, lightning schemes based on microphysics principles have been parameterized upon these models from regional to global scales (Barthe et al., 2010; Lynn et al., 2012; Price and Rind, 1994b; Wong et al., 2013; Yair et al., 2010). Simple strategies were also adopted to improve the modeling capability with WRF simulations (Giannaros et al., 2015; Zepka et al., 2014).

In addition to physical parameterizations, empirical-based methods such as logistic regression (Bates et al., 2018; Shafer and Fuelberg, 2006) and random forest (RF; Blouin et al., 2016; Schön et al., 2018) were developed in recent studies to

model CG lightning occurrence based on dynamic meteorological conditions and thunderstorm characteristics. Opportunities for integrating dynamic NWP and statistical models have been explored to improve the modeling capability of lightning potential. Burrows et al. (2005) and Burrows (2008) trained tree-structured regression models to forecast lightning probability using predictors generated from the Global Environmental Multiscale (GEM) model. Sousa et al. (2013) and Gijben et al. (2017) also combined NWP models such as WRF with logistic regression to develop statistical-dynamical methods for lightning prediction in different regions.

Due to the remoteness of the tundra, meteorological observations, including weather stations and atmospheric soundings, are sparsely distributed and thus unsuitable for describing the spatial variation of tundra conditions. Although reanalysis products provide atmospheric variables with spatial-temporal consistency, their performances are limited by the coarse spatial resolution, availability of observations, and uncertainty of diagnostic variables (Dee et al., 2016). Therefore, purely empirical models trained with observations or reanalysis data are unsuitable for lightning modeling in data-scarce regions like tundra.

Although NWP has not been specifically applied in tundra studies, existing research has demonstrated its suitability and effectiveness for modeling lightning potential (Burrows et al., 2005; Reap, 1991) and fire danger (Di Giuseppe et al., 2016; Mölders, 2010, 2008) in the boreal forests. Considering that tundra has different land-atmosphere interactions and fewer meteorological stations available for measuring near-surface and atmospheric conditions when compared to boreal forests, this study focuses on improving the modeling capacity for CG lightning probability

and understanding what atmospheric factors drive CG lightning in Alaskan tundra through the integration of WRF and RF, a commonly used machine learning algorithm. I first assessed WRF parameterization schemes to identify an optimal combination for reproducing the observed meteorological conditions in the tundra. I then examined data from 2001 to 2019 to understand what atmospheric factors drive CG lightning probability across Alaskan tundra.

3.3 Study Area

In Alaska, more than 99% of CG lightning occurs from May to August, particularly during June and July (Mcguiney et al., 2005; Reap, 1991). A typical diurnal pattern exists starting from noon and lasting until midnight with a peak between 4pm and 8pm. Elevation and forest cover can affect the spatial variation of lightning in Alaska by altering the convective activity (Dissing and Verbyla, 2003). In particular, large-scale atmospheric instability and local convergence are the major contributors to thunderstorm formation and lightning occurrence in Alaska (Reap, 1991). Here I defined Alaskan tundra using the Circumpolar Arctic Vegetation Map (CAVM; Figure 3.1 a; Walker et al. 2005). Fire regimes vary by year and across different tundra regions (Figure 1.2).

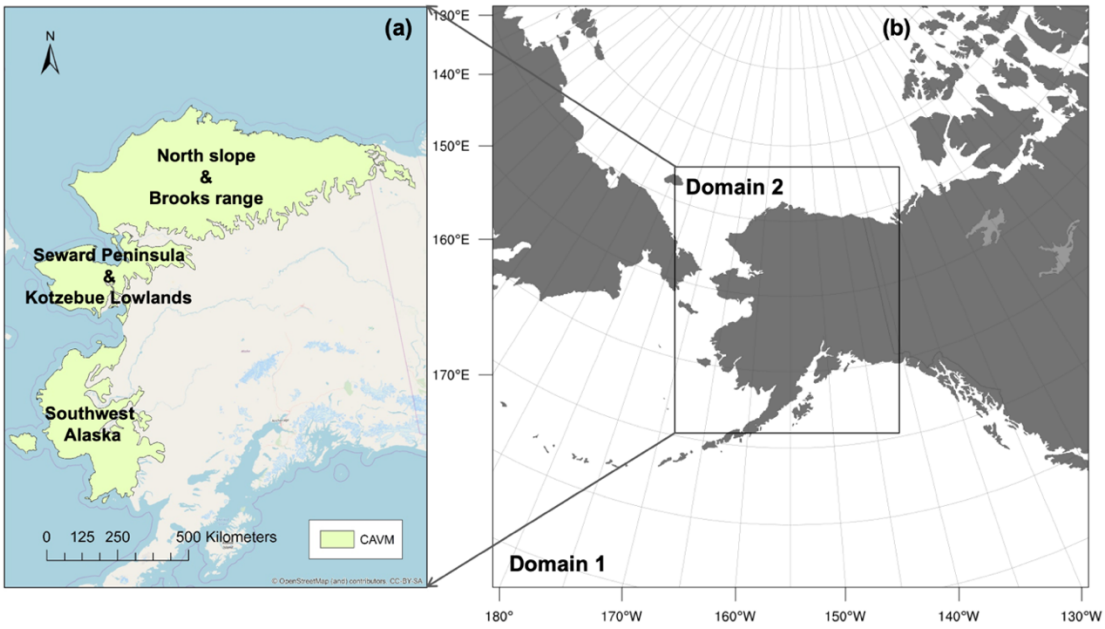

Figure 3.1. Study area: (a) Alaskan tundra defined by CAVM; (b) WRF simulation domains.

3.4 Materials and Methods

I designed an empirical-dynamic method combining WRF-simulated atmospheric variables and ground-based lightning observations to model CG lightning probability in Alaskan tundra (Figure 3.2). I first conducted a sensitivity analysis to identify an optimal WRF parameterization scheme that best describes tundra meteorological conditions. I then ran WRF for selected case studies and trained RF models for predicting CG lightning probability.

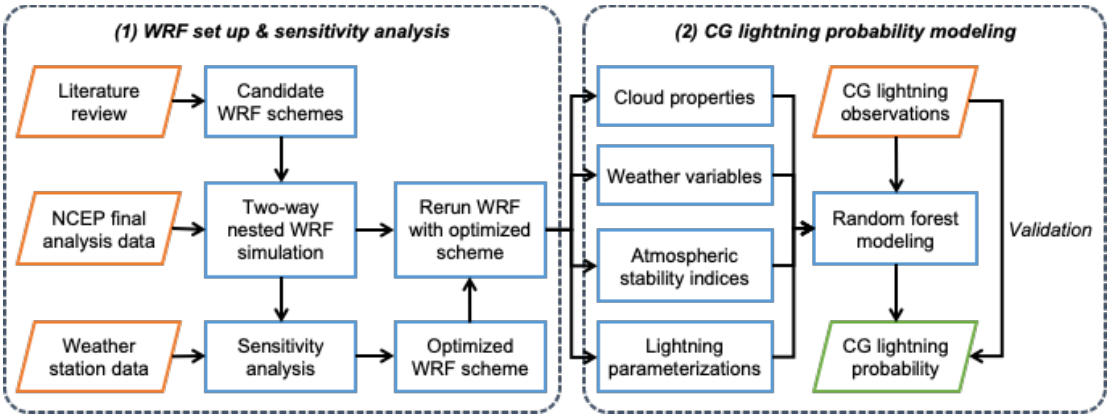

Figure 3.2. Overall workflow of Chapter 3

3.4.1 Cloud-to-ground lightning observations

I obtained lightning data from the Alaska Lightning Detection Network (ALDN) maintained by the Bureau of Land Management (Fronterhouse, 2012). This system has a detection efficiency better than 5km and positional accuracy higher than 70%, as estimated by early studies (Dissing and Verbyla, 2003; Reap, 1991). It has been updated multiple times to improve detection performance (Fronterhouse, 2012). Specifically, devices employed before 2012, developed by Vaisala, Inc., recorded lightning flash with multiplicity (i.e., lightning strikes per flash). The new system, provided by TOA Systems, Inc., records lightning strikes instead (Fronterhouse, 2012). To ensure the consistency of lightning records between systems, I utilized lightning strikes rather than flashes in this study.

3.4.2 WRF model setup and sensitivity analysis

I adopted the Advanced Research WRF version 4.0 (Skamarock et al., 2019) to simulate weather conditions in the tundra. I used the National Centers for Environmental Prediction Final Operational Model Global Tropospheric Analysis

data (NCEP FNL) at 1°×1° resolution and 6-hour interval for model initialization (NCEP, 2000). Developed with the Global Data Assimilation System (GDAS), this product provides a variety of parameters to describe initial and boundary meteorological conditions on the surface and at 26 mandatory pressure levels. I defined two domains with 25-km (Domain 1) and 5-km (Domain 2) grid spacing for two-way nested WRF simulation (Figure 3.1b). The vertical dimension was configured with 33 unevenly spaced full sigma levels with the model top at 50hPa. WRF provides multiple parameterization schemes for its major physics components (Table 3.1; Skamarock et al., 2019). The various assumptions and mechanisms adopted in these schemes can affect simulation results for a specific region.

Since existing applications of WRF in the HNL primarily focus on the boreal forests or the pan-Arctic region, their schemes may not be suitable for tundra. Therefore, I employed a sensitivity analysis to determine WRF settings that achieve the closest description of tundra conditions compared to meteorological observations. I first reviewed existing literature to explore a list of WRF schemes as candidates (Table 3.1). The majority of the literature utilized the same schemes for land surface model, radiation, and cumulus components, namely Noah, Rapid Radiative Transfer Model (RRTM), and Grell-Devenyi, respectively (Table 3.1). These schemes were then applied with updated versions in WRF 4.0. Microphysics schemes explicitly resolve physical processes related to water vapor, cloud, and precipitation, with mixed-phase ones recommended for simulating icing or convective conditions at horizontal resolution finer than 10 km (Skamarock et al., 2019). I thus selected Morrison 2-moment, Thompson 2-moment, and WRF 2-moment 6-class (WRF6) for

microphysics in the sensitivity analysis. Mellor-Yamada-Janjic (MYJ)/ Monin-Obukhov MM5, and Yonsei University (YSU) / Monin-Obukhov Eta combinations were also considered for Planetary Boundary Layer (PBL) / Surface Layer (SL) representation. All six candidates of schemes are summarized in Table 3.2.

Table 3.1. WRF schemes used for the pan-Arctic region in existing literature

Components	Schemes	References
Microphysics	Morrison 2-moment	(Bieniek et al., 2016)
	Thompson 2-moment	(Kim et al., 2014; Mölders, 2010, 2008)
	WRF single-moment 6-class	(Cai et al., 2016; Hines and Bromwich, 2008)
	Goddard Cumulus Ensemble Model	(Cassano et al., 2011; Glisan et al., 2013)
Longwave radiation	Rapid Radiative Transfer Model (RRTM) Longwave	(Bieniek et al., 2016; Cai et al., 2016; Glisan et al., 2013; Hines et al., 2011; Kim et al., 2014; Mölders, 2010, 2008)
	Community Atmospheric Model (CAM) Longwave	(Cassano et al., 2011; Glisan et al., 2013)
Shortwave radiation	RRTM Shortwave	(Bieniek et al., 2016; Glisan et al., 2013; Kim et al., 2014)
	Dubhia Shortwave	(Cai et al., 2016; Mölders, 2010, 2008)
	Goddard Shortwave	(Hines et al., 2011)
	CAM Shortwave	(Cassano et al., 2011; Glisan et al., 2013)
Cumulus	Grell-Devenyi ensemble	(Bieniek et al., 2016; Cassano et al., 2011; Glisan et al., 2013)
	Kain-Fritsch	(Cai et al., 2016)
Planetary Boundary Layer (PBL) / Surface layer	Mellor-Yamada-Janjic (MYJ) / Monin-Obukhov Eta (Eta)	(Bieniek et al., 2016; Cassano et al., 2011; Glisan et al., 2013; Hines et al., 2011)
	Yonsei University (YSU) / Monin-Obukhov MM5 (MM5)	(Cai et al., 2016; Kim et al., 2014; Mölders, 2010, 2008)
Land surface model	Noah	(Bieniek et al., 2016; Cai et al., 2016; Cassano et al., 2011; Glisan et al., 2013; Hines et al., 2011)
	Rapid Update Cycle	(Mölders, 2010, 2008)

Table 3.2. Six candidates of parameterization combinations for sensitivity analysis

Combination notation	Microphysics	PBL + SL
Morrison_MYJ	Morrison 2-moment	MYJ + Eta
Thompson_MYJ	Thompson 2-moment	MYJ + Eta
WRF6_MYJ	WRF6	MYJ + Eta
Morrison_YSU	Morrison 2-moment	YSU + MM5
Thompson_YSU	Thompson 2-moment	YSU + MM5
WRF6_YSU	WRF6	YSU + MM5

Near-surface weather observations collected by Remote Automated Weather Stations (RAWS; https://raws.nifc.gov) provide the densest weather network in Alaska to date. Four weather variables recorded by RAWS, including air temperature, dew point temperature, relative humidity, and solar radiation were utilized as "ground truth" for sensitivity analysis. To consider different fire regimes (Figure 1.2), I selected four cases for 24-hr simulations in years of varying fire season intensity (2006 – low, 2007 – moderate, 2010 and 2015 – intense, Figure 1.2; Table 3.3). Daily observations were obtained for all available RAWS stations in the tundra. To identify the optimal combination group, I calculated three statistical metrics, including root-mean-square error (RMSE), mean absolute error (MAE) and Pearson's r correlation between simulations and observations. For each weather variable, I ranked the three metrics from all candidates for each year from 1 (lowest) to 6 (highest). For each metric, the yearly rankings were then summed up to create a single rank sum (ranging from 4 to 24), with the larger rank sum representing better overall performance.

Table 3.3. Summary of case studies for sensitivity analysis

Year	Number of RAWS stations	Simulation period (UTC time)
2006	8	08/16 00:00 - 08/17 00:00
2007	9	05/01 00:00 - 05/02 00:00
2010	12	07/01 00:00 - 07/02 00:00
2015	29	06/18 00:00 - 06/19 00:00

3.4.3 RF modeling of cloud-to-ground lightning probability

RF classification algorithm (Breiman, 2002, 2001) was used for modeling CG lightning probability with the atmospheric variables simulated from WRF. As an ensemble method, RF generates a large number of individual decision trees through permutation and integrates its results for a more stable modeling performance. I designed two separate modeling experiments referred to as the "24-hr model" and "48-hr model" in this study, to compare the consistency of modeling performance and variable importance with different WRF simulation periods (0-24hrs and 0-48hrs respectively; Figure 3.3). For each experiment, atmospheric variables of interest were extracted from WRF outputs simulated at 24hrs or 48hrs after initialization, respectively. Four groups of predictors were summarized from existing literature (Blouin et al., 2016; Burrows, 2008; Burrows et al., 2005; Reap, 1991; Sousa et al., 2013) including atmospheric stability indices, cloud properties, weather conditions at multiple pressure levels (500, 700, 850, and 1000 hPa), and two lightning parameterizations from WRF (Table 3.4). Both the Price and Rind (PR92; Wong et al., 2013) and Lightning Potential Index (LPI; Yair et al., 2010) lightning schemes were included for modeling.

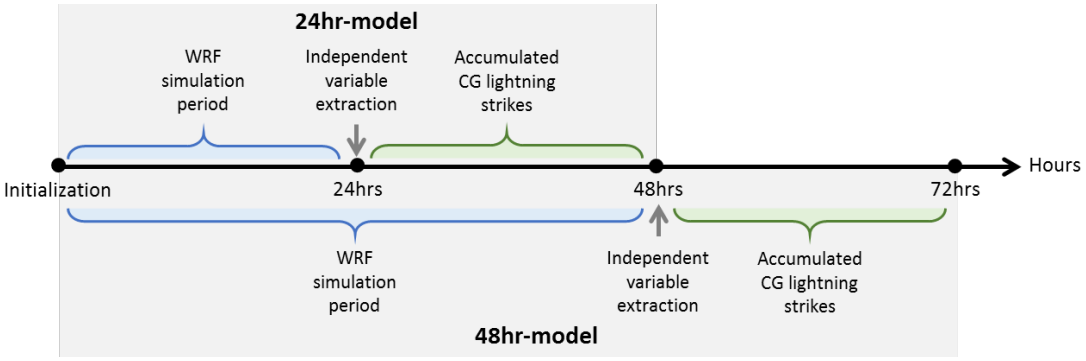

Figure 3.3. Illustration of the "24-hr model" and "48-hr model" components

Table 3.4. List of independent variables retrieved from WRF output for RF modeling

Categories	Variables	Description
Atmospheric stability indices	CAPE	Convective Available Potential Energy
	CIN	Convective Inhibition
	LCL	Lifted Condensation Level
	LFC	Level of Free Convection
	TT	Total Totals
	KI	K Index
	PLI	Parcel Lifted Index (to 500 hPa)
	BI	Boyden Index
	SHOW	Showalter Index
Cloud properties	CF_{total}	Total cloud cover fraction
	CF_{high}	High-level cloud cover fraction
	CF_{mid}	Mid-level cloud cover fraction
	CF_{low}	Low-level cloud cover fraction
	CTT	Cloud top temperature
	CTH	Cloud top height
	CTP	Cloud top pressure
	IWP	Ice water path
	LWP	Liquid water path
	ER_{Ice}	Effective radius of cloud ice
	ER_{Water}	Effective radius of cloud water
	Q_{Cloud}	Cloud water mixing ratio
	Q_{Ice}	Ice mixing ratio
	Q_{Rain}	Rain mixing ratio
	BT	Brightness temperature
Weather variables	T	Air temperature at surface & multiple pressure levels
	T_d	Dewpoint temperature at surface and multiple pressure levels
	$T.T_d$	Temperature-dewpoint spread at multiple pressure levels
	RH	Relative humidity at surface and multiple pressure levels
	GPZ	Geopotential height at multiple pressure levels
	DZ	Thickness between any two pressure layers
	W	Vertical velocity at multiple pressure levels
	Helicity	Helicity
	UH	Updraft helicity
	Rain	Total precipitation
	PW	Precipitable water
	SLP	Sea level pressure

Lightning parameterizations	PR92	Flash distribution of CG lightning with PR92
	LPI	Lightning probability index

All predictors were retrieved with WRF outputs of Domain 2 using the NCAR Command Language (NCL) and the NCEP Unified Post Processor System (UPP). Then I used these atmospheric factors to model the presence and absence of CG lightning strikes during the following day (24hrs) after the timing of variable extraction, which were considered as dependent variables in my RF models. CG lightning points extracted from the ALDN dataset during the corresponding period were labeled as the presence of lightning, while sample points with no lightning occurred (labeled as absence) were randomly generated within Alaskan tundra region during the same period.

To ensure the representative of our models in describing tundra lightning conditions, three lightning severity levels were identified based on the total number of daily CG lightning strikes for model training, following a similar method by Farukh et al. (2011): > 2000 strikes per day as severe, 500 – 2000 strikes per day as moderate, and 0 – 500 strikes per day as low. For each level, I selected five cases for WRF simulation using a stratified random sampling strategy (Table 5). I then randomly selected 70% of presence and absence points for model training and reserved the rest 30% for validation. Training and testing points from all levels were combined for model development and accuracy assessment, respectively. I set the number of trees to 500 and the number of variables at each split as 8 in the RF algorithm.

Table 3.5. Cases studies of WRF simulations for CG lightning modeling

Initialization of simulation (UTC)	Total CG lightning strokes during 0~24hrs	Total CG lightning strokes during 24~48hrs
2003/06/23 00:00	1305	1560
2005/06/11 00:00	732	1027
2005/06/29 00:00	3449	2151
2005/08/16 00:00	5	15
2007/07/04 00:00	4280	479
2007/07/11 00:00	2321	2247
2008/06/25 00:00	2030	295
2009/06/09 00:00	335	64
2010/07/01 00:00	1015	1991
2013/06/20 00:00	3073	3641
2013/08/16 00:00	60	10
2015/07/14 00:00	847	4320
2015/06/21 00:00	974	905
2015/07/23 00:00	175	80
2016/07/11 00:00	93	109

I reported the out-of-bag (OOB) error rate provided by the RF classification algorithm to evaluate the overall accuracy of the trained models. I further calculated the commonly used statistical criteria using the prediction results of the validation dataset for accuracy assessment (Tables 3.6 and 3.7). Receiver Operating Characteristics (ROC) curves and area under curve (AUC) were also generated based on the validation dataset. Additionally, I examined the contribution of predictors in determining CG lightning potential in the tundra with variable importance quantified by Mean Decrease in Accuracy (MDA; Breiman, 2002, 2001).

Table 3.6. Contingency matrix of variables used to calculate statistical scores

		CG lightning event observed	
		Presence	Absence
CG lightning event predicted	Presence	a (hit)	b (false alarm)
	Absence	c (miss)	d (correct non-event)

Table 3.7. Statistical criteria used for assessing modeling performance

Statistical scores	Abbreviation	Formula
Probability of Detection	POD	$a/(a+c)$
Critical Success Index	CSI	$a/(a+b+c)$
False Alarm Ratio	FAR	$b/(a+c)$
False Alarm Rate	F	$b/(b+d)$

3.4.4 Forecasting capability assessment

In addition to empirical modeling, I further tested the capability of our empirical-dynamic method in forward forecasting of CG lightning probability at a future timing, by applying the RF model developed for a previous period. Here I utilized the "24-hr model" to forecast the CG lightning probability with atmospheric conditions simulated 48hrs after initialization. Statistical criteria listed in Table 7 and ROC curves were also generated for quantifying the forecasting capability of CG lightning potential.

3.5 Results

3.5.1 Sensitivity analysis of WRF simulation

The results of the sensitivity analysis indicate a substantial variability in performance of different WRF parameterizations by individual meteorological variable and across different case study periods (Figure 3.4; Tables S1 – S4). The combined statistical ranking for each variable can range between 4 (the lowest rank across all four sensitivity cases, see Table 3.3) and 24 (the highest rank across all four cases). Based on these results, Thompson_MYJ and Morrison_MYJ emerged as strongest performing settings for tundra meteorology simulations (Figure 3.4). Although majority of the correlation values for all metrological variables are around

0.7 ~ 0.8, the overall simulation results for air temperature and dew point temperature across all six candidates outperform those for relative humidity and solar radiation according to the RMSE and MAE values (Tables S1 – S4).

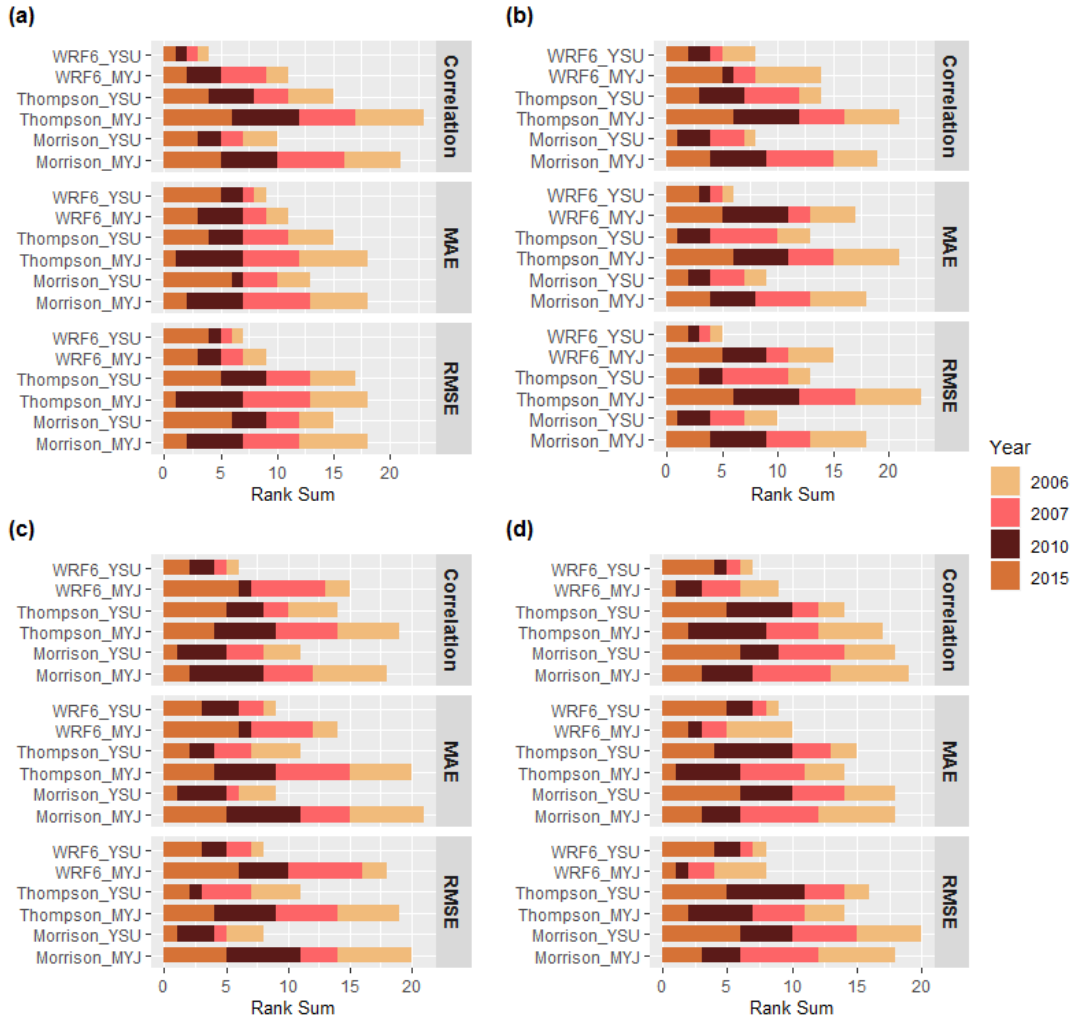

Figure 3.4. Bar plots summarizing the ranks of six candidate schemes based on Pearson's r correlation, MAE and RMSE for: (a) air temperature, (b) dew point temperature, (c) relative humidity, and (d) solar radiation. The largest rank sum value represents the best overall performance.

Specifically, Thompson_MYJ shows the best results when compared to other schemes for air temperature and dew point temperature (Figure 3.4 a-b; Tables S1 –

S2). For RH, using MYJ for the PBL scheme show superior results than adopting YSU, particularly when combined with the Morrison and Thompson schemes (Figure 3.4 c). While for solar radiation, the Morrison scheme outperforms other microphysics schemes, followed by Thompson. Since lightning activity is largely related to convection activity, I further examined the spatial distribution of Convective Available Potential Energy (CAPE), as a representative of convection, generated by both Thompson_MYJ and Morrison_MYJ schemes for comparison. The Thompson_MYJ scheme shows a more detailed distribution of CAPE values for describing convective activities (Figure 3.5). I therefore chose to adopt the Thompson_MYJ combination and summarized the optimized WRF schemes for CG lighting modeling experiments in Table 3.8.

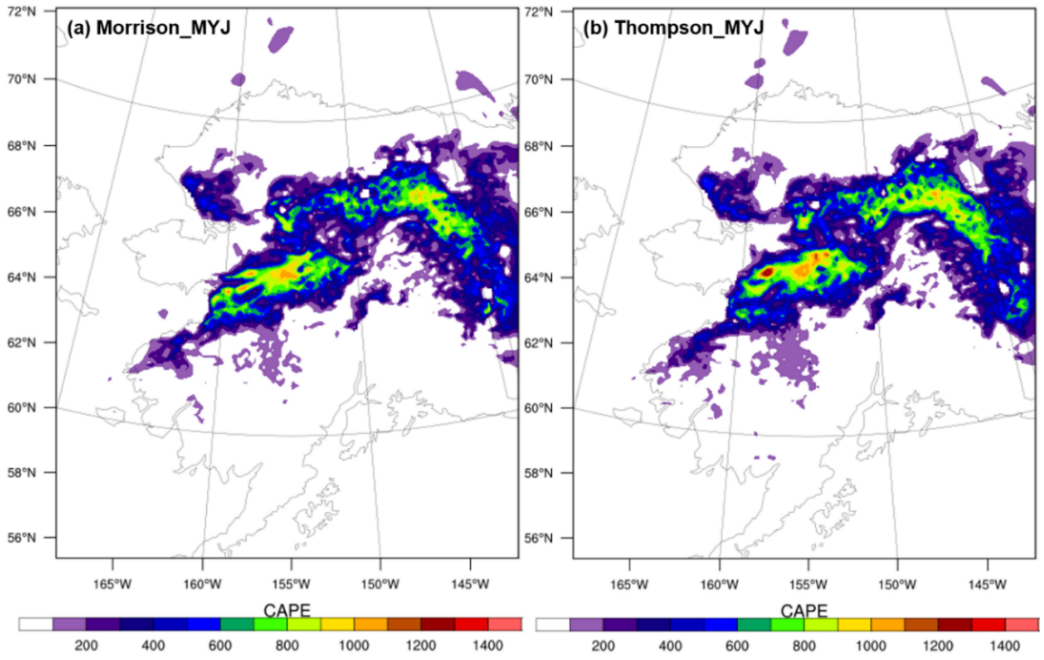

Figure 3.5. Comparison of CAPE simulation in Domain 2 between (a) Morrison_MYJ and (b) Thompson_MYJ for the 2010 case as an example.

Table 3.8. Optimized combination of physical parameterizations

Physical component	Parameterization scheme	Setting option in WRF
Microphysics	Thompson 2-moment	mp_physics = 8
Cumulus	Grell-Freitas ensemble	cu_physics = 3
PBL	MYJ	bl_pbl_physics = 2
SL	Eta	sf_sfclay_physics = 2
Land surface model	Noah	sf_surface_physics = 2
Longwave radiation	RRTMG	ra_lw_physics = 4
Shortwave radiation	RRTMG	ra_sw_physics = 4

3.5.2 Accuracy assessment of RF models

The overall OOB estimate of error rate and the class errors have shown high accuracy in predicting CG lightning strikes in Alaskan tundra. For the "24-hr model", the OOB is 4.64% and the overall accuracy reaches 95.36%. Specifically, the absence of CG lightning has a class error of 7.26%, while that of the presence reaches 2.54% (Table 3.9 a). For the "48-hr model", the OOB is 6.81% with an overall accuracy of about 93.19%. The class errors of the absence and presence of lightning events are 11.15% and 3.43%, respectively (Table 3.9 b).

Table 3.9. Confusion matrix for (a) "24-hr model" and (b) "48-hr model"

(a) 24-hr model				
Confusion matrix		CG lightning predictions		Class error
		Absence	Presence	
CG lightning observations	Absence	7013	549	0.0726
	Presence	241	9239	0.0254
(b) 48-hr model				
Confusion matrix		CG lightning predictions		Class error
		Absence	Present	
CG lightning observations	Absence	4872	612	0.1115
	Presence	243	6837	0.0343

The validation results against the reserved dataset show that both models have overall high accuracy in predicting CG lightning strikes. I assessed the overall

statistical metrics (Table 3.10) and the ROC curves (Figure 3.6). I also reported them separately by severity level and found a notably stronger performance during severe and moderate lightning days when compared to the low severity level. For the severe and moderate levels, the "24-hr model" produces a Probability of Detection (POD) value of 0.96 and a Critical Success Index (CSI) of 0.91, while the two error metrics False Alarm Ratio (FAR) and False Alarm Rate (F) are below 0.1 (see Table 3.7). While the POD and CSI values are below 0.8 for the validation data from the low-level lightning cases. The AUC values estimated from the ROC curves are above 0.95 across lightning days in all severity levels.

Table 3.10. Statistical criteria calculated using the validation data for: (a) 24-hr model; (b) 48-hr model.

Models	**Metrics**	**All**	**Severe level**	**Moderate level**	**Low level**
24-hr model	POD	0.9628	0.9821	0.9456	0.7885
	CSI	0.9065	0.9365	0.8569	0.7454
	FAR	0.0606	0.0472	0.0987	0.0682
	F	0.0858	0.1167	0.0794	0.0277
	AUC	0.9869	0.9898	0.9818	0.9743
48-hr model	POD	0.9668	0.9701	0.9643	0.2273
	CSI	0.8815	0.8808	0.8833	0.1829
	FAR	0.0909	0.0946	0.0868	0.5161
	F	0.1247	0.1291	0.1196	0.0366
	AUC	0.9810	0.9810	0.9809	0.8751

The "48-hr model" shows an overall POD value of 0.97 and a CSI of 0.88, while the FAR is below 0.1 and the F metric is about 0.12. Similar to the "24-hr model", it also has the best performance for the validation records collected during the severe lightning days, followed by those collected during moderate lightning days. However, the POD and CSI values are below 0.5 for the low severity cases.

Similar patterns can be observed from the ROC curves (Figure 3.6 b). The AUC reported from validation data collected during severe and moderate lightning days are higher than 0.95, while its value drops to 0.87 for the low severity level days (Table 3.10).

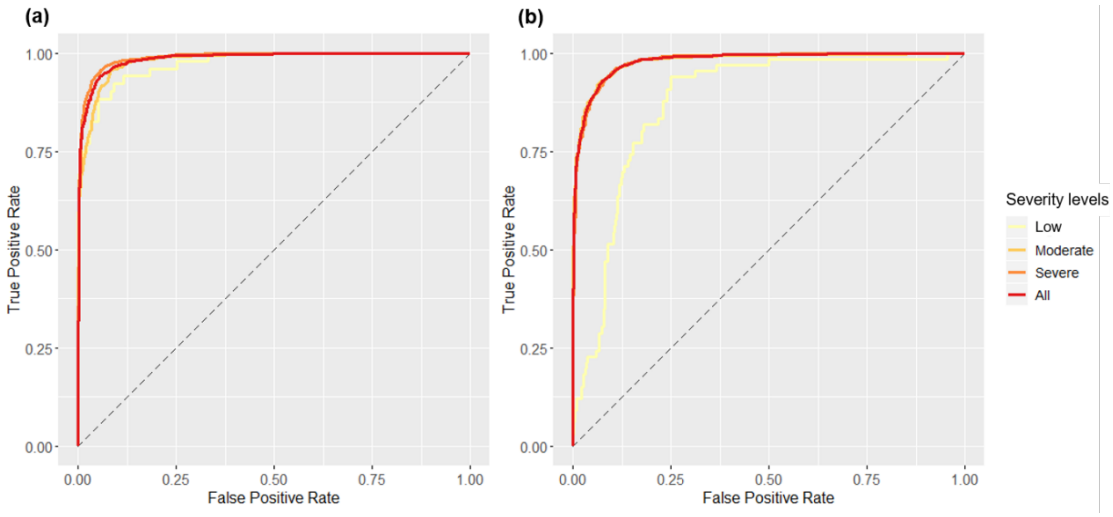

Figure 3.6. ROC curves of validation results on lightning days with different severity levels: (a) 24-hr model, (b) 48-hr model.

In addition to the purely statistical accuracy assessment, I generated CG lightning probability maps across the entire Alaskan tundra to visually compare the predicted spatial patterns to observed patterns of lightning strike distribution (see an example for a severe lightning day in Figure 3.7.

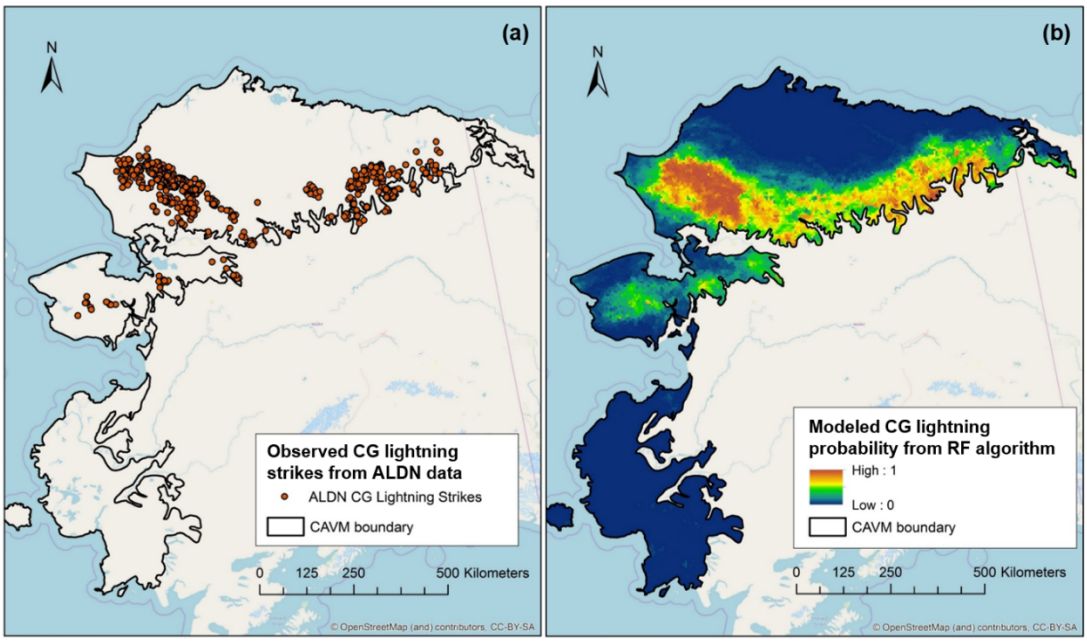

Figure 3.7. (a) Observed CG lightning strikes during 2010/07/02 00:00 and 2010/07/03 00:00UTC and (b) modeled CG lightning probability with the "24-hr model" in Alaskan tundra as an example.

3.5.3 Forecasting performance

The forecasting test using the "24-hr model" for the 48-hr simulation demonstrates strong statistical performance of my method in forecasting forward, with POD as 0.71 and CSI as 0.67 (Table 3.11). The two false ratios FAR and F are below 0.08. When separated by different severity levels of lightning days, the forecasting performance is consistent with previously reported results: the accuracy appears to be substantially higher for severe and moderate lightning conditions compared to low severity days. Similar patterns can be found from the ROC curves (Figure 3.8), with the AUC values around 0.9 for the entire data and those from the moderate level cases (Table 3.11).

Table 3.11. Statistical criteria calculated for the forecasting test

Metrics	All	Severe level	Moderate level	Low level
POD	0.7063	0.6372	0.7707	0.1515
CSI	0.6660	0.5898	0.7397	0.1397
FAR	0.0788	0.1119	0.0516	0.2
F	0.0780	0.1024	0.0547	0.0132
AUC	0.9203	0.8766	0.9519	0.769

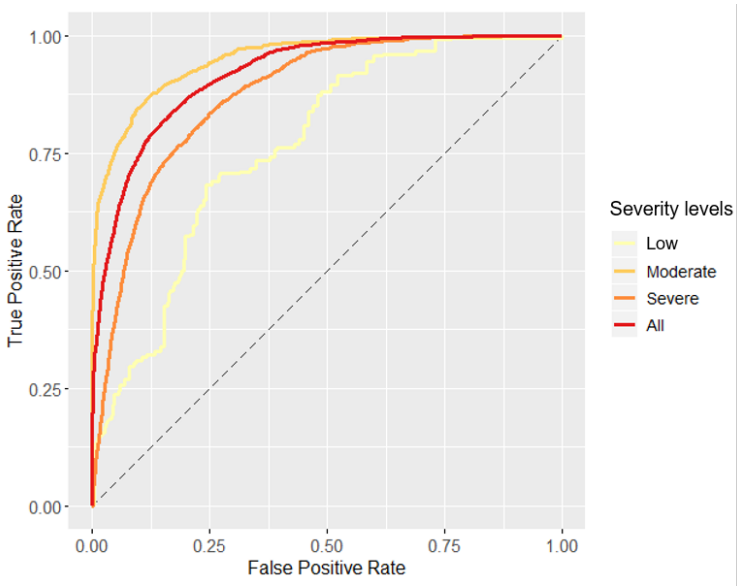

Figure 3.8. ROC curves of forecasting tests on lightning days with different severity levels

3.5.4 Evaluation of variable importance

To understand the roles of the predictors in determining the CG lightning potential in the tundra, I examined the top 20 important variables ranked according to MDA from both the "24-hr model" and the "48-hr model" for comparison (Figure 3.9). According to both models, Parcel Lifted Index (PLI) is found to be the most important variable in determining the accumulated lightning strikes among all the predictors. For the "24-hr model", weather variables at multiple pressure levels, including geopotential height, dew temperature, relative humidity, and velocity speed,

also show their importance in determining CG lightning occurrence in the tundra (Figure 3.9 a). In addition, cloud fraction, sea level pressure, helicity, lifted condensation level, and atmospheric stability indices like the Total Totals and the Showalter Index (SHOW) are also among the top 20 important indicators. Although the variable ranking order of the "48-hr model" differs from that of the "24-hr model", the majority of the top 20 important variable remains the same. Only layer thickness between 700 and 850 hPa levels ($DZ_{700\text{-}850}$) and brightness temperature appear to play an important role in determining the lightning potential for the "48-hr model" but not in the "24-hr model".

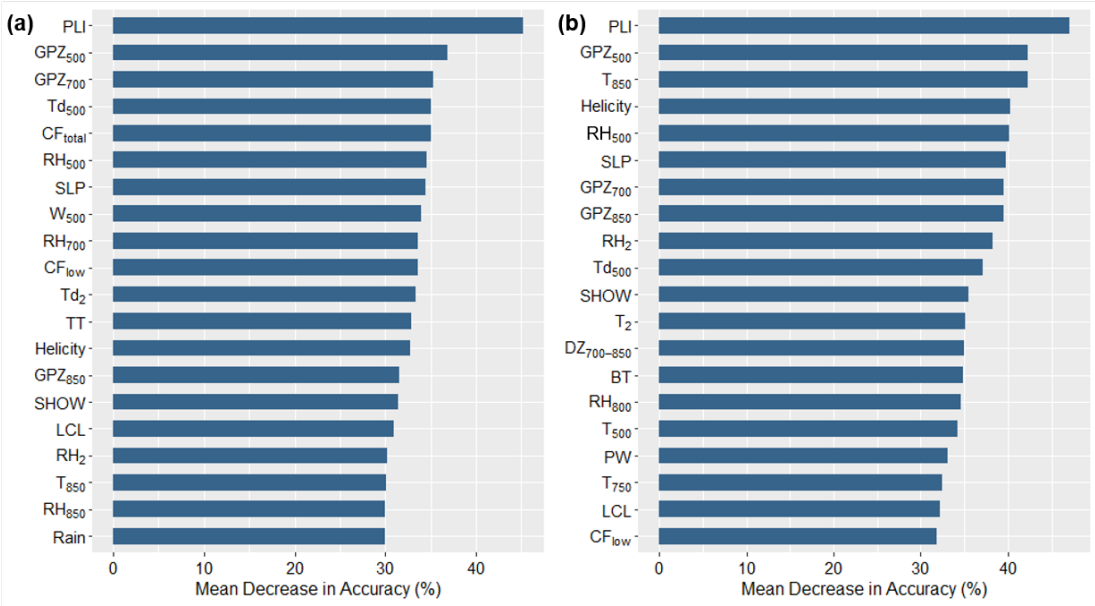

Figure 3.9. Top 20 important variables ranked by MDA in (a) "24-hr model" and (b) "48-hr model".

3.6 Discussions

In general, my results successfully demonstrate the strong capability of the empirical-dynamic method in representing meteorological conditions that support CG

lightning well in Alaskan tundra. As integration of WRF (using the selected parameterization schemes) and RF algorithm, this method shows excellent performance in both modeling CG lightning strikes with 24hr and 48hr WRF simulations, and forward forecasting of lightning probability. This supports the effectiveness of the empirical-dynamical framework in accurate prediction of future CG lightning potential in the data-scarce regions like the HNL. Considering the primary role of lightning in igniting wildland fire in the boreal forest and tundra ecosystems (French et al., 2015; Veraverbeke et al., 2017), this study can further support the monitoring of fire weather conditions and probability as well.

The results indicate that atmospheric conditions supporting CG lightning activity in Alaskan tundra may differ from those in the boreal. Although instability indices SHOW and CAPE were recognized as the top-ranking indicators for lightning potential in boreal forests (Blouin et al., 2016; Burrows et al., 2005), I found PLI as the most important factor in modeling lightning activity than any other indices in Alaskan tundra. This highlights the key role of the lift potential in providing sufficient convection to support lightning formation in the tundra than in the boreal forests in general, which is consistent with the modeling results of Burrows et al. (2005) in the far west and north region of the North America dominated by tundra. While Burrows et al. (2005) suggested that the occurrence of lightning was influenced by the interaction between strong convection and precipitable water (PW) in the cloud, here I found much lower rankings of PW than instability indices like PLI and SHOW in both models. This indicates that convection plays a more critical role than PW in determining the lightning potential in the tundra, which is consistent with the findings

of Reap (1991). Besides, I also found the vertical profiles of variables like geopotential height, relative humidity, dew point temperature, and layer thickness important in modeling lightning activity (Figure 9). However, neither of the two lighting parameterizations (PR92 and LPI) reflect lightning potential in the tundra at the regional scale well. This is not surprising because these parameterizations were not specifically developed for the HNL.

Additionally, the justification of using Thompson 2-moment and MYJ for WRF simulation in the tundra is consistent with existing findings of WRF application in lightning modeling. With a more detailed distribution of CAPE values for describing convective activities (Figure 4), the Thompson scheme is also recommended in existing studies (Giannaros et al., 2015; Zepka et al., 2014), given a detailed representation of ice-phase processes and improved simulation performance for convection related events like precipitation. For lightning modeling purpose, the MYJ scheme is also suitable for describing PBL conditions considering its optimal representation of atmospheric conditions for triggering convection activities (Giannaros et al., 2015; Sousa et al., 2013).

Despite WRF's strong capabilities in regional modeling and dynamic downscaling of atmospheric conditions, its performance of describing physical processes is limited by the assumptions and mechanisms employed for developing the parameterization schemes. Polar WRF is now under development for an improved description of near-surface and atmospheric conditions for the Arctic regions with improved WRF schemes, which has the potential for improving lightning modeling for Alaska in future (Cai et al., 2018; Hines et al., 2011; Wilson et al., 2012).

Although our modeling results show very impressive prediction capabilities, they are subject to uncertainties inherent in CG lightning observations detected from either the ground-based networks. Satellite-based sensors such as Lightning Imaging Sensor or Geostationary Lightning Mapper monitor lightning at large spatial scale. Their datasets, however, are not available for the HNL due to the limited spatial coverage and resolution (Matsangouras et al., 2016; Nag et al., 2014). Separating the CG and intra-cloud lightning from satellite observations can introduce errors as well (Nag et al., 2014). Although ground-based systems are constrained by position accuracy and detection efficiency, I found reporting probability a more effective way to describe CG lightning activity.

Although atmospheric factors function as the key predictors for lightning, synoptic-scale dynamic forcings control meteorological mechanisms driving lightning and fire weather (Flannigan and Wotton, 2001; Reap, 1994; Santos et al., 2013). For example, Kochtubajda et al. (2019) found more frequent ridging and ridge displacements during the 2014 wildfire season in the Northwest Territories of Canada. Synoptic weather conditions should be explored and incorporated in future modeling efforts to improve our understanding of lightning and fire regimes in the tundra.

3.7 Conclusions

Wildfire dominates the disturbance regimes in the Arctic and boreal ecosystems in North America. In recent decades, these regimes have been notably changing and, thus, necessitating a better understanding of the current regimes and their feedbacks to the climate system (Fisher et al., 2018). This study makes the first

effort in examining the factors driving lightning activity, the primary ignition source for wildfire, in Alaska tundra with my statistical-dynamical modeling method. This study demonstrated the effectiveness of integrating WRF and machine learning for lightning modeling in Alaskan tundra at 5km spatial resolution. The results provide insights on understanding the mechanisms of lightning-ignited fires in the tundra. PLI and weather variables at multiple pressure levels were found to be the most important predictors for modeling lightning potential in the tundra, indicating the primary role of convection in the formation of thunderstorms and CG lightning. Moreover, applicable for other data-scare regions, this method can further support the lightning and fire prediction as well as management efforts in the HNL.

Chapter 4: Exploring environmental factors driving wildland fire ignitions in Alaskan tundra

4.1 Summary

Tundra fires are common across the pan-Arctic region, particularly in Alaska. Fires lead to significant impacts on terrestrial carbon balance and ecosystem functioning in the tundra. They can even affect the forage availability of herbivorous wildlife and living resources of local human communities. Also, interactions between fire and climate change can enhance the fire impacts on the Arctic ecosystems. However, the drivers and mechanisms of wildland fire ignitions in Alaskan tundra are still poorly understood. Research on modeling contemporary fire probability in the tundra is also lacking. This study focuses on exploring the critical environmental factors controlling wildfire ignitions in Alaskan tundra and modeled the fire ignition probability, accounting for ignition source, fuel types, fire weather conditions, and topography. The fractional cover maps of fuel type components developed Chapter 2 serve as input data for fuel type distribution. The probability of cloud-to-ground (CG) lightning and fire weather conditions are simulated using WRF. Topographic features are also calculated from the Digital Elevation Model (DEM) data. Additionally, fire ignition locations are extracted from Moderate Resolution Imaging Spectroradiometer (MODIS) active fire product for Alaskan tundra from 2001 to 2019. Empirical modeling methods, including RF and logistic regression, are then utilized to model the relationships between environmental factors and wildfire ignitions in the tundra and to evaluate the roles of these factors. The results suggest that CG lightning is the primary driver controlling fire ignitions in the tundra, while warmer and drier weather

conditions also support fires. The results of this study highlight the important role of CG lightning in driving tundra fires and that incorporating CG lightning modeling is necessary and essential for fire monitoring and management efforts in the High Northern Latitudes (HNL).

4.2 Introduction

Wildland fires have played an important role in altering ecosystem functioning, driving land cover change and affecting carbon balance in the boreal forest and tundra ecosystems (Gustine et al., 2014; Kasischke et al., 2010; Mack et al., 2011; Randerson et al., 2006; Rocha and Shaver, 2011; Turetsky et al., 2011). Although tundra fires are typically less severe than the fires in the boreal forests, they are common and widespread across the pan-Arctic region according to satellite based observations (He et al., 2019). In recent years, several large fire seasons have occurred in Alaskan tundra, such as the 2010 fire season in the Noatak River Valley and the 2015 fire season in the Southwest Alaska. Tundra fires also have the potential to release the ancient carbon stored in the permafrost underneath the land surface and lead to widespread development of thermokarst (Jones et al., 2015; Mack et al., 2011). Moreover, fires in the tundra can influence the habitats and forage availability of wildlife like caribou, which would further affect the resources of local human communities (Gustine et al., 2014; Jandt et al., 2008; Rupp et al., 2006). Furthermore, fire activities are likely to increase in the tundra under climate warming in the future (French et al., 2015).

Despite the importance of tundra fires, they are less studied compared to fires in other ecosystems. Current research primarily focuses on evaluating post-fire

impacts such as fire severity (Loboda et al., 2013), ecosystem responses (Bret-Harte et al., 2013), and carbon budget change (Mack et al., 2011) within comparatively little attention to modeling tundra fire occurrence. Previous studies have modeled historical or future tundra fire regimes with either empirical methods or an ecosystem model Alaska Frame-Based Ecosystem Code (ALFRESCO; Higuera et al., 2011; Joly et al., 2012; Young et al., 2017). However, research on modeling contemporary fire occurrence is lacking in current English language peer-reviewed literature. Although numerous studies have modeled the interactions between environmental factors and wildfire occurrences in boreal forests, their results are not directly applicable to tundra ecosystems due to the different ecosystem functioning and responses (French et al., 2015; Van Heerwaarden and Teuling, 2014).

Wildfire occurrences are primarily ignited by cloud-to-ground lightning strikes and human activities. In addition to the ignition sources, wildfire behaviors are typically controlled by three types of influencing forces including fuel, weather and topography, as summarized by the *Fire Environment Triangle* (Pyne et al., 1996). Fuel type and state are critically important factors that control fire-environment interactions through altering fire characteristics and affecting ignition easiness (Pyne et al., 1996). Fuel type represents properties of the fuel itself, such as fuel composition, continuity and loading. Fuel state is mainly related to moisture content primarily driven by the changing weather conditions at different temporal scales. Topography also has the potential to affect the fire behaviors through controlling exposure to sunlight and moisture pooling. Weather conditions can also function as the dominant contributors to the fire environment from hourly to daily scales, by

influencing the fuel conditions and ignition sources. A variety of rating systems have been developed to quantify the danger of fire weather conditions and to predict the fire potential, such as National Fire Danger Rating System (NFDRS) and Canadian Forest Fire Weather Index System (CFFWIS).

Majority of the existing studies exploring the impacts of these environmental factors in driving wildland fires are focused on boreal forests in the HNL, from the perspectives of both fire occurrence and fire spread. Liu et al. (2012) studied both lightning and human ignited fires in the boreal forests of Northeast China and found out that lightning fires are mainly controlled by fuel moisture and vegetation type. Veraverbeke et al. (2017), however, suggested the primary role of lightning in driving burned areas in recent large fire years in the boreal forests of North American. Peterson et al. (2010) also demonstrated the effects of atmospheric stability, lightning strike counts, and dry weather conditions on fire activity in the boreal forests of North America. Though lightning characteristics like polarity and peak current were found to be significant predictors of fire occurrences (Müller and Vacik, 2017; Vecín-Arias et al., 2016), they did not function as major contributors that drive fire ignitions in some other studies (Adámek et al., 2018; Pineda et al., 2014). These differences could be caused by different matching methods between lightning strikes and fires (Moris et al., 2020). Recently, Masrur et al. (2018) found out that warm and dry conditions affect the spatiotemporal patterns across the entire circumpolar tundra regions. However, their analyses were conducted across the pan-Arctic region and may not explain the situation of fires in Alaskan tundra.

Due to the lack of weather stations in the remote tundra, datasets developed based on station observations with interpolation methods such as Daymet are not suitable for capturing these environmental factors, particularly fire weather conditions, in this data-scare region. Reanalysis data products also have their limitations regarding the coarse spatial resolution. Meteorological variables simulated with Numerical Weather Prediction (NWP) models like Weather Research and Forecast (WRF) model have demonstrated their suitability for describing fire weather conditions and capturing their spatial variations in regions with limited observations available (Mölders, 2010, 2008), although the simulated indices may not always be trustworthy in accurate characterization of fire risk likely caused by the inaccurate simulation of wind and precipitation (Mölders, 2010; Simpson et al., 2014). In addition, remote sensing observations have also been widely adopted for capturing the spatial distribution of fuel types, fuel moisture states and topographical features (He et al., 2019; Loboda, 2009; Loboda and Csiszar, 2007; Ottmar et al., 2007; Yebra et al., 2013, 2008).

Two types of models have been developed to uncover the impacts of the environmental factors on driving lightning-ignited wildfire occurrences and to model their relationships. Earliest attempts of fire occurrence modeling developed physical-based models with explicit representations of wildland fire processes(Anderson, 2002; Anderson et al., 2000; Kourtz and Todd, 1991). Specifically, major steps related to fire occurrences including the start of lightning, fire ignition, fire smoldering and fire detection were accounted for and represented in these physical-based models. Through a series of equations developed upon experiments and

assumptions, these models were able to incorporate the related environmental drivers of fires and to model the probability of fire occurrences.

Empirical based methods have been commonly adopted for modeling wildfire ignitions in recent-year research (Prestemon et al., 2013). The spatial point modeling methods have been adopted by several studies on modeling fires in different ecosystems (Liu et al., 2012; Woo et al., 2017; Yang et al., 2015). Generalized Linear Models have also been commonly utilized to predict fire occurrences (Ager et al., 2018; Barbero et al., 2014; Vilar et al., 2016). In addition, with strong predictive capability, logistic regression and random forest (RF) based algorithms have been frequently applied to understand the relationships between environmental factors and fire occurrences (Guo et al., 2016; Keyser and Leroy Westerling, 2017; Van Beusekom et al., 2018; Vecín-Arias et al., 2016; Viedma et al., 2018; Wotton and Martell, 2005).

Therefore, in this study, I aim to understand "*What environmental factors drive fire ignition probability across Alaskan tundra?*" Here fire ignition is referred as the detectable start of fire occurrence using satellite sensors. To address this research question, I plan to develop an empirical model using RF algorithm for predicting fire ignition probability in Alaskan tundra with environmental drivers derived from WRF simulations and satellite observations from 2001 to 2019.

4.3 Study Area

This study covers the entire Alaskan tundra beyond the northern tree line, as defined by the Circumpolar Arctic Vegetation Map (CAVM) data (Walker et al., 2005; Figure 3.1 a), focusing on the shrub or graminoid dominated tundra in

particular. Major vegetation fuels in this region include evergreen or deciduous shrub, sedge, grass, moss, and lichen (Bliss et al., 1973). This region is underlain by continuous and discontinuous permafrost. Though varying by ecoregions, the study area has an average temperature below 0°C throughout the year. Despite the low annual precipitation, tundra lands tend to be wet because of the low evaporation rates and poor drainage conditions. Wildland fire activities in Alaskan tundra also have a large variability across different ecoregions (French et al., 2015; Rocha et al., 2012). Over the past half-century, the mean fire return intervals for Alaskan tundra ecoregions vary from 13 to 22 years, and the fire rotation periods have a range from roughly 400 to thousands of years (Rocha et al., 2012). Though most Alaskan tundra fires are small in spatial scale, the large ones are not rare. Particularly, Kotzebue Lowlands and Seward Peninsula tend to have higher frequency and larger burned extent compared to the others (French et al., 2015).

4.4 Data and Methods

To achieve the research goals, I considered five groups of environmental factors related to wildfire ignition, including fuel type distribution, fuel state conditions, fire weather conditions, topographical features, and fire ignition source (Figure 4.1). Fire ignition locations in Alaskan tundra extracted from satellite observations were used as the dependent variable. I then developed an empirical model for predicting the fire ignition probability in the tundra using RF algorithm. In particular, the fractional cover maps developed in Chapter 2 were used to represent fuel type distribution in this study. The empirical-dynamical method developed in Chapter 3 was adopted to model the probability of CG lightning strikes, the primary

ignition source of wildfire in Alaskan tundra. Additional environmental variables, including satellite-derived fuel state characterization, surface topography and weather conditions, are described in this chapter.

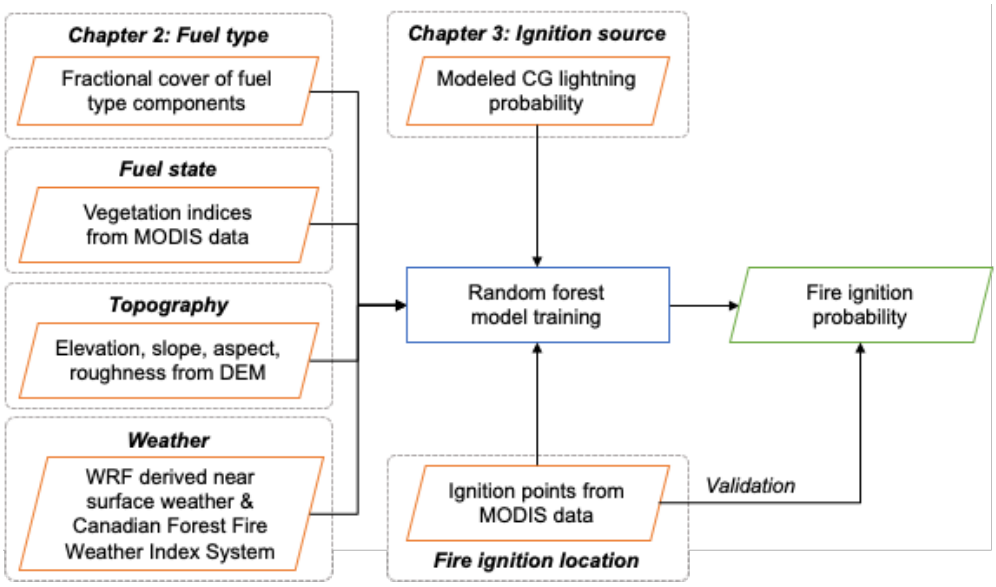

Figure 4.1. Methodology framework of modeling fire ignition probability in Alaskan tundra in Chapter 4.

In addition to the overall framework, the modeling workflow of this chapter is further summarized in Figure 4.2. All input environmental factors were first categorized into variables of relatively high and low temporal variability referred to as dynamic and static, respectively. Static variables including both topographical features (ref?) and fractional coverages of major fuel type components (He et al., 2020). Although vegetation shifts and fuel type transitions can occur from years to decades under disturbances or climatic variability and change, the vegetation compositions are relatively stable when compared to the seasonal and diurnal changes of meteorological variables and fire weather conditions. The fuel types were therefore considered as static variables in this dissertation. Weather related variables, including

near surface, CFFWIS, and CG lightning probability, are dynamic throughout a short time period. Compared to fuel type, fuel moisture state can change under the influence of meteorological conditions in a few days, thus considered as dynamic variables.

To characterize the dynamic components of fire ignition, I extracted the earliest detections from the space-time contiguous point clouds of MODIS active fire data (sec section 4.4.1) to determine ignition locations and dates for multiple years. These points served as "Fire" events in the fire ignition modeling. The dates of these ignition points were used for determining dynamic variables used for modeling. I used the leaf moisture related vegetation indices calculated from the closest day of year (DOY) before the ignition dates using MODIS 8-day surface reflectance composites (MOD09A1; Vermote et al., 2015). I then determined WRF simulation dates for modeling CG lightning probability and near-surface meteorological conditions. Since the calculation of some of the fire weather indices within the CFFWIS is based on long-term accumulation of weather variable starting from snowmelt dates, here I combined downscaled WRF output starting from a week since the ignition dates, and the relative coarse resolution reanalysis data from the mid-April to calculate indices from CFFWIS. After preparing all independent variables, two models were developed with RF algorithms using dynamic variable acquired on the fire ignition day and one day before ignition, to, first, assess the ability of the model to represent actual fire ignition instances (the day of ignition model) and, second, assess the model's forecasting capacity (one day before ignition).

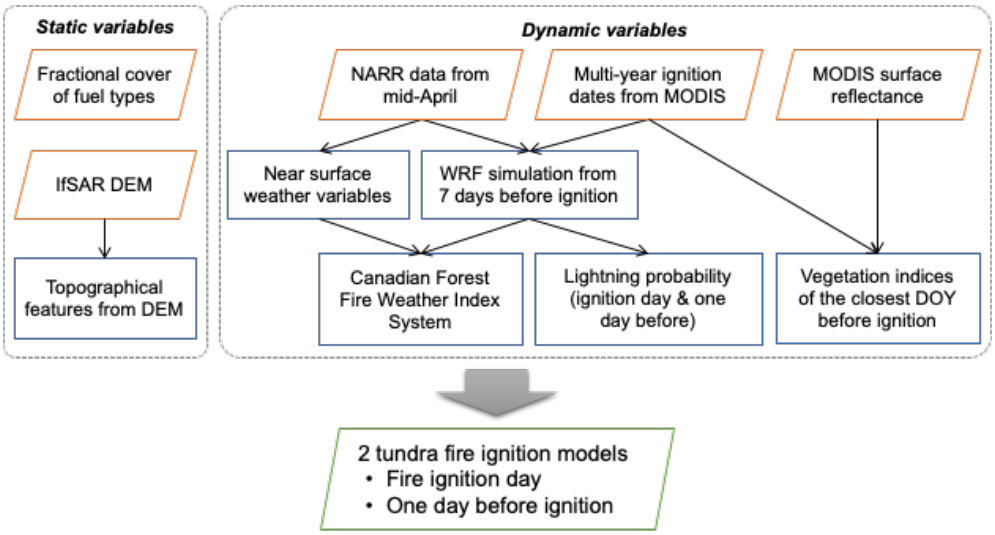

Figure 4.2. Modeling workflow

4.4.1 Determining fire ignition locations

Ignition point locations of tundra fires from 2001 to 2019 were determined using the 1km MODIS Thermal Anomalies/Fire locations data product (MCD14DL V006; Giglio et al., 2003) obtained from NASA's Fire Information for Resource Management System (FIRMS). Since fires have strong emission of mid-infrared radiation, this active fire product detects fires based on brightness temperatures from MODIS 4- and 11-μm bands using a contextual algorithm (Giglio et al., 2003). In addition to coordinates (latitude and longitude) of active fire points, attributes including brightness temperature, acquisition date, acquisition time, fire radiative power, and detection confidence are also recorded in the data product. Only fire points classified as nominal or high confidence levels (detection confidence above 30%) were considered in the processing.

MODIS active fire points in the tundra were first extracted using a 10km buffered boundary of the CAVM data. I designed a clustering method based on the

Density-Based Spatial Clustering of Applications with Noise (DBSCAN; Ester et al., 1996) algorithm to identify the tundra fire clusters (Figure 4.3). The DBSCAN algorithm separates points of high density from those of low density and locates these regions as clusters. Here the ε parameter in DBSCAN, which represents the maximum distance between two neighboring points, was set to 2.5 km based on the study of Loboda and Csiszar (2007). The DBSCAN algorithm was applied to tundra fire points for each year. Since fires occurring at different times could be grouped into the same cluster, I further examined the temporal gap (Gap_{time}) among fire points in each cluster and. The temporal gap was determined as 4 days to separate different fires in a certain spatial cluster (Loboda and Csiszar, 2007). The active fire points with the earliest acquisition time were considered as the ignition locations.

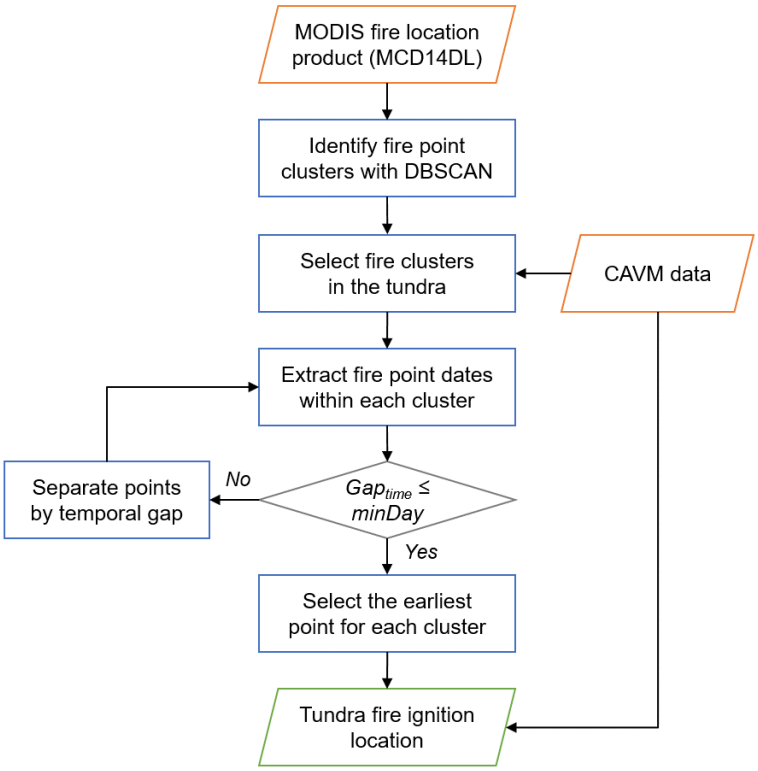

Figure 4.3. Workflow for extracting fire ignition locations in Alaskan tundra

Individual fire ignition events were then identified from the MODIS active fire records between 2001 and 2019 across Alaskan tundra using the algorithm described above, suggesting a variety of wildfire activity patterns in this region (Figure 4.4). Thirteen of the nineteen years in the available data record have a number of fire events between twenty (2001 – 2004, 2006, 2008 – 2009 , 2011 – 2014, 2016 – 2018), four years can be characterized as a moderate fire activity season with the number of fire events between 20 and 30 (2005, 2007, 2010, 2019), while the 2015 fire season has particularly high fire activity with 49 fire events detected within the boundary of Alaskan tundra defined by CAVM.

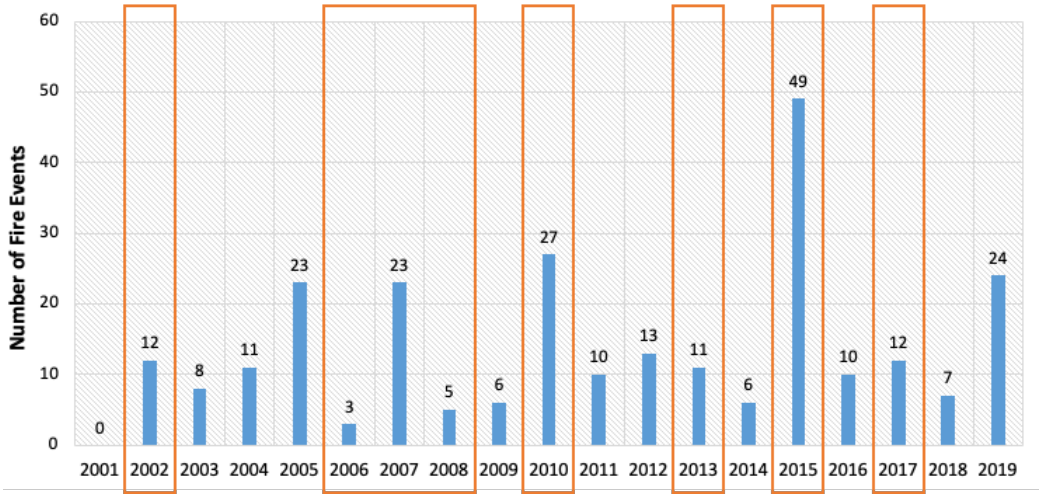

Figure 4.4. Number of fire ignition events detected from 2001 to 2019 with MCD14DL data. Sampled fire years are highlighted in orange boxes.

To cover a variety of fire seasons, I sampled five seasons of low fire activity (2002, 2006, 2008, 2013, 2017), two years with moderate fire season activity (2007, 2010), and one year with very high fire activity (2015), as illustrated in Figure 4.4. I then extracted the ignition points for individual fire events and defined the dates of ignition based on the time stamp of the ignition points to improve the computing

efficiency of WRF simulation. Fire ignition dates detected from the selected eight years were summarized in Table 4.1.

Table 4.1. Full list of fire ignition dates detected from sampled years

Year	Fire ignition dates
2002	5/23/2002, 6/3/2002, 6/18/2002, 7/10/2002, 7/20/2002, 7/28/2002, 8/2/2002, 8/5/2002, 8/15/2002, 8/22/2002, 9/22/2002
2006	5/31/2006, 7/7/2006
2007	6/4/2007, 6/10/2007, 7/5/2007, 7/6/2007, 7/7/2007, 7/12/2007, 7/14/2007, 7/16/2007, 7/17/2007, 8/2/2007, 8/29/2007, 9/8/2007, 9/9/2007, 9/19/2007, 9/30/2007
2008	6/4/2018, 6/5/2018, 6/7/2018, 6/8/2018, 6/13/2018
2010	6/1/2010, 6/8/2010, 6/9/2010, 6/21/2010, 6/22/2010, 6/23/2010, 6/24/2010, 7/1/2010, 7/2/2010, 7/3/2010, 7/4/2010, 7/8/2010, 7/10/2010
2013	5/31/2013, 6/5/2013, 6/20/2013, 6/21/2013, 7/11/2013, 7/30/2013
2015	6/1/2015, 6/2/2015, 6/16/2015, 6/20/2015, 6/21/2015, 6/22/2015, 6/23/2015, 6/24/2015, 6/25/2015, 6/29/2015, 6/30/2015, 7/2/2015, 7/3/2015, 7/4/2015, 7/6/2015, 7/7/2015, 7/13/2015, 7/14/2015, 7/20/2015, 7/24/2015, 7/25/2015, 8/1/2015, 8/6/2015
2017	6/6/2017, 6/7/2017, 6/8/2017, 6/16/2017, 6/19/2017, 6/28/2017

4.4.2 Modeling cloud-to-ground lightning probability with WRF simulations

The empirical-dynamical framework “24-hr model” developed in Chapter 3 was adopted here to describe the probability distribution of ignition source across Alaskan tundra. Since the National Centers for Environmental Prediction (NCEP) final analysis data used in Chapter 3 does not provide precipitation data, in this section I used the North American Regional Reanalysis (NARR) data instead to initialize the two-way nested WRF simulation, for the consistency of CFFWIS calculation in Section 4.4.3. Developed by the NCEP, the NARR dataset assimilates a large amount of observations to generate long term estimations of weather conditions across the entire North America at 32 km resolution and 3-hour time interval. All

observations used in NCEP/NCAR Global Reanalysis project, precipitation data, radiances from Television Infrared Observations Satellite (TIROS) Operational Vertical Sounder (TOVS), profiler data, and land surface and moisture data have been utilized to produce this dataset.

I then applied the modeling approach developed in Chapter 3 to develop CG probability grids at 5km resolution for the entire tundra region in Alaska, using WRF simulated atmospheric factors as independent variables. CG lightning probability was modeled and included in this analysis for each of the "fire ignition" dates extracted in section 4.4.1. and "the day before ignition" dates. The output 5km lightning probability grids were then used as input data for representing ignition sources of wildland fires.

4.4.3 Near surface weather conditions and calculation of the CFFWIS

As a sub-system of the Canadian Forest Fire Danger Rating System (CFFDRS), the CFFWIS has been developed since 1970 to account for the weather impacts on forest fuels and fires across the boreal forests of Canada (Van Wagner, 1987; Figure 4.5). Although not specifically designed for the tundra fuels and fires, this system is suitable for describing fire weather conditions in the ecosystems of the HNL and considers for more detailed fuel types than the NFDRS (French et al., 2015; Mölders, 2010).

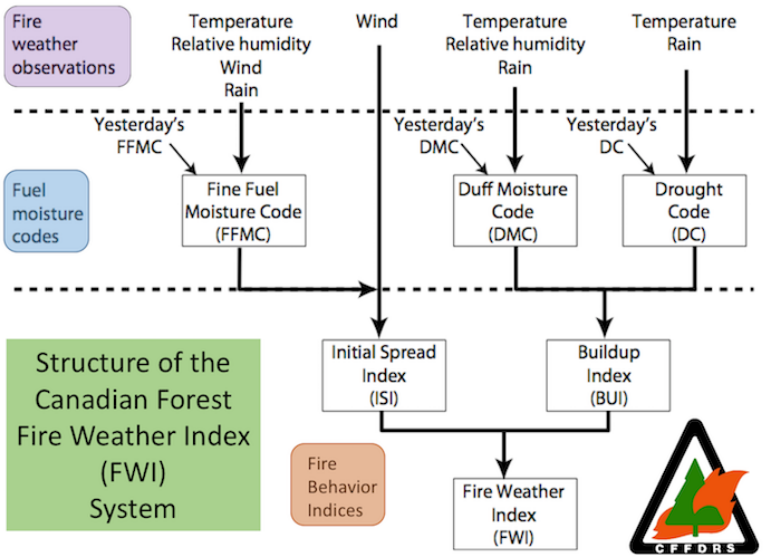

Figure 4.5. Flow chart of Canadian FWI system, source: National Wildfire Coordinating Group (https://www.nwcg.gov/publications/pms437/cffdrs/fire-weather-index-system)

The entire CFFWIS is comprised of six standard components, including three fuel moisture codes and three fire behavior indices (Van Wagner, 1987; Figure 4.5). The calculation of CFFWIS purely requires weather readings of air temperature, RH and wind at noon, as well as daily accumulated precipitation, which actually represents the peak fire danger during the midafternoon (Van Wagner, 1987). The design of three fuel moisture codes accounts for both water capacity and drying speed of the fuels. Fine Fuel Moisture Code (FFMC), Duff Moisture Code (DMC) and Drought Code (DC) represent the moisture content and flammability of litter and fine fuels, loosely compacted organic matter of moderate depth, and deep and compact organic layers, respectively. Both DMC and DC are slow-reacting codes that are largely affected by the changing daylength and long-term accumulation, while the fast-reacting FFMC is less responsive those effects. For all three codes, larger values

suggest drier conditions and higher flammability of the fuels. Calculated based on the moisture codes, the fire behavior indices, including Initial Spread Index (ISI), Buildup Index (BUI) and Fire Weather Index (FWI), are designed to describe the important variables related to fire behavior, including spread rate, fuel weight and fire intensity.

The CFFWIS requires long-term records of weather observations starting from snowmelt date for each year. Although the exact date of snowmelt varies across the regions, I set the startup date to a common day, as is common for calculating CFFWIS (Lawson and Armitage, 2008), in mid-April (DOY 101) for all years. Fire weather variables from NARR reanalysis data and WRF outputs were combined to support the calculation of CFFWIS to reduce the computing load caused by multi-year WRF simulation, while achieving the improved spatial resolution of the results. Specifically, WRF simulations were run for a week before the ignition dates to downscale the data to 5 km. Then the NARR data were resampled with the Nearest Neighbor method to describe the meteorological conditions from the startup date till the WRF simulations. In addition to the four weather observations (air temperature, RH, wind and precipitation), the daylength data of the selected years for the entire North America were obtained from Daymet (Thornton et al., 2017) provided by the Oak Ridge National Laboratory Distributed Active Archive Center (ORNL DAAC).

To prepare the input data for CFFWIS, the daily maximum values during daytime from noon to midafternoon were calculated based on the 3-hour intervals for air temperature, RH and wind. Daily accumulated precipitation values were also summed up based on the 3-hourly data. The initial conditions of seasonal start-up

values for FFMC, DMC, and DC were set to 85, 6, and 15, respectively (Lawson and Armitage, 2008). The three fuel moisture codes (FFMC, DMC, and DC) and three fire behavior indices (ISI, BUI, and FWI) from CFFWIS were then calculated according to the equations provided in Van Wagner and Pickett (1985) to describe long-term weather conditions for all the sampled eight years across the entire tundra.

4.4.4 Estimating fuel state with vegetation indices

A variety of vegetation indices have been developed to estimate vegetation moisture content for large-scale monitoring. Yebra et al. (2008) reviewed commonly used vegetation indices and suggested that Normalized Difference Infrared Index (NDII), Normalized Difference Water Index (NDWI) and Global Vegetation Moisture Index (GVMI) are directly related to leaf water content. I, therefore, decided to adopt these indices as a reference for fuel moisture state in this chapter (Table 4.2). MODIS 8-day surface reflectance data product MOD09A1 was used to compute these vegetation indices across Alaskan tundra. Only clear pixels were adopted for the calculation according to the state Quality Assurance (QA) flags. Indices from the closest DOY of 8-day composites were used for RF modeling.

Table 4.2. Vegetation indices for estimating live fuel moisture content

Vegetation index	Formula with MODIS bands	Reference
Normalized Difference Infrared Index ($NDII_6$)	$\frac{\rho_2 - \rho_6}{\rho_2 + \rho_6}$	(Hardisky et al., 1983)
Normalized Difference Infrared Index ($NDII_7$)	$\frac{\rho_2 - \rho_7}{\rho_2 + \rho_7}$	(Hardisky et al., 1983)
Normalized Difference Water Index (NDWI)	$\frac{\rho_2 - \rho_5}{\rho_2 + \rho_5}$	(Gao, 1996)
Global Vegetation Moisture Index (GVMI)	$\frac{(\rho_2 + 0.1) - (\rho_6 + 0.02)}{(\rho_2 + 0.1) + (\rho_6 + 0.02)}$	(Ceccato et al., 2002)

4.4.5 Extracting topographic features

The 5m DEM product collected with airborne Interferometric Synthetic Aperture Radar (IfSAR) data was obtained for the entire Alaska from the Alaska Elevation Portal supported by the State of Alaska (https://elevation.alaska.gov). The IfSAR data has been collected by USGS a 5-m post spacing throughout Alaska with since 2010. This data product has a vertical accuracy of 3-m with 90% confidence level for regions with slope between 0 – 10 degrees. It has provided a full coverage for the tundra regions in Alaska. Four topographical features were extracted based on the DEM, including elevation, slope, aspect, and roughness using the Geospatial Data Abstraction Library (GDAL). For a certain elevation grid cell, the roughness is defined as the maximum inter-cell difference between its elevation value and those from all surrounding cells (Wilson et al., 2007). Due to the extremely large size of the entire dataset covering Alaskan tundra, I resampled the DEM data to 30m for the extraction of topographical features considering the computing efficiency.

4.4.6 Empirical modeling of fire ignition probability

Empirical models were developed with RF classification algorithm to identify the important factors driving fire ignitions in the tundra and to predict the ignition probability. Fire ignition points extracted from the Section 4.4.1 were used to represent the presence of "Fire" in Alaskan tundra, which was coded as "1" in the modeling. I then randomly sampled similar amounts of points across the tundra regions on the same fire ignition dates as the "No Fire" conditions, which was coded as "0". For dynamic variables, I extracted the values acquired on fire ignition dates and the dates before ignition separately, to construct two different datasets of

predictors for the two models, referred as “Current model” and “Previous model” in this dissertation. For both models, 70% of the records were randomly selected for model training, and the rest 30% were reserved for validation.

Although spatial autocorrelation does not impact the accuracy of prediction within the RF models, it can impact the assessment of relative impact of individual input variables on the outcome. Since the ultimate goal of this study is to understand the relative importance of the drivers of fire ignitions in Alaskan tundra, I first tested the Pearson’s r correlation between each pair of the variables and removed those that are highly correlated from modeling. Although the algorithm has strong capability of accurate prediction, it only provides the relative rankings of variable importance while fails to show how the independent variables relate to the fire events (negatively or positively) and the strength of the relationship. To account for these limitations of the RF modeling algorithm, I visualized the distribution of the values for different variables within “fire” and “non-fire” conditions using boxplots, and quantified the significance of the observed differences in the mean values of environmental factors within “fire” and “non-fire” cases using Welch’s t-tests. Finally, logistic regressions were also developed with the two datasets to further support the exploration of driving factors of tundra fire ignitions.

4.5 Results

4.5.1 Variable selections based on correlations

The study design includes the development and testing of two models. The “Current” model represents the condition observed and modeled for the day of fire

ignition to test our ability to accurately model the ignition events. The "Previous" model is developed to add an assessment of fire ignition forecasting capabilities using weather and other environmental condition from the day before the actual date of fire ignition event. Before executing these empirical models, I first explored the Pearson's r correlations between independent variables to exclude the highly correlated ones. The correlation matrices of variables in both "Current" and "Previous" models are shown in Figures 4.6 and 4.7, respectively. For both matrices, three groups of variables exhibit very strong correlations with Pearson's r values above 0.8, including vegetation indices, fire weather variables, and topographic features. Specifically, all four vegetation indices are highly correlated with each other, with correlation values above 0.95. I therefore selected to include only NDII6 as a reference for the fuel state conditions in the modeling efforts. For the CFFWIS, I also found strong correlations between several pairs of CFFWIS fire weather indices, including FFMC-ISI and DMC-BUI, with correlation values above 0.95. FWI was not included in this analysis and further modeling steps because the dynamic range of the values remained at 0 for the dates. Therefore, only three fuel moisture codes – FFMC, DMC and DC – were included in the empirical modeling. Although near surface meteorological variables also show moderate correlations with fire weather indices, they are included to account for meteorological conditions irrespective of fuels. Finally, among topographic features, slope and roughness are closely related to elevation values for Alaskan tundra, and hence, are excluded from modeling.

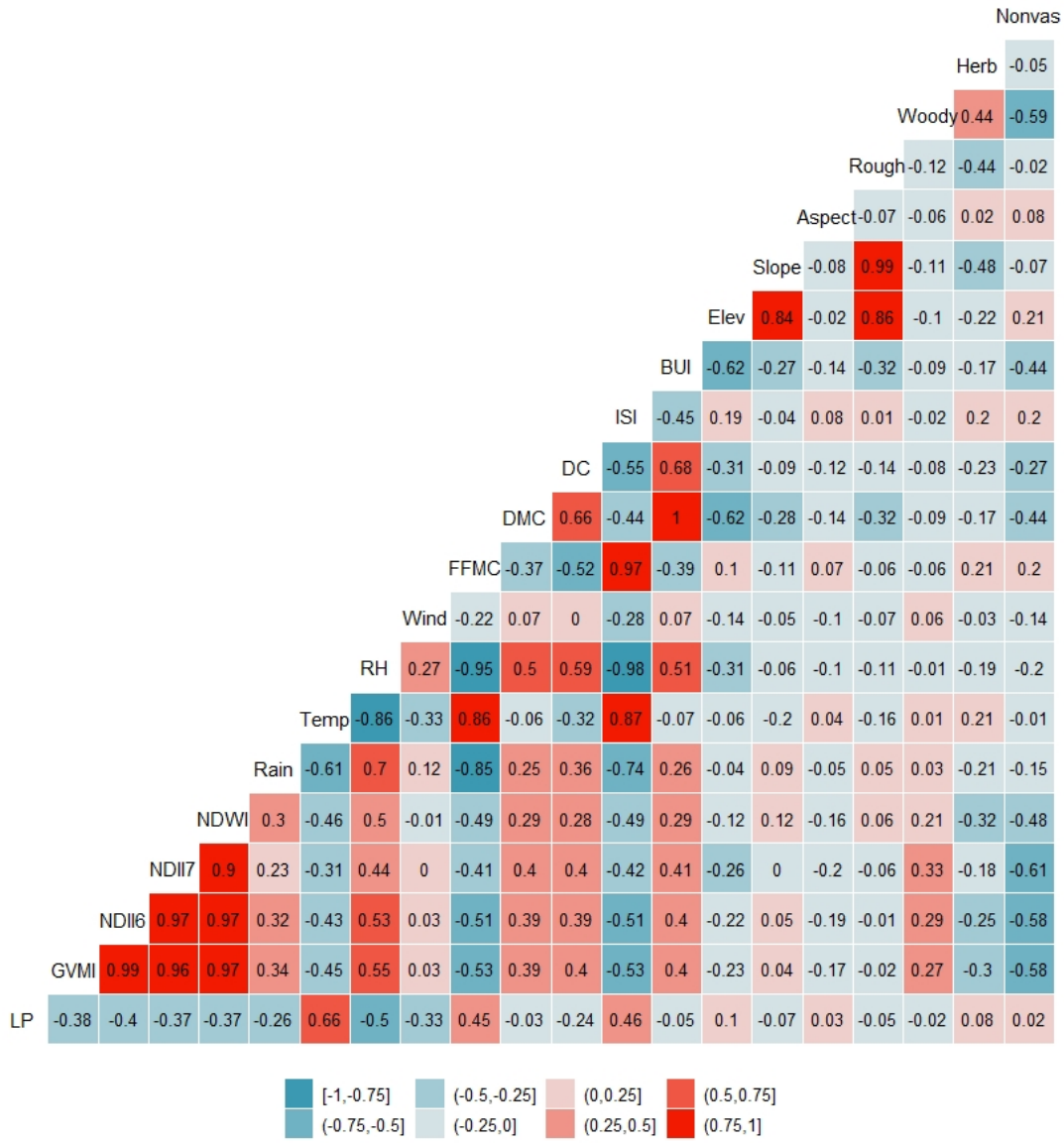

Figure 4.6. Correlation matrix for static and dynamic variables extracted on the fire ignition days. "LP": CG lightning probability, "Temp: air temperature, "Elev": elevation, "Rough": roughness, "Herb": herbaceous component, and "Nonva": nonvascular component.

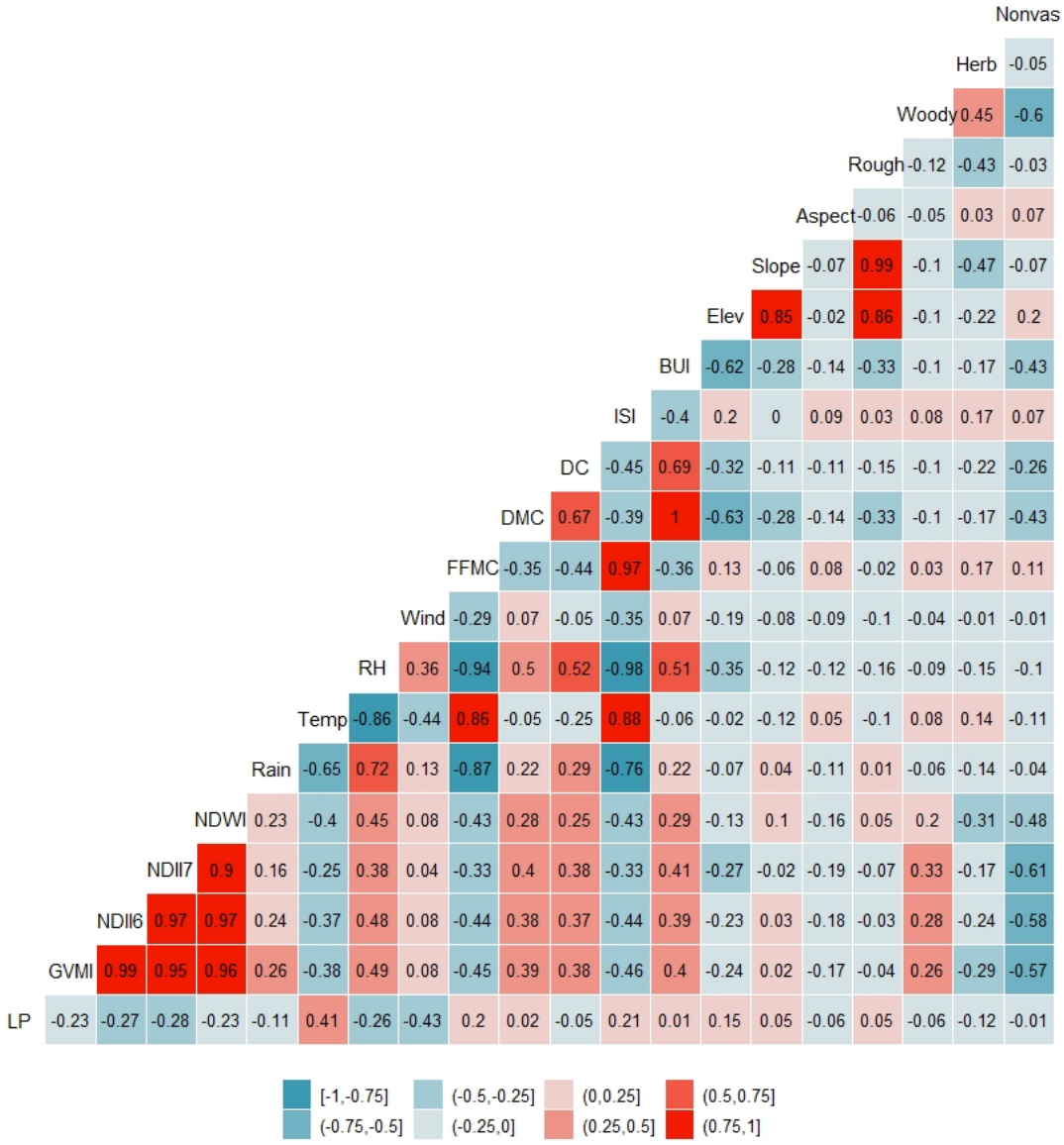

Figure 4.7. Correlation matrix for static and dynamic variables extracted on the dates before fire ignitions. "LP": CG lightning probability, "Temp: air temperature, "Elev": elevation, "Rough": roughness, "Herb": herbaceous component, and "Nonvas": nonvascular component.

4.5.2 Accuracy of empirical modeling

The RF models have shown strong capability and high accuracy in predicting wildfire ignition probability in Alaskan tundra, according to the overall OOB estimate of error rate and the class errors. The overall OOB error rate of the "Current" model is 6.03% with the overall accuracy of 93.97%. Specifically, the "Fire" condition has a class error of 5.05%, while that of the "No fire" reaches 7.17% (Table 4.3 a). The overall performance of the "Previous" model is slightly lower. Its overall OOB error rate is 8.75% with the overall accuracy of 91.25%. The class errors of the absence and presence of fire events are 6.86% and 10.97%, respectively (Table 4.3 b).

Table 4.3. RF modeling results of the two models for predicting fire ignitions

(a) Current model				
Confusion matrix		Predictions		Class error
		No fire	Fire	
Observations	No fire	263	14	0.0505
	Fire	17	220	0.0717
(b) Previous model				
Confusion matrix		Predictions		Class error
		No fire	Fire	
Observations	No fire	258	19	0.0686
	Fire	26	211	0.1097

Validation performed against the reserved dataset shows that both models have a strong capability to reflect (for "Current") and forecast (for "Previous") fire ignition probability, according to the ROC curves (Figure 4.8). The AUC values estimated from the ROC curves are above 0.95 in both models, with 0.9704 and 0.9683 for the "Current" for "Previous" models, respectively.

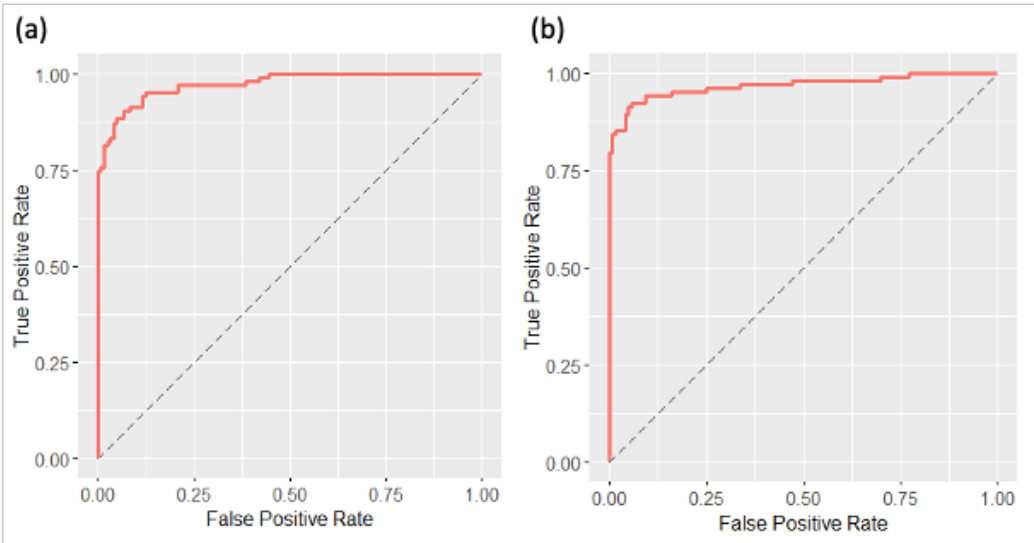

Figure 4.8. ROC curves estimated based on validation datasets for the two models: (a) "Current model"; (b) "Previous model".

4.5.3 Evaluation of variables driving tundra fire ignitions

RF Mean Decrease in Accuracy (MDA) metric identifies CG lightning probability as the most important independent variable, with MDA values of 50.06% and 34.58% for the "Current" and "Previous" models, respectively (Figure 4.9). Near surface weather variables and fuel moisture codes from CFFWIS are also found to be important in determining fire ignition events in the tundra, particularly air temperature, RH and DC. Compared to the weather-related variables, fuel types, satellite-based estimates of fuel state, and topographical features contribute but do not appear to drive fire ignitions in the tundra.

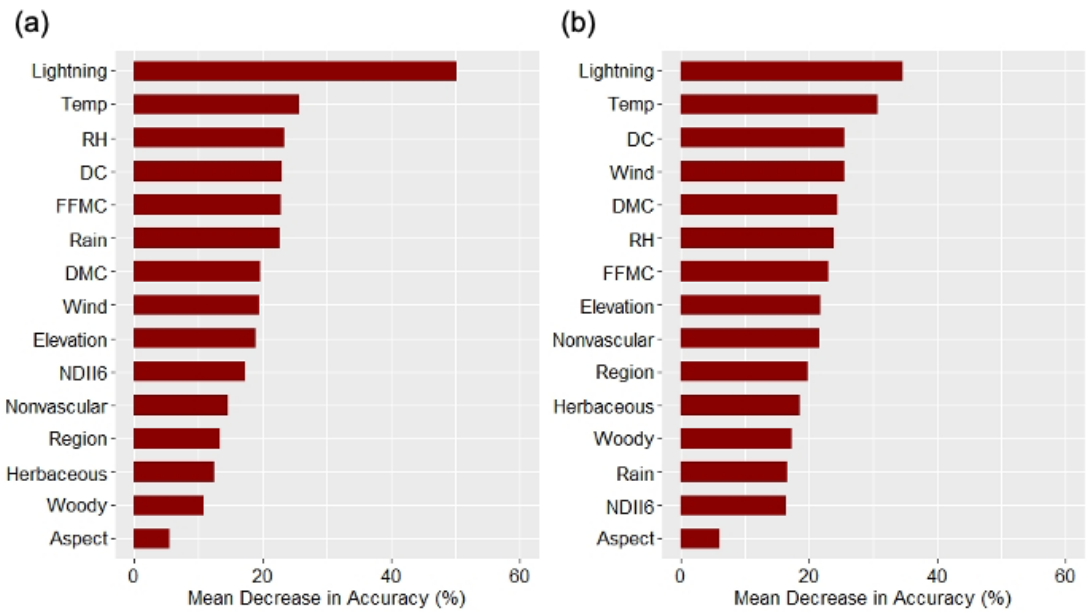

Figure 4.9. Variable importance rank for models: (a) "Fire ignition day", (b) "One day before ignition"

Although RF models provide relative ranking of variable importance in predicting the dependent variable, they are limited in showing the types and strengths of the relationships between each independent environmental factor and fire ignition probability. Logistic regression models were also developed to support analyzing the potential impacts of environmental factors on fire. I developed two logistic regression models for "Current" and "Previous" conditions similarly to the RF modeling framework (Table 4.4). CG lightning probability, air temperature and DC are confirmed as significant variables in the logistic regression models ($p < 0.05$). All three variables are positively correlated with fire ignitions, implying that the increase in the value of those variables (i.e. higher probability of CG lightning, higher air temperature and higher values of DC) ultimately leads to higher probability of fire ignitions. Although not ranked as the top predictor in RF results, $NDII_6$ is found to

have a significantly negative relationship with fire ignitions in both logistic models ($p < 0.05$). Other variables, like RH, rain, FFMC and fuel type covers are found significant in one of the two models. In particular, the fractional covers of woody and herbaceous components are positively related to the fire ignitions, while that of the nonvascular component has a negative relationship.

Table 4.4. Logistic regression results for the two models

Variables	**Current model**			**Previous model**		
	Estimate	Std. Error	Pr(>|z|)	Estimate	Std. Error	Pr(>|z|)
Intercept	-4.550	2.607	0.08	-2.003	2.367	0.7964
Lightning	5.428	0.591	< 2e-16 ***	3.430	0.543	1.0e-10 ***
$NDII_6$	-12.69	2.028	3.8e-10 ***	-18.360	5.581	6.4e-5 **
Rain	-0.136	0.064	0.0327*	-0.043	0.037	0.2083
Temp	0.166	0.053	0.0017 **	0.098	0.042	0.0211 *
RH	0.005	0.019	0.7910	-0.057	0.016	0.0001 ***
Wind	0.012	0.074	0.8657	-0.225	0.076	0.0029 **
FFMC	-0.029	0.016	0.0541	-0.034	0.014	0.0155 *
DMC	0.008	0.031	0.7814	0.0001	0.027	0.6910
DC	0.006	0.002	0.0002 ***	0.005	0.002	0.0027 **
Region (Seward)	-1.220	0.520	0.0190 *	-1.176	0.432	0.0047 **
Region (SW)	-0.192	0.793	0.8084	1.973	0.662	0.0071 **
Elevation	-0.002	0.001	0.0077 **	-0.001	0.001	0.0685
Aspect	-0.002	0.003	0.5904	-0.0004	0.003	0.8908
Woody	1.089	2.173	0.6163	0.073	1.793	0.7246
Herbaceous	3.625	1.953	0.0635	5.542	1.727	0.0005***
Nonvascular	-2.811	1.234	0.0223 *	-0.223	1.058	0.9110
Significance codes: 0 '***' 0.001 '**' 0.01 '*' 0.05						

A categorical variable "Region" was also included in the models to account for the potential variability across three major tundra regions, including the North Slope and Brook Range (referred as "North Slope"), Seward Peninsula and Kotzebue

Lowlands (referred as “Seward”), and Southwest Alaska (referred as “SW”) (Figure 3.1). Welch t-test results were summarized for environmental variables between “Fire” and “No fire” conditions for each tundra region in Table 4.5. The mean values of variables including CG lightning probability, air temperature, RH and vegetation indices for “Fire” and “No fire” conditions are consistently statistically separable across the three tundra regions with p-values below 0.05. In contrast, fire weather indices do not show significant differences of mean values between “Fire” and “No fire” conditions for the Seward Peninsula. Although topographical features and fuel type covers are less important in RF, their mean values of “Fire” and “No fire” events are significantly different, particularly slope, roughness, and woody component coverage.

Table 4.5. Welch t-test results across different tundra regions.

Variables	**North Slope**		**Seward Peninsula**		**Southwest Alaska**	
	t	**p-value**	**t**	**p-value**	**t**	**p-value**
Lightning (current)	-6.603	1.3e-6***	-5.113	5.9e-6***	-16.18	<2.2e-16***
Lightning (previous)	-2.337	0.0293*	-5.161	5.0e-6***	-6.414	6.9e-10***
Temperature (current)	-4.789	5.8e-5***	-1.142	0.2585	-16.59	<2.2e-16***
Temperature (previous)	-4.726	6.4e-5***	-2.410	0.0192*	-10.79	<2.2e-16***
RH (current)	2.985	0.0062**	0.819	0.4156	9.192	<2.2e-16***
RH (previous)	3.844	0.0007***	2.549	0.0134*	7.451	4.4e-13***
Rain (current)	-0.132	0.8961	4.487	8.9e-6***	3.755	0.0002**
Rain (previous)	2.215	0.0300*	-0.098	0.9225	4.461	1.0e-5***
Wind (current)	0.836	0.4121	-2.941	0.0045**	4.198	3.5e-5***
Wind (previous)	2.385	0.0246*	1.989	0.0519	3.523	0.0005**
FFMC (current)	-4.321	2.2e-5***	-1.571	0.1217	-9.433	<2.2e-16***

FFMC (previous)	-9.820	8.8e-5***	-0.021	0.9835	-8.876	<2.2e-16***
DMC (current)	-	-	-0.305	0.7616	-3.873	0.0001***
DMC (previous)	-	-	-0.280	0.7804	-3.375	0.0008***
DC (current)	-3.446	0.0007***	1.705	0.0933	0.601	0.5484
DC (previous)	-3.345	0.0010**	1.711	0.0921	0.735	0.463
ISI (current)	-6.010	1.1e-8***	0.162	0.8719	-9.587	<2.2e-16***
ISI (previous)	-6.497	9.1e-10***	0.341	0.7343	-8.502	2.7e-16***
BUI (current)	-3.807	0.0002***	-0.138	0.8905	-3.471	0.0006***
BUI (previous)	-3.664	0.0003***	-0.113	0.9107	-3.014	0.0027*
GVMI	2.124	0.0347*	3.879	0.0003***	8.981	<2.2e-16***
NDII6	4.043	7.9e-5***	3.916	0.0003***	8.002	9.6e-15***
NDII7	4.423	1.9e-5***	3.444	0.0012**	4.552	7.8e-6***
NDWI	3.111	0.0021**	3.278	0.0019**	5.414	1.0e-7***
Elevation	2.633	0.0088**	0.749	0.4569	-0.711	0.4775
Slope	2.200	0.0289*	3.679	0.0004***	3.394	0.0007***
Aspect	-2.903	0.0041**	-1.017	0.3147	2.832	0.0049*
Roughness	2.947	0.0035**	4.056	0.0001***	3.3943	0.0007***
Woody	-8.689	1.3e-15***	-5.661	4.9e-7***	9.818	<2.2e-16***
Herbaceous	-1.810	0.0717	-0.879	0.3835	-7.148	3.3e-12***
Nonvascular	9.525	<2.2e-16***	-0.441	0.6612	-13.08	<2.2e-16***
Significance codes: 0 ‘***’ 0.001 ‘**’ 0.01 ‘*’ 0.05						

Boxplots across different regions help with visualizing the extent in difference in environmental conditions between “Fire” and “No fire” settings. CG lightning probability values on both fire ignition days and the days before ignitions are significantly higher (p-value < 0.05 for all three regions) for fire ignition events (Figure 4.10 and Table 4.5). In particular, for the fire ignition days, the majority of the “No fire” events have CG lightning probabilities smaller than 0.25, while the

lightning probabilities for “Fire” events have an Interquartile Range (IQR) between 0 to 1, with mean values around 0.5.

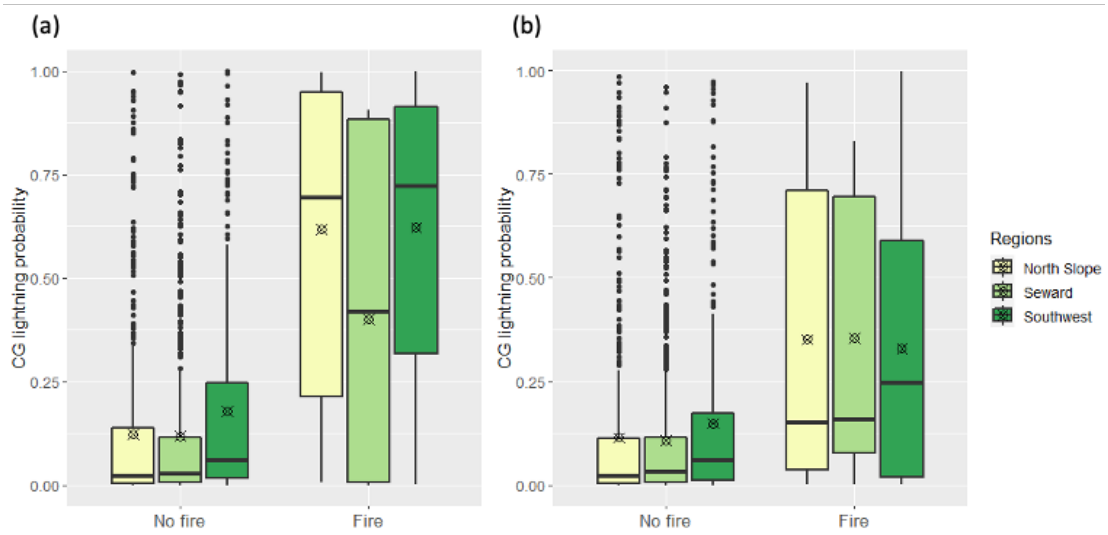

Figure 4.10. Boxplots of CG lightning probability between “Fire” and “No fire” conditions across three major fuel regions: (a) CG lightning probability on fire ignition day, (b) CG lightning on the previous day.

For near surface weather conditions, mean air temperature values are significantly higher while mean RH values are lower for “Fire” conditions for both the North Slope and Southwest Alaska regions (Figure 4.11 and Table 4.5). The values, however, do not differ significantly for the Seward Peninsula. Similarly, “Fire” conditions have significantly higher mean values of FFMC, ISI and BUI in the North Slope and Southwest Alaska (Figures 4.12 and 4.13). DMC and DC values of the “Fire” conditions are also higher than those of the “No fire” ones in the Southwest Alaska and North Slope. Mean values of the vegetation indices related fuel state are slightly but significantly lower within the “Fire” conditions compared to “No fire” (Figure 4.14).

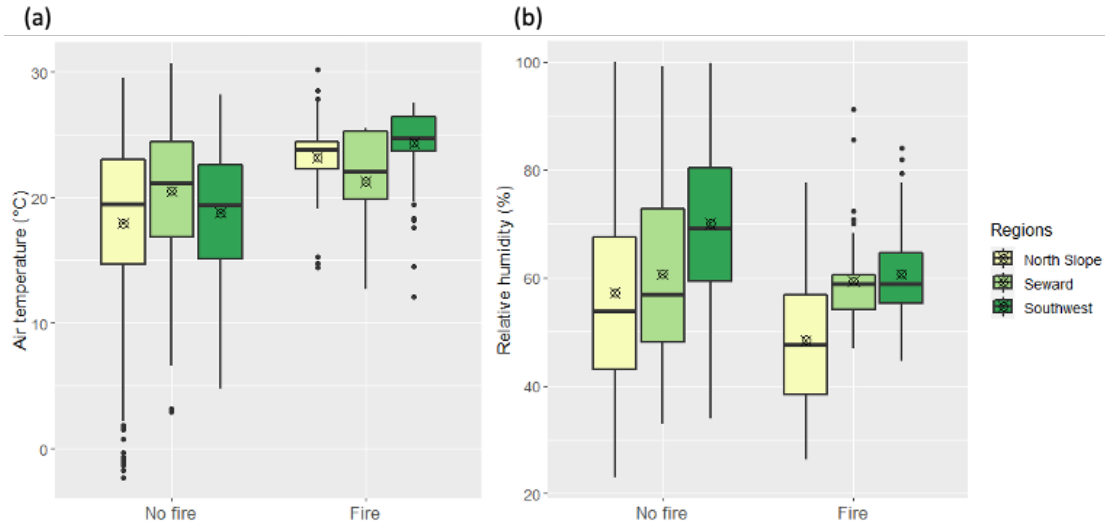

Figure 4.11. Boxplots of (a) air temperature and (b) RH on fire ignition days between "Fire" and "No fire" conditions across three major fuel regions.

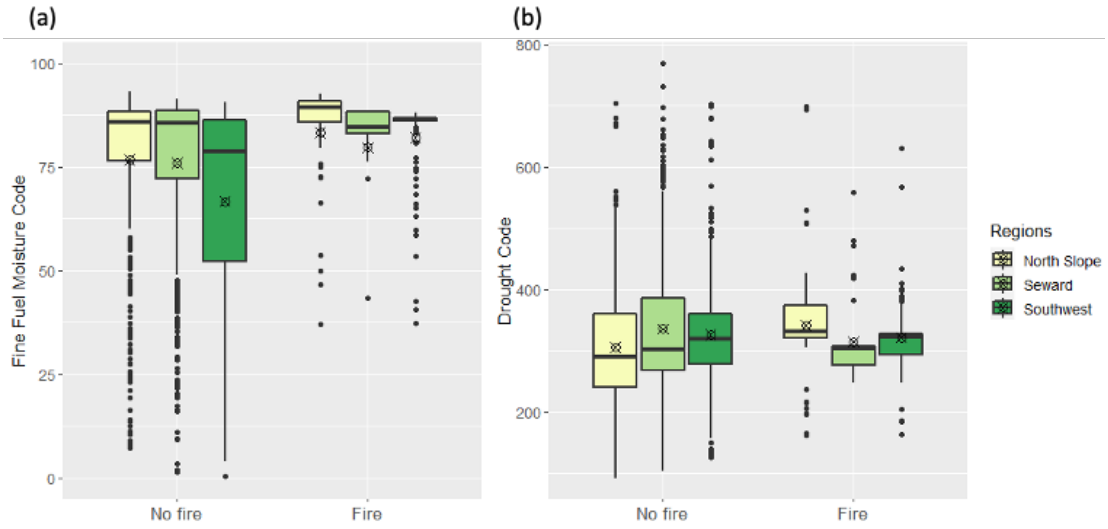

Figure 4.12. Boxplots of (a) FFMC and (b) DC on fire ignition days between "Fire" and "No fire" conditions across three major fuel regions.

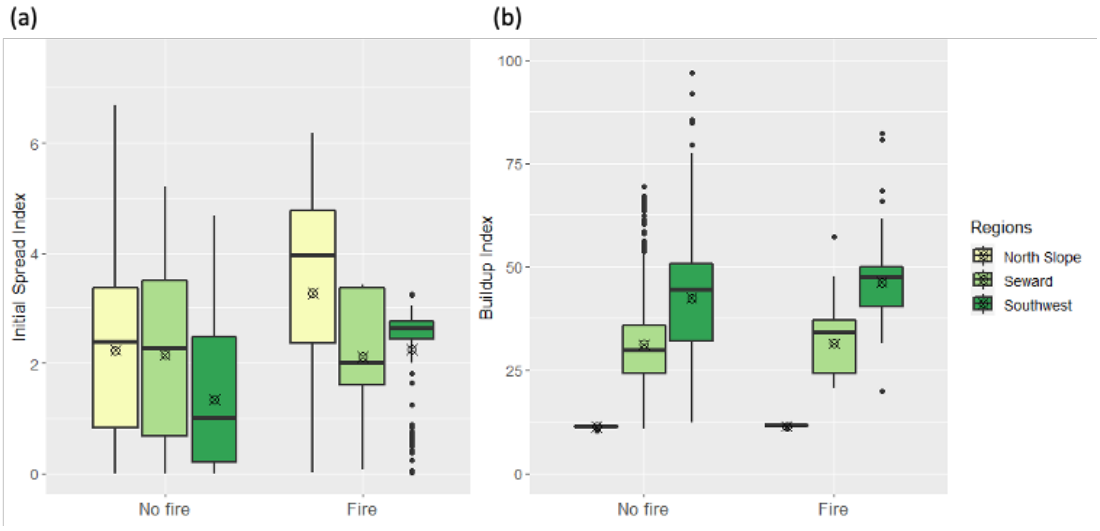

Figure 4.13. Boxplots of (a) ISI and (b) BUI on fire ignition days between "Fire" and "No fire" conditions across three major fuel regions.

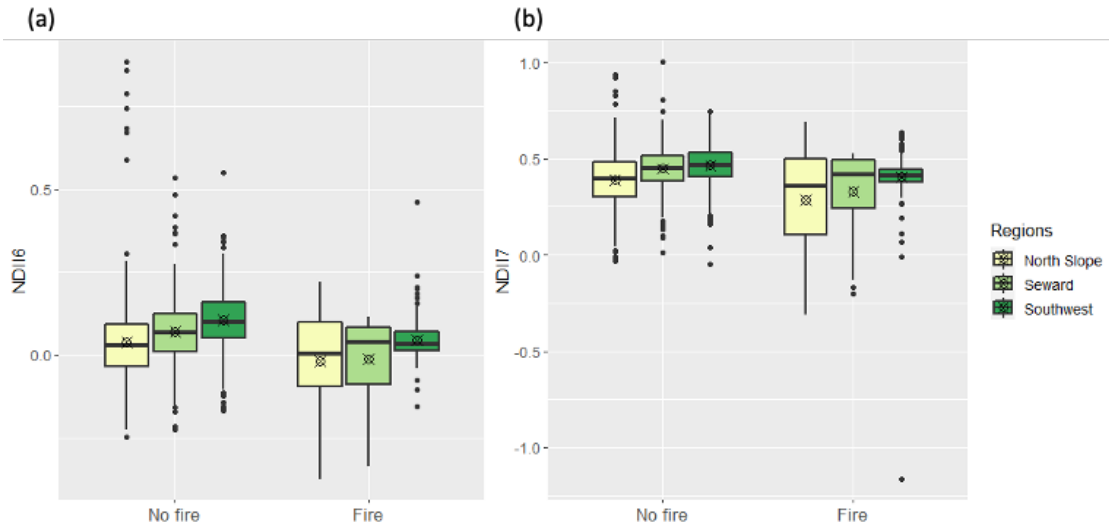

Figure 4.14. Boxplots of (a) $NDII_6$ and (b) $NDII_7$ on fire ignition days between "Fire" and "No fire" conditions across three major fuel regions.

Different from the variables described above, the overall patterns (higher or lower) of the mean fuel type coverages between "Fire" and "No fire" conditions vary across different regions (Figure 4.15), particularly for woody and nonvascular components. Although logistic regressions suggest positive relationship between

woody cover and fire ignition, “Fire” conditions in the North Slope and Seward Peninsula are linked to higher fractions of the woody component of the fuels, while those in the Southwest Alaska linked to the lower woody fuel fraction. Similarly, the significantly higher fraction of nonvascular plants is found within “Fire” conditions in the Southwest Alaska, but the relationship is reversed within the North Slope region.

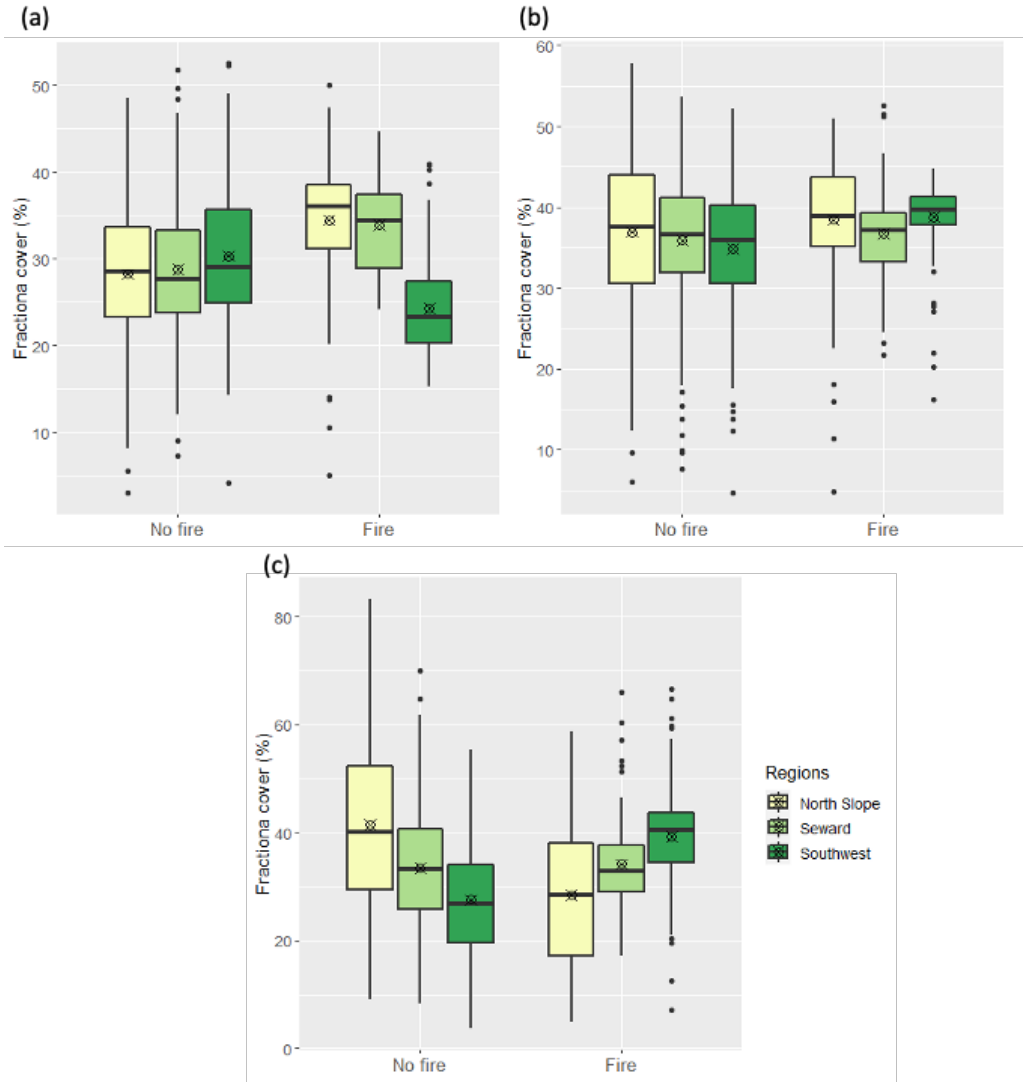

Figure 4.15. Boxplots of mean fractional covers of (a) woody component, (b) herbaceous, and (c) nonvascular components between “Fire” and “No fire” events across three major fuel regions.

4.6 Discussions

CG lightning is commonly assumed to be the primary source of ignition in the tundra ecosystems due to the remoteness of the region and the limited human activities. This study provides the first quantitative piece of evidence that fully justified this assumption, as the results from all models explored in this study point to CG lightning probability as the most influential factor that predicts fire ignition. This finding is also consistent with previous research conducted in the boreal forests of North America (Veraverbeke et al., 2017), while the role of ignition source is not always highlighted in research conducted for the other ecosystems (Díaz-avalos et al., 2001; Liu et al., 2012; Vecín-Arias et al., 2016). Previous studies have also established relationships between fires and lightning characteristics observed from ground-based detection networks, such as count of strikes, polarity, and peak current (Peterson et al., 2010). This study, whereas, suggest that the probability of CG lightning modeled purely with atmospheric variables is a powerful indicator of tundra fire potential.

Tundra is a very unusual environment with generally low temperatures and high water table, largely due to widespread underlying permafrost (Bliss et al., 1973; Wielgolaski and Goodall, 1997). This generally means that the ecosystems are rarely moisture limited and are not highly flammable. Evidences from both modeling and statistical analyses in this study emphasize the controls of warm and dry weather conditions over tundra fire ignitions in Alaska, with near surface air temperature and RH significantly related to fires. Higher temperature and lower moisture conditions have the potential to increase the flammability of the environment in general.

Similarly, the study of Masrur et al. (2018), which was conducted with reanalysis data at a coarser resolution and a larger spatial scale, indicated the same information. In addition to the impacts of air temperature and RH on fuel flammability, they might also reflect the high likelihood of convective potential which in turn leads to atmospheric instability and ultimately CG lightning.

In addition, the dominant fuels in the tundra are composed of herbaceous (grass and sedge) and dwarf shrub components (Innes, 2013), which are considered fine fuels as defined in the CFFWIS. FFMC is designed to describe the fine surface fuels in boreal forests (Lawson and Armitage, 2008). Larger FFMC values indicate higher flammability of the fine fuels. FFMC values with the "Fire" conditions in this study are generally higher than 70, typically representing dry fuels (Lawson and Armitage, 2008). This also shows the suitability of FFMC in describing the moisture conditions of tundra fuels. Therefore, it is not surprising that FFMC is highlighted as a highly predictive variable and the most influential among all fire weather indices in assessing fire ignition probability for the tundra. It is also important, that DC – a variable that tracks deeper drying of fuels and longer local "drought" conditions – has been shown to be responsive to changes in deep moisture levels in the tundra. Since DC is a slow-reacting and representative of the long-term dry conditions (Lawson and Armitage, 2008), its significance in the logistic regression models suggests that long-term dry conditions accumulated for days are also driving the ignition probability. All fire weather indices have been developed for boreal forest ecosystems and their ability to forecast tundra conditions has been most generally assumed rather than

tested. This study shows that both FFMC and DC provide a reasonable approximation of changes in fuel state that can more readily support fire ignition.

The inconsistency of the role of vegetation indices representing fuel moisture between different models indicates that remote sensing-based indices may not be a good representative of the fuel moisture state. Fuel type distributions also show different patterns between "Fire" and "No fire" conditions across the three major tundra regions. Though the flammability of vegetation composites varies according to experiment results (Sylvester and Wein, 1981), these patterns suggest that the interactions of fuel and weather can be more important in driving fire ignitions than the fuel type itself.

More importantly, this study has demonstrated the effectiveness and the strong capability of modeling fire ignition probability with WRF-simulated weather conditions in the remote tundra regions across space and time. The key role of CG lightning probability identified from the models suggests that current fire management efforts are inadequate regarding the integration of CG lightning probability in fire danger monitoring and modeling for the ecosystems in the HNL. By monitoring lightning potential, temperature and dry conditions, it is promising that fire ignition probability can be predicted with high accuracy in remote regions at 5km resolution with WRF. Besides, modeling experiments with two types of dynamic variables – on fire ignition days and one day before ignition – show that using data simulated from one day earlier can still achieve acceptable prediction results for estimating fire ignition probability. This suggests that by using data acquired before fire starts, the method developed from this study can still capture the probability of

fire ignition very well, indicating the potential improvement of fire forecasting performance.

Although existing efforts have incorporated lightning characteristics in fire modeling by matching recorded lightning strikes and fires (Peterson et al., 2010; Wotton and Martell, 2005), this research suggests the suitability of using simulated CG lightning probability for modeling fire ignitions for several reasons. First, modern ground-based lightning detection networks typically have a location accuracy ranging from below 1km to 4km and a detection efficiency of between 70% and over 90% (Biagi et al., 2007; Dissing and Verbyla, 2003; Koshak et al., 2015; Nag et al., 2014). This indicates that CG lightning strikes may not always be recorded by the system and that the strike location may not be accurately triangulated. Therefore, commonly used matching methods to link lightning characteristics and ignitions can miss the lightning strikes that actually ignite the fires, which would introduce errors and uncertainties when using detected lightning characteristics in the modeling. The selection of matching methods could also affect the results (Moris et al., 2020). Third, simulation of lightning characteristics has not been developed based on existing numerical weather prediction models, which limits the potential of integrating them for fire ignition modeling and forecasting.

Despite the capability of WRF simulated weather conditions in modeling fire ignition in this study, previous research questioned the suitability of utilizing WRF for calculating fire weather indices due to its limitations in accurate simulation of wind and precipitation (Mölders, 2010; Simpson et al., 2014). However, simulating weather variables with NWPs is probably the only available method for describing

near-surface conditions in the data-scarce regions with very sparsely distributed stations like Alaskan tundra.

Previous work has also found that lightning and fire weather are associated with synoptic-scale atmospheric circulation patterns in the HNL (Balzter et al., 2005; Fauria and Johnson, 2006; Hayasaka et al., 2016; Kim et al., 2020; Kochtubajda et al., 2019). Since this study has shown the importance of meteorological variables in predicting fire ignitions in the tundra, future work needs to be done to understand the synoptic weather conditions that drive the dynamic changes of lightning and fire weather, to improve our understanding about the mechanisms of wildland fires in the pan-Arctic ecosystems.

4.7 Conclusions

This study explores the key drivers of wildland fire ignitions in Alaskan tundra from 2001 to 2019 by modeling the impacts of environmental factors on fire ignition probability. Specifically, I consider environmental variables related to fuel type distribution, fuel state, fire weather, topography, and ignition source. Among all environmental factors, CG lightning probability is found to be the most important driver of tundra fire ignitions in Alaskan from 2001 to 2019. Higher CG lightning probability shows a significant positive relationship with fire ignition probability. In addition, warmer and drier weather conditions are also found to be important in determining fire ignitions. In particular, air temperature, FFMC, and DC show significant positive relationships in modeling fire ignition probability, while RH is negatively related with the ignition. Moreover, the empirical RF models developed in this study have shown a strong capability in predicting fire ignition probability, given

the input static variables (fuel types and topographical features) and dynamic variables (CG lightning probability and weather) simulated with WRF on both fire ignition day and one day before. The findings of this study highlight the necessity of incorporating CG lightning modeling and emphasize the benefits of WRF simulation for wildland fire monitoring efforts in data-scarce regions like Alaskan tundra. Future efforts need to be undertaken to improve both the modeling capability and understanding of the synoptic-scale climatic patterns that drive tundra fire ignitions.

Chapter 5: Conclusion

5.1 Major research findings

The objective of this dissertation was to advance the scientific understanding of wildland fire ignition in the tundra ecosystems of the High Northern Latitudes (HNL). Specifically, this dissertation focused on addressing the overarching scientific question: "*What environmental factors and mechanisms drive wildland fire ignitions in Alaskan tundra?*" To achieve my dissertation objective, I explored three integrated research questions that took advantage of a large data archive of satellite observations and Numerical Weather Prediction (NWP) modeling. The research questions were outlined in Section 1.4 of Chapter 1 and described in detail in Chapters 2 – 4.

The development of the fractional coverage product of fuel type components in Chapter 2 was driven by the lack of efforts in describing the detailed distribution of fuel type compositions in Alaskan tundra, where the surface vegetation fuels are highly mixed. Although categorical fuel classification systems have been developed for years at 30m resolution for the entire Alaska (Anderson, 1982; Hirsch, 1996; Ottmar et al., 2007; Scott and Burgan, 2005), their applications in the tundra are limited. This is mainly because the systems were designed to describe fuel components for the forests, and categorical values were not representative for highly mixed surface fuel distribution. Recent efforts have elaborated on developing fractional cover products of vegetation types (Beck et al., 2011; Berner et al., 2018; Macander et al., 2017). However, these maps were limited to certain regions (e.g., the

North Slope) and thus not helpful for answering of my overall research question, which relates to the entire Alaskan tundra ecosystems.

To overcome these limitations, I combined field observations collected by our team during three fieldtrips in the tundra, and Landsat 8 surface reflectance data from 2013 to 2018 to develop a fuel type distribution product that covers the entire Alaskan tundra circa 2015. I first generated mosaicked composites of the study area from more than 1800 Landsat 8 tiles for three seasons (pre-growing, peak-growing and post-growing) extracted from phenology information based on Moderate Resolution Imaging Spectroradiometer (MODIS) observations. I was then able to map the fractional cover distributions of three major fuel components, including wood (evergreen and deciduous shrub), herbaceous (sedge and grass) and nonvascular (lichen and moss). My mapping results not only capture the detailed spatial variations of vegetation fuel type components, but also depict the overall distributions of the related vegetation communities along the latitudes. The published manuscript (He et al., 2019) and data product (He et al., 2020) can support other tundra fire studies in the future.

In addition to fuel type, I explored the primary ignition source of wildfires, cloud-to-ground (CG) lightning strikes, in the HNL in Chapter 3 of this dissertation. Despite the important role of lightning in igniting wildfires in the tundra, CG lightning has never been examined specifically for this ecosystem. Although several previous studies have modeled CG lightning activity in the boreal forests of North America (Blouin et al., 2016; Burrows et al., 2005; Reap, 1991), their findings are not suitable for explaining lightning potential tundra, because of the different land-

atmospheric interactions in the two landscapes (Rivas Soriano et al., 2019; Van Heerwaarden and Teuling, 2014). Considering the downscaling and forecasting capability of the Weather Research and Forecast (WRF) model, I designed an empirical-dynamical framework to model CG lightning probability in the tundra through the integration of WRF and random forest (RF) algorithm and to understand the atmospheric factors driving lightning occurrence.

To achieve my goals, I first conducted a sensitivity analysis method to identify an optimized parameterization setting of WRF simulation for Alaskan tundra. After comparing the statistical metrics calculated between WRF simulated variables and observations from the Remote Automatic Weather Stations (RAWS) for several case studies, I decided to utilize the Thompson 2-moment and the Mellor-Yamada-Janjic (MYJ) schemes to represent the microphysics and Planetary Boundary Layer (PBL) physics options, respectively. I then identified case studies from lightning days with three different severity levels. WRF simulations were run for these cases to extract four groups of predictors for modeling CG lightning probability: cloud properties, meteorological variables at multiple pressure levels, atmospheric stability indices, and existing lightning parameterization schemes in WRF. I developed two RF models using variables simulated at 24hrs and 48hrs after WRF initialization time for comparison. Both models have shown strong capability of capturing CG lightning distribution in the tundra, with the parcel lifted index as the most important factor driving lighting distribution.

After achieving the first two objectives, in Chapter 4, I explored the environmental factors driving wildland fires ignitions in Alaskan tundra, which is also

the overarching research question. Although the factors driving boreal forest fires have been extensively studied around the globe at different scales (Balzter et al., 2005; Kim et al., 2020; Liu et al., 2012; Veraverbeke et al., 2017), much less is known for tundra fires. Recently, Masrur et al. (2018) examined the climatic factors contributing to tundra fire activity across the circumpolar Arctic region and found that warm and dry conditions important through statistical analyses and RF modeling. Despite their efforts on understanding climatic conditions suitable for tundra burning, more work is required to understand the mechanisms behind the fires. Contemporary modeling studies are also needed for accurate characterization of fire ignition probability in the tundra and for improved understanding of the driving factors that control tundra fire ignitions.

In this study, I considered four types of environmental factors related to fire ignitions: ignition source, fuel conditions (fuel type and moisture state), weather and topographical features. I utilized the empirical-dynamical framework developed in Chapter 3 to model CG lightning probability, as a representative of ignition source. Remote sensing based products were used to describe fuel conditions: fractional cover product from Chapter 2 to map fuel type distribution, and MODIS-derived vegetation indices to estimate fuel moisture state. Due to the lack of weather stations in the remote tundra, weather conditions, including both near-surface weather variables and the Canadian Forest Fire Weather Index System (CFFWIS), were extracted and calculated using the WRF simulated outputs at 5km resolution. I obtained the Interferometric Synthetic Aperture Radar (IfSAR) Digital Elevation Model (DEM) product to generate topographical features. After preparing all these

environmental factors, I utilized both RF and logistic regression methods to understand the roles of each factor in driving fire ignition probability. I identified the probability of CG lightning as the most important driver of fire ignitions, followed by warm and dry weather conditions. Both near-surface weather and fire weather indices have shown that fire ignitions tend to occur with higher air temperature, lower relative humidity (RH), higher Fine Fuel Moisture Code (FFMC), and higher Drought Code (DC). In addition to exploring the drivers, I developed two RF models using dynamic weather variables extracted on fire ignition day and one day before fire ignition, both of which have shown strong capability of predicting fire ignitions in the tundra. My results also highlight that incorporating the modeling of CG lightning potential is critical for fire monitoring and management efforts in the HNL.

5.2 Contribution to Broader Arctic Science Research

The Arctic region has experienced a higher rate of climate warming than the global average, as recorded by surface air temperature during the last two decades (Meredith et al., 2019). The warming in the Arctic has led to increasing loss of sea ice and glaciers, permafrost thawing, disturbances and carbon emissions, which can in return contribute to amplified warming and threaten the human communities and wildlife according to the Intergovernmental Panel on Climate Change (IPCC) report (Meredith et al., 2019). In particular, this report highlights the role of wildfire as a major driver among all disturbance types in regularly affecting the terrestrial ecosystems at the continental scale across the HNL, with increasing wildfire activity linked with climate warming (Randerson et al., 2006; Veraverbeke et al., 2017). To address the impacts of climate change on the Arctic, multiple agencies and

organizations, including the National Aeronautics and Space Administration (NASA), Department of Energy (DOE), National Research Council of the National Academies of Sciences and the Interagency Arctic Research Policy Committee (IARPC), have started specific scientific programs aimed at understanding the underlying processes and potential influences of ecosystem changes in the HNL.

The Arctic-Boreal Vulnerability Experiment (ABoVE) program initiated by NASA focuses on studying the terrestrial ecosystems of tundra and boreal forests in the HNL of North America. The ultimate goal of this program is to improve our understanding of the complex ecosystem processes and to prepare the society with rapid response and adaptation to the environmental and social changes at present and in the future (ABoVE, 2014). In particular, understanding the driving mechanisms and potential influences of wildfire disturbance regimes in the HNL responds to one of the key science questions of ABoVE (ABoVE, 2014): "*What processes are contributing to changes in disturbance regimes and what are the impacts of these changes?"* As part of the Next-Generation Ecosystem Experiments (NGEE) program funded by DOE, NGEE Arctic focuses on advancing the predictive understanding and the modeling capability of the climate and ecosystem on Earth. One of the key science questions of the NGEE Arctic also aims to address: "*What controls the vulnerability and resilience of Arctic ecosystems to disturbance, and how do disturbances alter the physical and ecological structure and function of these ecosystems?"*

Both questions from the two programs align very well with the underlying theme of this dissertation on advancing the understanding of factors driving wildfires

in the HNL. Besides, both programs emphasize the need for advancing the integrated modeling capabilities of the Arctic ecosystems to support future projections of climate change (Fisher et al., 2018). This dissertation has made the first efforts of contemporary modeling for wildfire ignitions and examined the driving factors of fires in Alaskan tundra, which supports the goals of these programs. The research findings of this dissertation, including the developed methods, models, and data product, provides the groundwork for an improved understanding of the contributors of tundra fires in Alaska, as well as a systematic modeling framework of fire danger prediction for the future.

5.3 Implications for fire management efforts in the HNL

The results of this dissertation provide insights from multiple perspectives for wildfire management efforts in both the tundra and the forest forests of the HNL. First, the empirical-dynamical modeling framework developed based on WRF and machine learning method in this study has demonstrated a strong capability of predicting wildfires in the data-poor regions and can be adopted easily for fire danger monitoring. The models developed with variables acquired on different dates in this dissertation also show potential for earlier prediction of lightning and fire ignition probabilities. However, since tundra weather typically fluctuates on a weekly basis, the performance of the modeling can be primarily affected by the capability of accurate weather forecasting with WRF. Additionally, modeling fire ignition is an essential start for estimating fire spread and quantifying carbon emissions and air quality impacts on human communities.

Second, the critical drivers of wildfire ignitions identified in this dissertation highlight the crucial roles of simulated weather conditions for fire danger modeling and prediction. CG lightning has been identified as the primary control of tundra fires in this dissertation and of boreal forest fires in previous studies (Veraverbeke et al., 2017). This dissertation makes the first attempt in contemporary modeling of tundra fire ignitions with CG lightning incorporated in the modeling system. However, the existing fire practices of CG lightning monitoring and modeling adopted by the fire management teams are not sufficient for supporting fire danger prediction in the HNL, where the fires are primarily ignited by lightning strikes. Current fire danger monitoring efforts in the HNL of North America mainly rely on the Canadian Forest Fire Danger Rating System (CFFDRS), in which lightning has been involved with the ground-based detection networks. Other attempts that integrated characteristics of lightning strikes have been made (Castedo-Dorado et al., 2011; Vecín-Arias et al., 2016; Wotton and Martell, 2005). This dissertation, nevertheless, suggests that CG lightning potential could be a better way of dealing with the ignition source in the models compared to the detected locations or characteristics of CG lightning strikes. Other factors like near-surface weather and commonly used CFFWIS simulated by WRF can greatly support fire danger monitoring. However, more work needs to be conducted to improve the WRF simulation for tundra environmental modeling and calibrating CFFWIS for representing the actual fire danger in the tundra.

Moreover, the methodology and data product developed in this dissertation for mapping fuel type distribution can be applied for monitoring and updating fuel conditions regularly at a large spatial scale, which can benefit the fire monitoring

efforts as well. Integration of Landsat 8 and Sentinel-2A/B imagery can achieve an average revisit time of about three days (Li and Roy, 2017), which can provide more data resources for accurate characterization of fuel type distribution and even fuel moisture state at 10 – 30m resolution. Fuel type system specifically developed for the tundra will also be necessary for determining the fuel characteristics in this region.

5.4 Future research directions

The key theme of this dissertation is to uncover the underlying processes and factors that control the ignition potential of wildland fires in the remote Alaskan tundra. According to the results of this dissertation, CG lightning is the most critical factor that leads to fire ignitions in the tundra. The ignition probability is then affected by warm and dry weather conditions, as indicated by higher temperature, lower RH, and higher fuel moisture codes (FFMC and DC) from CFFWIS. The primary control of these weather variables on the tundra fires in Alaskan strongly suggests that further research on synoptic weather and atmospheric circulation patterns driving these factors and processes is crucial for improving our understanding of underlying mechanisms behind these environmental factors. Previous studies have either explored the synoptic-scale weather patterns related to lighting or fire weather conditions in boreal forests (Flannigan and Wotton, 2001; Hayasaka et al., 2016; Kochtubajda et al., 2019) or explored the impacts of teleconnections on boreal forest fires (Balzter et al., 2005; Fauria and Johnson, 2008, 2006; Kim et al., 2020). However, these patterns have never been explored for the tundra fires across the entire pan-Arctic region. Further efforts need to be made to

gain a thorough understanding of the processes contributing to fire disturbances in the tundra.

Moreover, the interactions and feedbacks among different factors, including fires, surface fuels, weather, and climate, are worth of exploring to improve both our understanding and modeling capability of tundra fires in the future. In Chapter 4, the different responses of fire or no fire events to fuel type components in different tundra regions suggests the roles of the weather and fuel interactions in driving fire ignitions. French et al. (2015) have already shown that fire weather in Alaskan tundra will become more suitable for burnings under climate warming, regardless of the mitigation strategies. Vegetation communities could also shift in the tundra as a consequence of climate warming and fire disturbances (Kittel et al., 2000; Van Der Kolk et al., 2016), which could further affect fire activities by altering fuel type and load. Additionally, climate change can affect future CG lightning activity as well, although there is a lack of consensus on its future trends (Finney et al., 2018; Romps et al., 2014).

In addition to further efforts on understanding science, more work needs to be accomplished to improve the modeling and predicting capability of fires for resource management. Due to the vegetation shifts in the tundra, fuel type distribution and fuel load products should be updated regularly for accurate characterization to support fire ignition and spread modeling and post-fire impact assessment. The combination of Landsat 8 and Sentinel 2 imagery can provide frequency observations in the HNL at 10 – 30m resolution, which will benefit the mapping of fuel type and load mapping across a large spatial scale. More field campaigns, if possible, will also be necessary

for collecting measurements in the remote tundra to support mapping and validation efforts. Calibration and modification of WRF-simulated CFFWIS for the tundra will also be necessary for representing fuel moisture conditions and fire danger potential. The methodology framework developed in this study provides opportunities for modeling fire potential in other data-scarce regions as well.

Appendices

Table S1. Statistical metrics for sensitivity analysis for air temperature (°C)

Metrics	Schemes	2006	2007	2010	2015
Correlation	Morrison_MYJ	0.8516	0.8746	0.8188	0.8871
	Morrison_YSU	0.8177	0.8265	0.8125	0.8847
	Thompson_MYJ	0.853	0.8719	0.8198	0.8876
	Thompson_YSU	0.8223	0.8325	0.8152	0.8848
	WRF6_MYJ	0.7991	0.8566	0.8149	0.8827
	WRF6_YSU	0.7814	0.7953	0.8037	0.8773
RMSE	Morrison_MYJ	2.5009	3.4409	3.3134	2.3018
	Morrison_YSU	2.7685	3.9639	3.3512	2.2776
	Thompson_MYJ	2.5057	3.4206	3.3084	2.3047
	Thompson_YSU	2.7367	3.8569	3.3304	2.2789
	WRF6_MYJ	2.9804	4.0524	3.3782	2.2872
	WRF6_YSU	3.0685	4.6816	3.4462	2.2829
MAE	Morrison_MYJ	1.9731	2.5993	2.5481	1.9007
	Morrison_YSU	2.2029	2.9851	2.6099	1.8639
	Thompson_MYJ	1.9625	2.6014	2.5394	1.9041
	Thompson_YSU	2.191	2.9136	2.5855	1.8678
	WRF6_MYJ	2.3314	3.0725	2.5779	1.8877
	WRF6_YSU	2.4759	3.5405	2.6031	1.8653

Table S2. Statistical metrics for sensitivity analysis for dew point temperature (°C)

Metrics	Schemes	2006	2007	2010	2015
Correlation	Morrison_MYJ	0.8473	0.8058	0.2955	0.7083
	Morrison_YSU	0.8294	0.7961	0.2756	0.6761
	Thompson_MYJ	0.8505	0.7973	0.3024	0.7104
	Thompson_YSU	0.8314	0.7986	0.2823	0.678
	WRF6_MYJ	0.86	0.7888	0.2678	0.7097
	WRF6_YSU	0.8411	0.7645	0.2714	0.6771
RMSE	Morrison_MYJ	2.1353	2.1616	3.5545	1.6217
	Morrison_YSU	2.3401	2.202	3.7679	1.7151
	Thompson_MYJ	2.108	2.1449	3.5528	1.6147
	Thompson_YSU	2.3463	2.1009	3.7681	1.709
	WRF6_MYJ	2.2026	2.5742	3.6068	1.6179
	WRF6_YSU	2.4036	2.7192	3.7989	1.7119
MAE	Morrison_MYJ	1.6818	1.6496	2.405	1.257
	Morrison_YSU	1.7835	1.6777	2.5472	1.2803
	Thompson_MYJ	1.6072	1.6539	2.3997	1.2506
	Thompson_YSU	1.763	1.6157	2.5433	1.2817
	WRF6_MYJ	1.7363	2.0049	2.3924	1.251
	WRF6_YSU	1.854	2.1117	2.5506	1.28

Table S3. Statistical metrics for sensitivity analysis for relative humidity (%)

Metrics	Schemes	2006	2007	2010	2015
Correlation	Morrison_MYJ	0.7786	0.7184	0.8504	0.8217
	Morrison_YSU	0.7382	0.7037	0.8479	0.8212
	Thompson_MYJ	0.7567	0.7365	0.848	0.822
	Thompson_YSU	0.7436	0.7012	0.8407	0.8222
	WRF6_MYJ	0.7257	0.7545	0.8133	0.8232
	WRF6_YSU	0.7074	0.6949	0.8292	0.8217
RMSE	Morrison_MYJ	12.552	18.672	11.317	9.6938
	Morrison_YSU	13.737	18.823	12.093	9.8978
	Thompson_MYJ	13.173	18.507	11.42	9.6969
	Thompson_YSU	13.714	18.663	12.299	9.8849
	WRF6_MYJ	13.892	18.275	12.046	9.6362
	WRF6_YSU	14.503	18.724	12.147	9.8568
MAE	Morrison_MYJ	9.1164	14.65	8.7566	7.4311
	Morrison_YSU	10.289	15.226	9.2098	7.5925
	Thompson_MYJ	9.5386	14.489	8.8432	7.446
	Thompson_YSU	10.018	14.984	9.5095	7.5872
	WRF6_MYJ	10.328	14.559	9.6644	7.3945
	WRF6_YSU	10.648	15.093	9.2811	7.5548

Table S4. Statistical metrics for sensitivity analysis for downward solar radiation (shortwave and longwave, W/m^2)

Metrics	Schemes	2006	2007	2010	2015
Correlation	Morrison_MYJ	0.697	0.8255	0.6532	0.8368
	Morrison_YSU	0.6738	0.8203	0.6473	0.8415
	Thompson_MYJ	0.6804	0.8179	0.6642	0.8352
	Thompson_YSU	0.657	0.8066	0.6621	0.8405
	WRF6_MYJ	0.6447	0.807	0.6455	0.835
	WRF6_YSU	0.5894	0.7761	0.6343	0.8393
RMSE	Morrison_MYJ	153.06	152.03	187.82	158
	Morrison_YSU	158	154.05	187.07	155.81
	Thompson_MYJ	164.74	155.36	185.41	158.73
	Thompson_YSU	168.67	159.86	178.57	156.02
	WRF6_MYJ	161.14	162.61	190.53	158.9
	WRF6_YSU	178.66	173.71	189.71	156.99
MAE	Morrison_MYJ	93.529	83.737	120.51	74.334
	Morrison_YSU	98.417	86.255	118.22	73.847
	Thompson_MYJ	101.92	85.681	116.75	75.247
	Thompson_YSU	105.304	91.491	113.74	74.281
	WRF6_MYJ	98.185	93.542	123.87	75.081
	WRF6_YSU	108.03	99.16	121.95	74.061

Bibliography

ABoVE, 2014. A Concise Experiment Plan for the Arctic-Boreal Vulnerability Experiment. http://above.nasa.gov/acep/acep_final_pdf.pdf. Accessed 1/25/2015.

Adámek, M., Jankovská, Z., Hadincová, V., Kula, E., Wild, J., 2018. Drivers of forest fire occurrence in the cultural landscape of Central Europe. Landsc. Ecol. 33, 2031–2045. https://doi.org/10.1007/s10980-018-0712-2

Ager, A.A., Barros, A.M.G., Day, M.A., Preisler, H.K., Spies, T.A., Bolte, J., 2018. Analyzing fine-scale spatiotemporal drivers of wildfire in a forest landscape model. Ecol. Modell. 384, 87–102. https://doi.org/https://doi.org/10.1016/j.ecolmodel.2018.06.018

Alaska Department of Fish and Game, 2006. Our Wealth Maintained: A Strategy for Conserving Alaska's Diverse Wildlife and Fish Resources 1–25.

Anderson, H.E., 1982. Fire Behavior Fuel Model Descriptions B1–B7.

Anderson, K., 2002. A model to predict lightning-caused fire occurrences. Int. J. Wildl. Fire 11, 163–172.

Anderson, K., 1992. Forecasting Lightning Occurrence and Frequency 1–18.

Anderson, K., Martell, D.L., Flannigan, M.D., Wang, D., 2000. Modeling of Fire Occurrence in the Boreal Forest Region of Canada, in: Fire, Climate Change, and Carbon Cycling in the Boreal Forest. pp. 357–367.

Anderson, K.R., 1991. Models to predict lightning occurrence and frequency over Alberta. M.Sc. thesis. University of Alberta. 91 pp.

Andersson, T., Andersson, M., Jacobsson, C., Nilsson, S., 1989. Thermodynamic indices for forecasting thunderstorms in southern Sweden. Meteorol. Mag. 118, 141–146.

Baig, M.H.A., Zhang, L., Shuai, T., Tong, Q., 2014. Derivation of a tasselled cap transformation based on Landsat 8 at-satellite reflectance. Remote Sens. Lett. 5, 423–431. https://doi.org/10.1080/2150704X.2014.915434

Baker, M.B., Blyth, A.M., Christian, H.J., Latham, J., Miller, K.L., Gadian, A.M., 1999. Relationships between lightning activity and various thundercloud parameters: Satellite and modelling studies. Atmos. Res. 51, 221–236. https://doi.org/10.1016/S0169-8095(99)00009-5

Balzter, H., Gerard, F.F., George, C.T., Rowland, C.S., Jupp, T.E., McCallum, I., Shvidenko, A., Nilsson, S., Sukhinin, A., Onuchin, A., Schmullius, C., 2005. Impact of the Arctic Oscillation pattern on interannual forest fire variability in Central Siberia. Geophys. Res. Lett. 32, 1–4. https://doi.org/10.1029/2005GL022526

Barbero, R., Abatzoglou, J.T., Steel, E.A., Larkin, N.K., 2014. Modeling very large-fire occurrences over the continental United States from weather and climate

forcing. Environ. Res. Lett. 9. https://doi.org/10.1088/1748-9326/9/12/124009

Barthe, C., Deierling, W., Barth, M.C., 2010. Estimation of total lightning from various storm parameters: A cloud-resolving model study. J. Geophys. Res. Atmos. 115, 1–17. https://doi.org/10.1029/2010JD014405

Bates, B.C., Dowdy, A.J., Chandler, R.E., 2018. Lightning prediction for Australia using multivariate analyses of large-scale atmospheric variables. J. Appl. Meteorol. Climatol. 57, 525–534. https://doi.org/10.1175/JAMC-D-17-0214.1

Beamish, A., Coops, N., Chabrillat, S., Heim, B., 2017. A Phenological Approach to Spectral Differentiation of Low-Arctic Tundra Vegetation Communities, North Slope, Alaska. Remote Sens. 9, 1200. https://doi.org/10.3390/rs9111200

Beck, P.S.A., Horning, N., Goetz, S.J., Loranty, M.M., Tape, K.D., 2011. Shrub Cover on the North Slope of Alaska: a circa 2000 Baseline Map. Arctic, Antarct. Alp. Res. 43, 355–363. https://doi.org/10.1657/1938-4246-43.3.355

Beringer, J., Chapin, F.S., Thompson, C.C., McGuire, A.D., 2005. Surface energy exchanges along a tundra-forest transition and feedbacks to climate. Agric. For. Meteorol. 131, 143–161. https://doi.org/10.1016/j.agrformet.2005.05.006

Berner, L.T., Jantz, P., Tape, K.D., Goetz, S., 2018. Tundra plant aboveground biomass and shrub dominance mapped across the North Slope of Alaska. Environ. Res. Lett. 13, 035002. https://doi.org/10.1088/1748-9326/aaaa9a

Bhatt, U.S., Walker, D.A., Raynolds, M.K., Bieniek, P.A., Epstein, H.E., Comiso, J.C., Pinzon, J.E., Tucker, C.J., Polyakov, I. V., 2013. Recent declines in warming and vegetation greening trends over pan-arctic tundra. Remote Sens. 5, 4229–4254. https://doi.org/10.3390/rs5094229

Biagi, C.J., Cummins, K.L., Kehoe, K.E., Krider, E.P., 2007. National Lightning Detection Network (NLDN) performance in southern Arizona, Texas, and Oklahoma in 2003-2004. J. Geophys. Res. Atmos. 112, 1–17. https://doi.org/10.1029/2006JD007341

Bieniek, P.A., Bhatt, U.S., Walsh, J.E., Rupp, T.S., Zhang, J., Krieger, J.R., Lader, R., 2016. Dynamical Downscaling of ERA-Interim Temperature and Precipitation for Alaska. J. Appl. Meteorol. Climatol. 55, 635–654. https://doi.org/10.1175/JAMC-D-15-0153.1

Bliss, L.C., Courtin, G.M., Pattie, D.L., Riewe, R.R., Whitfield, D.W.A., Widden, P., 1973. Arctic Tundra Ecosystems, in: Annual Review of Ecology and Systematics. pp. 359–399.

Blouin, K.D., Flannigan, M.D., Wang, X., Kochtubajda, B., 2016. Ensemble lightning prediction models for the province of Alberta, Canada. Int. J. Wildl. Fire 25, 421–432. https://doi.org/10.1071/WF15111

Bond-Lamberty, B., Peckham, S.D., Ahl, D.E., Gower, S.T., 2007. Fire as the dominant driver of central Canadian boreal forest carbon balance. Nature 450, 89–92. https://doi.org/10.1038/nature06272

Bourgeau-Chavez, L.L., Leblon, B., Charbonneau, F., Buckley, J.R., 2013. Evaluation of polarimetric Radarsat-2 SAR data for development of soil moisture retrieval algorithms over a chronosequence of black spruce boreal forests. Remote Sens. Environ. 132, 71–85. https://doi.org/https://doi.org/10.1016/j.rse.2013.01.006

Bourgeau-Chavez, L.L., Kasischke, E.S., Riordan, K., Brunzell, S., Nolan, M., Hyer, E., Slawski, J., Medvecz, M., Walters, T., Ames, S., 2007. Remote monitoring of spatial and temporal surface soil moisture in fire disturbed boreal forest ecosystems with ERS SAR imagery. Int. J. Remote Sens. 28, 2133–2162. https://doi.org/10.1080/01431160600976061

Breiman, L., 2002. Manual on setting up, using, and understanding random forests v3. 1. Tech. Report, http//oz.berkeley.edu/users/breiman, Stat. Dep. Univ. Calif. Berkeley, … 29. https://doi.org/10.2776/85168

Breiman, L., 2001. Random forests. Mach. Learn. 45, 5–32.

Bret-Harte, M.S., Mack, M.C., Shaver, G.R., Huebner, D.C., Johnston, M., Mojica, C. a, Pizano, C., Reiskind, J. a, 2013. The response of Arctic vegetation and soils following an unusually severe tundra fire. Philos. Trans. R. Soc. B 368, 20120490. https://doi.org/10.1098/rstb.2012.0490

Buchhorn, M., Walker, D.A., Heim, B., Raynolds, M.K., Epstein, H.E., Schwieder, M., 2013. Ground-based hyperspectral characterization of Alaska tundra vegetation along environmental gradients. Remote Sens. 5, 3971–4005. https://doi.org/10.3390/rs5083971

Buiat, M., Porcù, F., Dietrich, S., 2017. Observing relationships between lightning and cloud profiles by means of a satellite-borne cloud radar. Atmos. Meas. Tech. 10, 221–230. https://doi.org/10.5194/amt-10-221-2017

Burrows, W.R., 2008. Dynamical-Statistical Models for Lightning Prediction to 48-hr, in: Third Conference on Meteorological Applications of Lightning Data.

Burrows, W.R., Price, C., Wilson, L.J., 2005. Warm Season Lightning Probability Prediction for Canada and the Northern United States. Weather Forecast. 20, 971–988. https://doi.org/10.1175/WAF895.1

Cai, L., Alexeev, V.A., Arp, C.D., Jones, B.M., Liljedahl, A., Gädeke, A., 2016. Dynamical Downscaling Data for Studying Climatic Impacts on Hydrology, Permafrost, and Ecosystems in Arctic Alaska. Earth Syst. Sci. Data Discuss. 1–39. https://doi.org/10.5194/essd-2016-31

Cai, L., Alexeev, V.A., Arp, C.D., Jones, B.M., Liljedahl, A.K., Gädeke, A., 2018. The Polar WRF Downscaled Historical and Projected Twenty-First Century Climate for the Coast and Foothills of Arctic Alaska. Front. Earth Sci. 5, 1–15. https://doi.org/10.3389/feart.2017.00111

Carroll, M.L., Wooten, M.R., Dimiceli, C., Sohlberg, R.A., Townshend, J.R.G., 2016. ABoVE: Surface Water Extent, Boreal and Tundra Regions, North America, 1991-2011. https://doi.org/10.3334/ornldaac/1324

Cassano, J.J., Higgins, M.E., Seefeldt, M.W., 2011. Performance of the Weather Research and Forecasting Model for Month-Long Pan-Arctic Simulations. Mon. Weather Rev. 139, 3469–3488. https://doi.org/10.1175/MWR-D-10-05065.1

Castedo-Dorado, F., Rodriguez-Perez, J.R., Marcos-Menendez, J.L., Alvarez-Taboada, M.., 2011. Modelling the probability of lightning-induced forest fire occurrence in the province of León (NW Spain). For. Syst. 20, 95–107.

Ceccato, P., Flasse, S., Grégoire, J.M., 2002. Designing a spectral index to estimate vegetation water content from remote sensing data: Part 1: Theoretical approach. Remote Sens. Environ. 82, 188–197. https://doi.org/10.1016/S0034-4257(02)00037-8

Chopping, M., Su, L., Rango, A., Martonchik, J. V, Peters, D.P.C., Laliberte, A., 2008. Remote sensing of woody shrub cover in desert grasslands using MISR with a geometric-optical canopy reflectance model. Remote Sens. Environ. 112, 19–34. https://doi.org/https://doi.org/10.1016/j.rse.2006.04.023

Davidson, S., Santos, M., Sloan, V., Watts, J., Phoenix, G., Oechel, W., Zona, D., 2016. Mapping Arctic Tundra Vegetation Communities Using Field Spectroscopy and Multispectral Satellite Data in North Alaska, USA. Remote Sens. 8, 978. https://doi.org/10.3390/rs8120978

Dee, D., Fasullo, J., Shea, D., Walsh, J., (Eds)., N.C. for A.R.S., 2016. The Climate Data Guide: Atmospheric Reanalysis: Overview & Comparison Tables.

Di Giuseppe, F., Pappenberger, F., Wetterhall, F., Krzeminski, B., Camia, A., Libertï¿½, G., Miguel, J.S., 2016. The potential predictability of fire danger provided by numerical weather prediction. J. Appl. Meteorol. Climatol. 55, 2469–2491. https://doi.org/10.1175/JAMC-D-15-0297.1

Díaz-avalos, C., Peterson, D.L., Alvarado, E., Ferguson, S.A., Besag, J.E., 2001. Space-time modelling of lightning-caused ignitions in the Blue Mountains , Oregon. Can. J. For. Res. 31, 1579–1593. https://doi.org/10.1139/cjfr-31-9-1579

Dissing, D., Verbyla, D.L., 2003. Spatial patterns of lightning strikes in interior Alaska and their relations to elevation and vegetation. Can. J. For. Res. 782, 770–782. https://doi.org/10.1139/X02-214

Dyrness, C.T., Norum, R.A., 1983. The effects of experimental fires on black spruce forest floors in interior Alaska. Can. J. For. Res. 13, 879–893. https://doi.org/10.1139/x83-118

Ester, M., Kriegel, H.-P., Sander, J., Xu, X., 1996. A density-based algorithm for discovering clusters in large spatial databases with noise., in: Kdd. pp. 226–231.

Farukh, M.A., Hayasaka, H., Kimura, K., 2011. Characterization of lightning occurrence in Alaska using various weather indices for Lightning Forecasting. J. Disaster Res. 6, 343–355.

Fauria, M.M., Johnson, E.A., 2006. Large-scale climatic patterns control large lightning fire occurrence in Canada and Alaska forest regions. J. Geophys. Res. Biogeosciences 111. https://doi.org/10.1029/2006JG000181

Finney, D.L., Doherty, R.M., Wild, O., Stevenson, D.S., MacKenzie, I.A., Blyth, A.M., 2018. A projected decrease in lightning under climate change. Nat. Clim. Chang. 8, 1–4. https://doi.org/10.1038/s41558-018-0072-6

Fisher, J.B., Hayes, D.J., Schwalm, C.R., Huntzinger, D.N., Stofferahn, E., Schaefer, K., Luo, Y., Wullschleger, S.D., Goetz, S., Miller, C.E., Griffith, P., Chadburn, S., Chatterjee, A., Ciais, P., Douglas, T.A., Genet, H., Ito, A., Neigh, C.S.R., Poulter, B., Rogers, B.M., Sonnentag, O., Tian, H., Wang, W., Xue, Y., Yang, Z.L., Zeng, N., Zhang, Z., 2018. Missing pieces to modeling the Arctic-Boreal puzzle. Environ. Res. Lett. 13. https://doi.org/10.1088/1748-9326/aa9d9a

Flannigan, M.., Stocks, B.., Wotton, B.., 2000. Climate change and forest fires. Sci. Total Environ. 262, 221–229. https://doi.org/10.1016/S0048-9697(00)00524-6

Flannigan, M.D., Wotton, B.M., 2001. Climate, weather, and area burned, in: Forest Fires. Elsevier, pp. 351–373.

Flannigan, M.D., Wotton, B.M., Marshall, G.A., de Groot, W.J., Johnston, J., Jurko, N., Cantin, A.S., 2016. Fuel moisture sensitivity to temperature and precipitation: climate change implications. Clim. Change 134, 59–71. https://doi.org/10.1007/s10584-015-1521-0

French, N.H.F., Jenkins, L.K., Loboda, T. V., Flannigan, M., Jandt, R., Bourgeau-Chavez, L.L., Whitley, M., 2015. Fire in arctic tundra of Alaska: Past fire activity, future fire potential, and significance for land management and ecology. Int. J. Wildl. Fire 24, 1045–1061. https://doi.org/10.1071/WF14167

French, N.H.F., Whitley, M.A., Jenkins, L.K., 2016. Fire disturbance effects on land surface albedo in Alaskan tundra. J. Geophys. Res. Biogeosciences 121, 841–854. https://doi.org/10.1002/2015JG003177

Fronterhouse, B.A., 2012. Alaska Lightning Detection Network (ALDN) Briefing Document. Ft. Wainwright, AK Bur. L. Manag. Alaska Fire Serv. 1–4.

Frost, G. V., Epstein, H.E., Walker, D.A., 2014. Regional and landscape-scale variability of Landsat-observed vegetation dynamics in northwest Siberian tundra. Environ. Res. Lett. 9, 1–11. https://doi.org/10.1088/1748-9326/9/2/025004

Frost, G. V, Loehman, R.A., Saperstein, L.B., Macander, M.J., Nelson, P.R., Paradis, D.P., Natali, S.M., 2020. Multi-decadal patterns of vegetation succession after tundra fire on the Yukon-Kuskokwim Delta, Alaska. Environ. Res. Lett. 15, 25003. https://doi.org/10.1088/1748-9326/ab5f49

Fuquay, D.M., 1980. Forecasting lightning activity level and associated weather. USDA For. Serv. Res. Pap. INT-244.

Gallant, A.L., Binnian, E.F., Omernik, J.M., Shasby, M.B., 1995. Ecoregions of Alaska - U.S. Geological Survey Professional Paper 1567 73. https://doi.org/0160482909\r0607010010

Gao, B., 1996. NDWI – A Normalized Difference Water Index for Remote Sensing of Vegetation Liquid Water from Space. Remote Sens. Environ. 58, 257.

https://doi.org/10.1016/S0034-4257(96)00067-3

García, M.J.L., Caselles, V., 1991. Mapping burns and natural reforestation using thematic Mapper data. Geocarto Int. 6, 31–37. https://doi.org/10.1080/10106049109354290

Gessner, U., Machwitz, M., Conrad, C., Dech, S., 2013. Estimating the fractional cover of growth forms and bare surface in savannas. A multi-resolution approach based on regression tree ensembles. Remote Sens. Environ. 129, 90–102. https://doi.org/10.1016/j.rse.2012.10.026

Giannaros, T.M., Kotroni, V., Lagouvardos, K., 2015. Predicting lightning activity in Greece with the Weather Research and Forecasting (WRF) model. Atmos. Res. 156, 1–13. https://doi.org/10.1016/j.atmosres.2014.12.009

Giglio, L., Descloitres, J., Justice, C.O., Kaufman, Y.J., 2003. An Enhanced Contextual Fire Detection Algorithm for MODIS. Remote Sens. Environ. 87, 273–282. https://doi.org/https://doi.org/10.1016/S0034-4257(03)00184-6

Gijben, M., Dyson, L.L., Loots, M.T., 2017. A statistical scheme to forecast the daily lightning threat over southern Africa using the Unified Model. Atmos. Res. 194, 78–88. https://doi.org/10.1016/j.atmosres.2017.04.022

Glisan, J.M., Gutowski, W.J., Cassano, J.J., Higgins, M.E., 2013. Effects of spectral nudging in WRF on arctic temperature and precipitation simulations. J. Clim. 26, 3985–3999. https://doi.org/10.1175/JCLI-D-12-00318.1

Goetz, S.J., Bunn, A.G., Fiske, G.J., Houghton, R. a, 2005. Satellite-observed photosynthetic trends across boreal North America associated with climate and fire disturbance. Proc. Natl. Acad. Sci. U. S. A. 102, 13521–5. https://doi.org/10.1073/pnas.0506179102

Guan, K., Wood, E.F., Caylor, K.K., 2012. Multi-sensor derivation of regional vegetation fractional cover in Africa. Remote Sens. Environ. 124, 653–665. https://doi.org/10.1016/j.rse.2012.06.005

Guo, F., Wang, G., Su, Z., Liang, H., Wang, W., Lin, F., Liu, A., 2016. What drives forest fire in Fujian, China? Evidence from logistic regression and Random Forests. Int. J. Wildl. Fire 25, 505–519.

Gustine, D.D., Brinkman, T.J., Lindgren, M.A., Schmidt, J.I., Rupp, T.S., Adams, L.G., 2014. Climate-driven effects of fire on winter habitat for Caribou in the Alaskan-Yukon Arctic. PLoS One 9. https://doi.org/10.1371/journal.pone.0100588

Hansen, M.C.C., Potapov, P. V, Moore, R., Hancher, M., Turubanova, S.A. a, Tyukavina, A., Thau, D., Stehman, S.V. V, Goetz, S.J.J., Loveland, T.R.R., Kommareddy, A., Egorov, A., Chini, L., Justice, C.O.O., Townshend, J.R.G.R.G., Patapov, P.V., Moore, R., Hancher, M., Turubanova, S.A. a, Tyukavina, A., Thau, D., Stehman, S.V. V, Goetz, S.J.J., Loveland, T.R.R., Kommaredy, A., Egorov, A., Chini, L., Justice, C.O.O., Townshend, J.R.G.R.G., 2013. High-Resolution Global Maps of 21st-Century Forest Cover Change.

Science (80-.). 342, 850–854. https://doi.org/10.1126/science.1244693

Hardisky, M.A., Klemas, V., Smart, R.M., 1983. The influence of soil salinity, growth form, and leaf moisture on the spectral radiance of Spartina alterniflora canopies. Photogramm. Eng. Remote Sens. 49, 77–83.

Hayasaka, H., Tanaka, H.L., Bieniek, P.A., 2016. Synoptic-scale fire weather conditions in Alaska. Polar Sci. 10, 217–226. https://doi.org/10.1016/j.polar.2016.05.001

He, J., Loboda, T. V, Jenkins, L., Chen, D., 2020. ABoVE: Distribution Maps of Wildland Fire Fuel Components across Alaskan Tundra, 2015. https://doi.org/10.3334/ORNLDAAC/1761

He, J., Loboda, T. V, Jenkins, L., Chen, D., 2019. Mapping fractional cover of major fuel type components across Alaskan tundra. Remote Sens. Environ. 232, 111324. https://doi.org/https://doi.org/10.1016/j.rse.2019.111324

Higuera, P.E., Chipman, M.L., Barnes, J.L., Urban, M.A., Hu, F.S., 2011. Variability of tundra fire regimes in Arctic Alaska: Millennial-scale patterns and ecological implications. Ecol. Appl. 21, 3211–3226. https://doi.org/10.1890/11-0387.1

Hines, K.M., Bromwich, D.H., 2008. Development and Testing of Polar Weather Research and Forecasting (WRF) Model. Part I: Greenland Ice Sheet Meteorology*. Mon. Weather Rev. 136, 1971–1989. https://doi.org/10.1175/2007MWR2112.1

Hines, K.M., Bromwich, D.H., Bai, L.-S., Barlage, M., Slater, A.G., 2011. Development and Testing of Polar WRF. Part III: Arctic Land. J. Clim. 24, 26–48. https://doi.org/10.1175/2010JCLI3460.1

Hinzman, L.D., Bettez, N.D., Bolton, W.R., Chapin, F.S., Dyurgerov, M.B., Fastie, C.L., Griffith, B., Hollister, R.D., Hope, A., Huntington, H.P., Jensen, A.M., Jia, G.J., Jorgenson, T., Kane, D.L., Klein, D.R., Kofinas, G., Lynch, A.H., Lloyd, A.H., McGuire, A.D., Nelson, F.E., Oechel, W.C., Osterkamp, T.E., Racine, C.H., Romanovsky, V.E., Stone, R.S., Stow, D.A., Sturm, M., Tweedie, C.E., Vourlitis, G.L., Walker, M.D., Walker, D.A., Webber, P.J., Welker, J.M., Winker, K.S., Yoshikawa, K., 2005. Evidence and implications of recent climate change in Northern Alaska and other Arctic regions. Clim. Change 72, 251–298. https://doi.org/10.1007/s10584-005-5352-2

Hirsch, K.G., 1996. Canadian Forest Fire Behavior Prediction (FBP) System : user's guide, Special Report 7. Northern Forestry Centre, Edmonton.

Holben, B.N., 1986. Characteristics of maximum-value composite images from temporal AVHRR data. Int. J. Remote Sens. 7, 1417–1434. https://doi.org/10.1080/01431168608948945

Hu, F.S., Higuera, P.E., Duffy, P., Chipman, M.L., Rocha, A. V., Young, A.M., Kelly, R., Dietze, M.C., 2015. Arctic tundra fires: Natural variability and responses to climate change. Front. Ecol. Environ. https://doi.org/10.1890/150063

Huemmrich, K.F., Gamon, J.A., Tweedie, C.E., Campbell, P.K.E., Landis, D.R., Middleton, E.M., 2013. Arctic tundra vegetation functional types based on photosynthetic physiology and optical properties. IEEE J. Sel. Top. Appl. Earth Obs. Remote Sens. 6, 265–275. https://doi.org/10.1109/JSTARS.2013.2253446

Innes, R.J., 2013. Fire regimes of Alaskan tundra communities, Fire Effects Information System, [Online].

Jandt, R., Joly, K., Meyers, C.R., Racine, C., 2008. Slow Recovery of Lichen on Burned Caribou Winter Range in Alaska Tundra : Potential Influences of Climate Warming and Other Disturbance Factors 40, 89–95. https://doi.org/10.1657/1523-0430(06-122)

Jenkins, L., Bourgeau-Chavez, L., French, N., Loboda, T., Thelen, B., 2014. Development of methods for detection and monitoring of fire disturbance in the Alaskan tundra using a two-decade long record of synthetic aperture radar satellite images. Remote Sens. 6, 6347–6364.

Jolly, W.M., Cochrane, M. a, Freeborn, P.H., Holden, Z. a, Brown, T.J., Williamson, G.J., Bowman, D.M.J.S., 2015. Climate-induced variations in global wildfire danger from 1979 to 2013. Nat. Commun. 6, 7537. https://doi.org/10.1038/ncomms8537

Joly, K., Duffy, P. a., Rupp, T.S., 2012. Simulating the effects of climate change on fire regimes in Arctic biomes: implications for caribou and moose habitat. Ecosphere 3, art36. https://doi.org/10.1890/ES12-00012.1

Jones, B.M., Grosse, G., Arp, C.D., Miller, E., Liu, L., Hayes, D.J., Larsen, C.F., 2015. Recent Arctic tundra fire initiates widespread thermokarst development. Sci. Rep. 5, 15865. https://doi.org/10.1038/srep15865

Kasischke, E.S., Hoy, E.E., 2012. Controls on carbon consumption during Alaskan wildland fires. Glob. Chang. Biol. 18, 685–699. https://doi.org/10.1111/j.1365-2486.2011.02573.x

Kasischke, E.S., Verbyla, D.L., Rupp, T.S., McGuire, A.D., Murphy, K.A., Jandt, R., Barnes, J.L., Hoy, E.E., Duffy, P.A., Calef, M., Turetsky, M.R., 2010. Alaska's changing fire regime — implications for the vulnerability of its boreal forestsThis article is one of a selection of papers from The Dynamics of Change in Alaska's Boreal Forests: Resilience and Vulnerability in Response to Climate Warming. Can. J. For. Res. 40, 1313–1324. https://doi.org/10.1139/X10-098

Keyser, A., Leroy Westerling, A., 2017. Climate drives inter-annual variability in probability of high severity fire occurrence in the western United States. Environ. Res. Lett. 12. https://doi.org/10.1088/1748-9326/aa6b10

Kim, C.K., Stuefer, M., Schmitt, C.G., Heymsfield, A., Thompson, G., 2014. Numerical Modeling of Ice Fog in Interior Alaska Using the Weather Research and Forecasting Model. Pure Appl. Geophys. 171, 1963–1982. https://doi.org/10.1007/s00024-013-0766-7

Kim, J.S., Kug, J.S., Jeong, S.J., Park, H., Schaepman-Strub, G., 2020. Extensive

fires in southeastern Siberian permafrost linked to preceding Arctic Oscillation. Sci. Adv. 6, 1–8. https://doi.org/10.1126/sciadv.aax3308

Kittel, T. G. F., Steffen, W. L., & Chapin, F.S., 2000. Global and regional modelling of Arctic-boreal vegetation distribution and its sensitivity to altered forcing. Glob. Chang. Biol. 6, 1–18. https://doi.org/10.1046/j.1365-2486.2000.06011.x

Kochtubajda, B., Stewart, R.E., Flannigan, M.D., Bonsal, B.R., Cuell, C., Mooney, C.J., 2019. An Assessment of Surface and Atmospheric Conditions Associated with the Extreme 2014 Wildfire Season in Canada's Northwest Territories. Atmosphere-Ocean 57, 73–90. https://doi.org/10.1080/07055900.2019.1576023

Koshak, W.J., Cummins, K.L., Buechler, D.E., Vant-Hull, B., Blakeslee, R.J., Williams, E.R., Peterson, H.S., 2015. Variability of CONUS lightning in 2003-12 and associated impacts. J. Appl. Meteorol. Climatol. 54, 15–41. https://doi.org/10.1175/JAMC-D-14-0072.1

Kourtz, P., Todd, B., 1991. Predicting the daily occurrence of lightning-caused forest fires. Forestry Canada, Petawawa National Forestry Institute.

Krause, A., Kloster, S., Wilkenskjeld, S., Paeth, H., 2014. The sensitivity of global wildfires to simulated past, present, and future lightning frequency. J. Geophys. Res. Biogeosciences 119, 312–322. https://doi.org/10.1002/2013JG002502

Kushida, K., Kim, Y., Tsuyuzaki, S., Fukuda, M., 2009. Spectral vegetation indices for estimating shrub cover, green phytomass and leaf turnover in a sedge-shrub tundra. Int. J. Remote Sens. 30, 1651–1658. https://doi.org/10.1080/01431160802502632

Lara, M.J., Nitze, I., Grosse, G., McGuire, A.D., 2018. Tundra landform and vegetation productivity trend maps for the Arctic Coastal Plain of northern Alaska. Sci. Data 5, 180058.

Larsen, J.N., Anisimov, O.A., Constable, A., Hollowed, A.B., Maynard, N., Prestrud, P., Prowse, T.D., Stone, J.M.R., n.d. Polar regions, in: Barros, V.R., Field, C.B., Dokken, D.J., Mastrandrea, M.D., Mach, K.J., Bilir, T.E., Chatterjee, M., Ebi, K.L., Estrada, Y.O., Genova, R.C., Girma, B., Kissel, E.S., Levy, A.N., MacCracken, S., Mastrandrea, P.R., White, L.L. (Eds.), Climate Change 2014: Impacts, Adaptation, and Vulnerability. Part B: Regional Aspects. Contribution of Working Group II to the Fifth Assessment Report of the Intergovernmental Panel of Climate Change. Cambridge University Press, Cambridge, United Kingdom and New York, NY, USA, pp. 1567–1612.

Lawson, B.D., Armitage, O.B., 2008. Weather Guide Canadian Forest Fire Danger Rating System, Canadian Forest Service Northern Forestry Centre.

Li, J., Roy, D.P., 2017. A Global Analysis of Sentinel-2A, Sentinel-2B and Landsat-8 Data Revisit Intervals and Implications for Terrestrial Monitoring. Remote Sens. 9. https://doi.org/10.3390/rs9090902

Liu, N., Budkewitsch, P., Treitz, P., 2017. Examining spectral reflectance features related to Arctic percent vegetation cover: Implications for hyperspectral remote

sensing of Arctic tundra. Remote Sens. Environ. 192, 58–72. https://doi.org/10.1016/j.rse.2017.02.002

Liu, Z., Yang, J., Change, Y., Weisberg, P.J., He, H.S., 2012. Spatial patterns and drivers of fire occurrence and its future trend under climate change in a boreal forest of Northeast China. Glob. Chang. Biol. 18, 2041–2056. https://doi.org/10.1111/j.1365-2486.2012.02649.x

Loboda, T.V., Hall, J.V., Hall, A.H., Shevade, V.S., 2017. ABoVE: Cumulative Annual Burned Area, Circumpolar High Northern Latitudes, 2001-2015. https://doi.org/10.3334/ornldaac/1526

Loboda, T. V., 2009. Modeling fire danger in data-poor regions: A case study from the Russian Far East. Int. J. Wildl. Fire 18, 19–35. https://doi.org/10.1071/WF07094

Loboda, T. V., Csiszar, I.A., 2007. Assessing the risk of ignition in the Russian Far East within a modeling framework of fire threat. Ecol. Appl. 17, 791–805. https://doi.org/10.1890/05-1476

Loboda, T. V., French, N.H.F., Hight-Harf, C., Jenkins, L., Miller, M.E., 2013. Mapping fire extent and burn severity in Alaskan tussock tundra: An analysis of the spectral response of tundra vegetation to wildland fire. Remote Sens. Environ. 134, 194–209. https://doi.org/10.1016/j.rse.2013.03.003

Loboda, T. V, Csiszar, I.A., 2007. Reconstruction of fire spread within wildland fire events in Northern Eurasia from the MODIS active fire product. Glob. Planet. Change 56, 258–273. https://doi.org/10.1016/j.gloplacha.2006.07.015

Louppe, G., Wehenkel, L., Sutera, A., Geurts, P., 2013. Understanding variable importances in forests of randomized trees. Adv. Neural Inf. Process. Syst. 26 431–439. https://doi.org/NIPS2013_4928

Lynn, B.H., Yair, Y., Price, C., Kelman, G., Clark, A.J., 2012. Predicting Cloud-to-Ground and Intracloud Lightning in Weather Forecast Models. Weather Forecast. 1470–1478. https://doi.org/10.1175/WAF-D-11-00144.1

Ma, L., Zhou, Y., Chen, J., Cao, X., Chen, X., 2015. Estimation of Fractional Vegetation Cover in Semiarid Areas by Integrating Endmember Reflectance Purification Into Nonlinear Spectral Mixture Analysis. IEEE Geosci. Remote Sens. Lett. 12, 1175–1179. https://doi.org/10.1109/LGRS.2014.2385816

Macander, M.J., Frost, G. V., Nelson, P.R., Swingley, C.S., 2017. Regional quantitative cover mapping of tundra plant functional types in Arctic Alaska. Remote Sens. 9, 1–26. https://doi.org/10.3390/rs9101024

Macias Fauria, M., Johnson, E.A., 2008. Climate and wildfires in the North American boreal forest. Philos. Trans. R. Soc. B Biol. Sci. 363, 2317–2329. https://doi.org/10.1098/rstb.2007.2202

Mack, M.C., Bret-Harte, M.S., Hollingsworth, T.N., Jandt, R.R., Schuur, E.A.G., Shaver, G.R., Verbyla, D.L., 2011. Carbon loss from an unprecedented Arctic tundra wildfire. Nature 475, 489–92. https://doi.org/10.1038/nature10283

Marino, E., Ranz, P., Tom??, J.L., Noriega, M. ??ngel, Esteban, J., Madrigal, J., 2016. Generation of high-resolution fuel model maps from discrete airborne laser scanner and Landsat-8 OLI: A low-cost and highly updated methodology for large areas. Remote Sens. Environ. 187, 267–280. https://doi.org/10.1016/j.rse.2016.10.020

Masrur, A., Petrov, A.N., DeGroote, J., 2018. Circumpolar spatio-temporal patterns and contributing climatic factors of wildfire activity in the Arctic tundra from 2001-2015. Environ. Res. Lett. 13. https://doi.org/10.1088/1748-9326/aa9a76

Matsangouras, I.T., Nastos, P.T., Kapsomenakis, J., 2016. Cloud-to-ground lightning activity over Greece: Spatio-temporal analysis and impacts. Atmos. Res. 169, 485–496. https://doi.org/10.1016/j.atmosres.2015.08.004

McFeeters, S.K., 1996. The use of the Normalized Difference Water Index (NDWI) in the delineation of open water features. Int. J. Remote Sens. 17, 1425–1432.

Mcguiney, E., Shulski, M., Wendler, G., 2005. Alaska lightning climatology and application to wildfire science, in: Proceedings of the 85th American Meteorological Society Annual Meeting.

McManus, K.M., Morton, D.C., Masek, J.G., Wang, D., Sexton, J.O., Nagol, J.R., Ropars, P., Boudreau, S., 2012. Satellite-based evidence for shrub and graminoid tundra expansion in northern Quebec from 1986 to 2010. Glob. Chang. Biol. 18, 2313–2323. https://doi.org/10.1111/j.1365-2486.2012.02708.x

Meredith, M., Sommerkorn, M., Cassotta, S., Derksen, C., Ekaykin, A., Hollowed, A., Kofinas, G., Mackintosh, A., Melbourne-Thomas, J., Muelbert, M.M.C., Ottersen, G., Pritchard, H., Schuur, E.A.G., 2019. Polar regions. In: IPCC Special Report on the Ocean and Cryosphere in a Changing Climate [H.-O. Pörtner, D.C. Roberts, V. Masson-Delmotte, P. Zhai, M. Tignor, E. Poloczanska, K. Mintenbeck, A. Alegría, M. Nicolai, A. Okem, J. Petzold, B. Rama, N.M. Weyer. https://doi.org/10.1016/S1366-7017(01)00066-6

Mölders, N., 2010. Comparison of Canadian Forest Fire Danger Rating System and National Fire Danger Rating System fire indices derived from Weather Research and Forecasting (WRF) model data for the June 2005 Interior Alaska wildfires. Atmos. Res. 95, 290–306. https://doi.org/10.1016/j.atmosres.2009.03.010

Mölders, N., 2008. Suitability of the Weather Research and Forecasting (WRF) Model to Predict the June 2005 Fire Weather for Interior Alaska. Weather Forecast. 23, 953–973. https://doi.org/10.1175/2008WAF2007062.1

Moris, J. V, Conedera, M., Nisi, L., Bernardi, M., Cesti, G., Pezzatti, G.B., 2020. Lightning-caused fires in the Alps: Identifying the igniting strokes. Agric. For. Meteorol. 290, 107990. https://doi.org/https://doi.org/10.1016/j.agrformet.2020.107990

Moritz, M.A., Morais, M.E., Summerell, L.A., Carlson, J.M., Doyle, J., 2005. Wildfires, complexity, and highly optimized tolerance. Proc. Natl. Acad. Sci. 102, 17912–17917. https://doi.org/10.1073/pnas.0508985102

Mu, X., Song, W., Gao, Z., McVicar, T.R., Donohue, R.J., Yan, G., 2018. Fractional vegetation cover estimation by using multi-angle vegetation index. Remote Sens. Environ. 216, 44–56. https://doi.org/https://doi.org/10.1016/j.rse.2018.06.022

Müller, M.M., Vacik, H., 2017. Characteristics of lightnings igniting forest fires in Austria. Agric. For. Meteorol. 240–241, 26–34. https://doi.org/https://doi.org/10.1016/j.agrformet.2017.03.020

Muller, S. V., Racoviteanu, A.E., Walker, D.A., 1999. Landsat MSS-derived land-cover map of northern Alaska: Extrapolation methods and a comparison with photo-interpreted and AVHRR-derived maps. Int. J. Remote Sens. 20, 2921–2946. https://doi.org/10.1080/014311699211543

Murray, L.T., 2018. An uncertain future for lightning. Nat. Clim. Chang. 8, 191–192. https://doi.org/10.1038/s41558-018-0094-0

Nag, A., Murphy, M.J., Schulz, W., Cummins, K.L., 2014. Lightning locating systems: Characteristics and validation techniques. 2014 Int. Conf. Light. Prot. ICLP 2014 1070–1082. https://doi.org/10.1109/ICLP.2014.6973283

National Centers for Environmental Prediction/National Weather Service/NOAA/U.S. Department of Commerce, 2000. NCEP FNL Operational Model Global Tropospheric Analyses, continuing from July 1999. https://doi.org/10.5065/D6M043C6

Nowacki, G.J., Spencer, P., Fleming, M., Brock, T., Jorgenson, T., 2003. Unified Ecoregions of Alaska: 2001, Open-File Report. https://doi.org/10.3133/ofr2002297

Olthof, I., Fraser, R.H., 2007. Mapping northern land cover fractions using Landsat ETM+. Remote Sens. Environ. 107, 496–509. https://doi.org/10.1016/j.rse.2006.10.009

Ottmar, R.D., Sandberg, D. V, Riccardi, C.L., Prichard, S.J., 2007. An overview of the Fuel Characteristic Classification System — Quantifying, classifying, and creating fuelbeds for resource planningThis article is one of a selection of papers published in the Special Forum on the Fuel Characteristic Classification Syste. Can. J. For. Res. 37, 2383–2393. https://doi.org/10.1139/X07-077

Pearson, R.G., Phillips, S.J., Loranty, M.M., Beck, P.S.A., Damoulas, T., Knight, S.J., Goetz, S.J., 2013. Shifts in Arctic vegetation and associated feedbacks under climate change. Nat. Clim. Chang. 3, 673–677. https://doi.org/10.1038/nclimate1858

Peterson, D., Wang, J., Ichoku, C., Remer, L.A., 2010. Effects of lightning and other meteorological factors on fire activity in the North American boreal forest: implications for fire weather forecasting. Atmos. Chem. Phys. 10, 6873–6888. https://doi.org/10.5194/acp-10-6873-2010

Pineda, N., Montanyà, J., van der Velde, O.A., 2014. Characteristics of lightning related to wildfire ignitions in Catalonia. Atmos. Res. 135–136, 380–387. https://doi.org/10.1016/j.atmosres.2012.07.011

Post, E., Forchhammer, M.C., Bret-Harte, M.S., Callaghan, T. V, Christensen, T.R., Elberling, B., Fox, A.D., Gilg, O., Hik, D.S., Høye, T.T., Ims, R.A., Jeppesen, E., Klein, D.R., Madsen, J., McGuire, a D., Rysgaard, S., Schindler, D.E., Stirling, I., Tamstorf, M.P., Tyler, N.J.C., van der Wal, R., Welker, J., Wookey, P.A., Schmidt, N.M., Aastrup, P., 2009. Ecological dynamics across the Arctic associated with recent climate change. Science 325, 1355–1358. https://doi.org/10.1126/science.1173113

Potapov, P., Hansen, M.C., Stehman, S. V., Loveland, T.R., Pittman, K., 2008. Combining MODIS and Landsat imagery to estimate and map boreal forest cover loss. Remote Sens. Environ. 112, 3708–3719. https://doi.org/10.1016/J.RSE.2008.05.006

Prestemon, J.P., Hawbaker, T.J., Bowden, M., Carpenter, J., Brooks, M.T., Abt, K.L., Sutphen, R., Scranton, S., 2013. Wildfire ignitions : A review of the science and recommendations for empirical modeling 20.

Price, C., Rind, D., 1994a. Possible implications of global climate change on global lightning distributions and frequencies. J. Geophys. Res. 99, 10823–10831.

Price, C., Rind, D., 1994b. Modeling Global Lightning Distributions in a General Circulation Model. Mon. Weather Rev. https://doi.org/10.1175/1520-0493(1994)122<1930:MGLDIA>2.0.CO;2

Pyne, S.J., Andrews, P.L., Laven, R.D., 1996. Introduction to Wildland Fire, Second Edi. ed. John Wiley & Sons, Inc.

Racine, C., Jandt, R., Meyers, C., Dennis, J., 2004. Tundra Fire and Vegetation Change along a Hillslope on the Seward Peninsula, Alaska, U.S.A. Arctic, Antarct. Alp. Res. 36, 1–10. https://doi.org/10.1657/1523-0430(2004)036[0001:TFAVCA]2.0.CO;2

Racine, C.H., Johnson, L.A., Viereck, L.A., 1987. Patterns of Vegetation Recovery after Tundra Fires in Northwestern Alaska, U.S.A. Arct. Alp. Res. 19, 461–469.

Rakov, V.A., Uman, M.A., 2003. Lightning: physics and effects. Cambridge University Press.

Randerson, J.T., Liu, H., Flanner, M.G., Chambers, S.D., Jin, Y., Hess, P.G., Pfister, G., Mack, M.C., Treseder, K.K., Welp, L.R., Chapin, F.S., Harden, J.W., Goulden, M.L., Lyons, E., Neff, J.C., Schuur, E. a G., Zender, C.S., 2006. The impact of boreal forest fire on climate warming. Science 314, 1130–1132. https://doi.org/10.1126/science.1132075

Raynolds, M.K., Comiso, J.C., Walker, D.A., Verbyla, D., 2008. Relationship between satellite-derived land surface temperatures, arctic vegetation types, and NDVI. Remote Sens. Environ. 112, 1884–1894. https://doi.org/10.1016/j.rse.2007.09.008

Reap, R., 1994. Analysis and prediction of lightning strike distributions associated with synoptic map types over Florida. Mon. Weather Rev. https://doi.org/10.1175/1520-0493(1994)122<1698:AAPOLS>2.0.CO;2

Reap, R.M., 1991. Climatological characteristics and objective prediction of thunderstorms over Alaska. Weather Forecast. https://doi.org/10.1175/1520-0434(1991)0062.0.CO;2

Reap, R.M., Foster, D.S., 1979. Automated 12–36 Hour Probability Forecasts of Thunderstorms and Severe Local Storms. J. Appl. Meteorol. 18, 1304–1315. https://doi.org/10.1175/1520-0450(1979)018<1304:AHPFOT>2.0.CO;2

Reap, R.M., MacGorman, D.R., 1989. Cloud-to-Ground Lightning: Climatological Characteristics and Relationships to Model Fields, Radar Observations, and Severe Local Storms. Mon. Weather Rev. 117, 518–535. https://doi.org/10.1175/1520-0493(1989)117<0518:CTGLCC>2.0.CO;2

Rivas Soriano, L., Sánchez Llorente, J.M., González Zamora, A., de Pablo Dávila, F., 2019. Influence of land cover on lightning and convective precipitation over the European continent. Prog. Phys. Geogr. 43, 352–364. https://doi.org/10.1177/0309133318825285

Rocha, A. V., Shaver, G.R., 2011. Postfire energy exchange in arctic tundra: The importance and climatic implications of burn severity. Glob. Chang. Biol. 17, 2831–2841. https://doi.org/10.1111/j.1365-2486.2011.02441.x

Rocha, A. V, Loranty, M.M., Higuera, P.E., Mack, M.C., Hu, F.S., Jones, B.M., Breen, A.L., Rastetter, E.B., Goetz, S.J., Shaver, G.R., 2012. The footprint of Alaskan tundra fires during the past half-century: implications for surface properties and radiative forcing. Environ. Res. Lett. 7, 044039. https://doi.org/10.1088/1748-9326/7/4/044039

Rollins, M.G., 2009. LANDFIRE: A nationally consistent vegetation, wildland fire, and fuel assessment. Int. J. Wildl. Fire 18, 235–249. https://doi.org/10.1071/WF08088

Romps, D.M., Seeley, J.T., Vollaro, D., Molinari, J., Schumann, U., Huntrieser, H., Levy, H., Moxim, W.J., Kasibhatla, P.S., Grewe, V., Bond, W.J., Keeley, J.E., Pausas, J.G., Keeley, J.E., Price, C., Rind, D., Michalon, N., Nassif, A., Saouri, T., Royer, J.F., Pontikis, C.A., Williams, E.R., Price, C., Rind, D., Price, C., Rind, D., Banerjee, A., Archibald, A.T., Maycock, A., Telford, P., Abraham, N.L., Yang, X., Braesicke, P., Pyle, J., Krause, A., Kloster, S., Wilkenskjeld, S., Paeth, H., Williams, E.R., Reeve, N., Toumi, R., Christian, H.J., Christian, H.J., Blakeslee, R.J., Boccippio, D.J., Boeck, W.L., Buechler, D.E., Driscoll, K.T., Goodman, S.J., Hall, J.M., Koshak, W.J., Mach, D.M., Stewart, M.F., Battan, L.J., Tapia, A., Smith, J.A., Dixon, M., Petersen, W.A., Rutledge, S.A., Meijer, E.W., Velthoven, P.F.J. van, Brunner, D.W., Huntrieser, H., Kelder, H., Williams, E.R., Geotis, S.G., Renno, N., Rutledge, S.A., Rasmussen, E., Rickenbach, T., Williams, E., Williams, E., Rosenfeld, D., Madden, N., Gerlach, J., Gears, N., Atkinson, L., Dunnemann, N., Frostrom, G., Antonio, M., Biazon, B., Camargo, R., Franca, H., Gomes, A., Lima, M., Machado, R., Manhaes, S., Nachtigall, L., Piva, H., Quintiliano, W., Machado, L., Artaxo, P., Roberts, G., Renno, N., Blakeslee, R., Bailey, J., Boccippio, D., Betts, A., Wolff, D., Roy, B., Halverson, J., Rickenbach, T., Fuentes, J., Avelino, E., Pawar, S.D., Lal, D.M.,

Murugavel, P., Murugavel, P., Pawar, S.D., Gopalakrishan, V., Kitzmiller, D., Miller, D., Fulton, R., Ding, F., Wacker, R.S., Orville, R.E., Orville, R.E., Huffines, G.R., Holle, R.L., Ye, B., Genio, A.D. Del, Lo, K.K.W., Sobel, A.H., Camargo, S.J., Trapp, R.J., Diffenbaugh, N.S., Brooks, H.E., Baldwin, M.E., Robinson, E.D., Pal, J.S., Trapp, R.J., Diffenbaugh, N.S., Gluhovsky, A., Romps, D.M., Muller, C.J., O'Gorman, P.A., Back, L.E., Singh, M.S., O'Gorman, P.A., Held, I.M., Soden, B.J., Taylor, K.E., Stouffer, R.J., Meehl, G.A., 2014. Projected increase in lightning strikes in the United States due to global warming. Science (80-.). 346, 851–854. https://doi.org/10.1126/science.1259100

Roy, D.P., Ju, J., Kline, K., Scaramuzza, P.L., Kovalskyy, V., Hansen, M., Loveland, T.R., Vermote, E., Zhang, C., 2010. Web-enabled Landsat Data (WELD): Landsat ETM+ composited mosaics of the conterminous United States. Remote Sens. Environ. 114, 35–49. https://doi.org/10.1016/j.rse.2009.08.011

Rupp, T.S., Olson, M., Adams, L.G., Dale, B.W., Joly, K., Henkelman, J., Collins, W.B., Starfield, A.M., 2006. Simulating the influence of various fire regimens on caribou winter habitat. Ecol. Appl. 16, 1730–1743. https://doi.org/10.1890/1051-0761(2006)016[1730:stiovf]2.0.co;2

Santos, J.A., Reis, M.A., De Pablo, F., Rivas-Soriano, L., Leite, S.M., 2013. Forcing factors of cloud-to-ground lightning over Iberia: Regional-scale assessments. Nat. Hazards Earth Syst. Sci. 13, 1745–1758. https://doi.org/10.5194/nhess-13-1745-2013

Saunders, C., 2008. Charge separation mechanisms in clouds. Space Sci. Rev. 137, 335–353. https://doi.org/10.1007/s11214-008-9345-0

Schön, C., Dittrich, J., Müller, R., 2018. The Error is the Feature: how to Forecast Lightning using a Model Prediction Error 2979–2988. https://doi.org/10.1145/3292500.3330682

Scott, J.H., Burgan, R.E., 2005. Standard fire behavior fuel models: a comprehensive set for use with Rothermel's surface fire spread model. https://doi.org/10.2737/RMRS-GTR-153

Selkowitz, D.J., 2010. A comparison of multi-spectral, multi-angular, and multi-temporal remote sensing datasets for fractional shrub canopy mapping in Arctic Alaska. Remote Sens. Environ. 114, 1338–1352. https://doi.org/10.1016/j.rse.2010.01.012

Shafer, P.E., Fuelberg, H.E., 2006. A statistical procedure to forecast warm season lightning over portions of the Florida peninsula. Weather Forecast. 21, 851–868. https://doi.org/10.1175/WAF954.1

Shaver, G.R., Kummerow, J., 1991. Phenology, resource allocation, and growth of arctic vascular plants, in: Arctic Ecosystems in a Changing Climate. Elsevier, pp. 193–211.

Simpson, C.C., Pearce, H.G., Sturman, A.P., Zawar-Reza, P., 2014. Verification of WRF modelled fire weather in the 2009–10 New Zealand fire season. Int. J.

Wildl. Fire 23, 34–45.

Skamarock, W.C., Klemp, J.B., Dudhia, J., Gill, D.O., Zhiquan, L., Berner, J., Wang, W., Powers, J.G., Duda, M.G., Barker, D.M., Huang, X.-Y., 2019. A Description of the Advanced Research WRF Model Version 4 NCAR Technical Note. Natl. Cent. Atmos. Res. 145. https://doi.org/10.5065/1dfh-6p97

Sly, W.K., 1965. A convective index in relation to lightning strikes in Northwestern Alberta, CIR 4220 TEC 566. Dept. of Transport, Canada. 11 pp.

Somers, B., Asner, G.P., Tits, L., Coppin, P., 2011. Endmember variability in Spectral Mixture Analysis: A review. Remote Sens. Environ. 115, 1603–1616. https://doi.org/https://doi.org/10.1016/j.rse.2011.03.003

Sousa, J.F., Fragoso, M., Mendes, S., Corte-Real, J., Santos, J.A., 2013. Statistical-dynamical modeling of the cloud-to-ground lightning activity in Portugal. Atmos. Res. 132–133, 46–64. https://doi.org/10.1016/j.atmosres.2013.04.010

Stewart, B.C., Kunkel, K.E., Steven, L.E., Sun, L., Walsh, J.E., 2013. Regional Climate Trends and Scenarios : Alaska 1–2.

Stocks, B.J., Lynham, T.J., Lawson, B.D., Alexander, M.E., Wagner, C.E. Van, McAlpine, R.S., Dubé, D.E., 1989. The Canadian Forest Fire Danger Rating System: An Overview. For. Chron. 65, 450–457. https://doi.org/10.5558/tfc65450-6

Stow, D.A., Burns, B.H., Hope, A.S., 1993. Spectral, spatial and temporal characteristics of Arctic tundra reflectance. Int. J. Remote Sens. 14, 2445–2462. https://doi.org/10.1080/01431169308904285

Stow, D.A., Hope, A., McGuire, D., Verbyla, D., Gamon, J., Huemmrich, F., Houston, S., Racine, C., Sturm, M., Tape, K., Hinzman, L., Yoshikawa, K., Tweedie, C., Noyle, B., Silapaswan, C., Douglas, D., Griffith, B., Jia, G., Epstein, H., Walker, D., Daeschner, S., Petersen, A., Zhou, L., Myneni, R., 2004. Remote sensing of vegetation and land-cover change in Arctic Tundra Ecosystems. Remote Sens. Environ. 89, 281–308. https://doi.org/10.1016/j.rse.2003.10.018

Strauss, J., Ulrich, M., Buchhorn, M., 2012. Expeditions to permafrost 2012:" Alaskan North Slope/Itkillik"," Thermokarst in Central Yakutia"," EyeSight-NAAT-Alaska". Berichte zur Polar-und Meeresforschung= Reports polar Mar. Res. 655.

Sulla-Menashe, D., Woodcock, C.E., Friedl, M.A., 2018. Canadian boreal forest greening and browning trends: An analysis of biogeographic patterns and the relative roles of disturbance versus climate drivers. Environ. Res. Lett. 13. https://doi.org/10.1088/1748-9326/aa9b88

Sylvester, T.W., Wein, R.W., 1981. Fuel characteristics of arctic plant species and simulated plant community flammability by Rothermel's model. Can. J. Bot. 59, 898–907. https://doi.org/10.1139/b81-125

Taylor, S.W., Alexander, M.E., 2006. Science, technology, and human factors in fire

danger rating: The Canadian experience. Int. J. Wildl. Fire 15, 121–135. https://doi.org/10.1071/WF05021

Thornton, P.E., Thornton, M.M., Mayer, B.W., Wilhelmi, N., Wei, Y., Devarakonda, R., Cook, R.B., 2017. Daymet: daily surface weather data on a 1-km grid for North America, Version 3. ORNL DAAC, Oak Ridge, Tennessee, USA. ORNL DAAC, Oak Ridge, Tennessee, USA.

Tucker, C.J., 1979. Red and photographic infrared linear combinations for monitoring vegetation. Remote Sens. Environ. 8, 127–150. https://doi.org/https://doi.org/10.1016/0034-4257(79)90013-0

Turetsky, M.R., Kane, E.S., Harden, J.W., Ottmar, R.D., Manies, K.L., Hoy, E., Kasischke, E.S., 2011. Recent acceleration of biomass burning and carbon losses in Alaskan forests and peatlands. Nat. Geosci. 4, 27–31. https://doi.org/10.1038/ngeo1027

Van Beusekom, A.E., Gould, W.A., Monmany, A.C., Khalyani, A.H., Quiñones, M., Fain, S.J., Andrade-Núñez, M.J., González, G., 2018. Fire weather and likelihood: characterizing climate space for fire occurrence and extent in Puerto Rico. Clim. Change 146, 117–131. https://doi.org/10.1007/s10584-017-2045-6

Van Der Kolk, H.J., Heijmans, M.M.P.D., Van Huissteden, J., Pullens, J.W.M., Berendse, F., 2016. Potential Arctic tundra vegetation shifts in response to changing temperature, precipitation and permafrost thaw. Biogeosciences 13, 6229–6245. https://doi.org/10.5194/bg-13-6229-2016

Van Heerwaarden, C.C., Teuling, A.J., 2014. Disentangling the response of forest and grassland energy exchange to heatwaves under idealized land-atmosphere coupling. Biogeosciences 11, 6159–6171. https://doi.org/10.5194/bg-11-6159-2014

Van Wagner, C.E., 1987. Development and Structure of the Canadian Forest FireWeather Index System, in: Canadian Forestry Service. Forestry Technical Report 35.

Van Wagner, C.E., Pickett, T.L., 1985. Equations and FORTRAN program for the Canadian forest fire weather index system. Canadian Forestry Service, Petawawa National Forestry Institute, Chalk River, Ontario. Forestry Technical Report 33. 18 p.

Vecín-Arias, D., Castedo-Dorado, F., Ordónez, C., Rodríguez-Pérez, J.R., 2016. Biophysical and lightning characteristics drive lightning-induced fire occurrence in the central plateau of the Iberian Peninsula. Agric. For. Meteorol. 225, 36–47. https://doi.org/10.1016/j.agrformet.2016.05.003

Veraverbeke, S., Rogers, B.M., Goulden, M.L., Jandt, R.R., Miller, C.E., Wiggins, E.B., Randerson, J.T., 2017. Lightning as a major driver of recent large fire years in North American boreal forests. Nat. Clim. Chang. 7, 529–534. https://doi.org/10.1038/nclimate3329

Vermote, E., Justice, C., Claverie, M., Franch, B., 2016. Preliminary analysis of the

performance of the Landsat 8/OLI land surface reflectance product. Remote Sens. Environ. 185, 46–56. https://doi.org/10.1016/j.rse.2016.04.008

Vermote, E.F., Roger, J.C., Ray, J.P., 2015. MODIS Surface Reflectance User's Guide Correspondence. Http://Modis-Sr.Ltdri.Org 35.

Viedma, O., Urbieta, I.R., Moreno, J.M., 2018. Wildfires and the role of their drivers are changing over time in a large rural area of west-central Spain. Sci. Rep. 8, 17797. https://doi.org/10.1038/s41598-018-36134-4

Viereck, L.A., 1979. Preliminary results of experimental fires in the black spruce type of interior Alaska. Dept. of Agriculture, Forest Service, Pacific Northwest Forest and Range~….

Viereck, L.A., Dyrness, C.T., Batten, A.R., Wenzlick, K.J., 1992. The Alaska Vegetation Classification. USDA Gen. Tech. Rep. 284.

Vierling, L.A., Deering, D.W., Eck, T.F., 1997. Differences in arctic tundra vegetation type and phenology as seen using bidirectional radiometry in the early growing season. Remote Sens. Environ. 60, 71–82. https://doi.org/10.1016/S0034-4257(96)00139-3

Vilar, L., Gómez, I., Martínez-Vega, J., Echavarría, P., Riaño, D., Martín, M.P., 2016. Multitemporal Modelling of Socio-Economic Wildfire Drivers in Central Spain between the 1980s and the 2000s: Comparing Generalized Linear Models to Machine Learning Algorithms. PLoS One 11, e0161344.

Walker, D.A., Raynolds, M.K., Daniëls, F.J.A., Einarsson, E., Elvebakk, A., Gould, W.A., Katenin, A.E., Kholod, S.S., Markon, C.J., Melnikov, E.S., Moskalenko, N.G., Talbot, S.S., Yurtsev, B.A., Team, the other members of the C., 2005. The Circumpolar Arctic vegetation map. J. Veg. Sci. 16, 267–282. https://doi.org/10.1111/j.1654-1103.2005.tb02365.x

Wang, X., Wotton, B.M., Cantin, A.S., Parisien, M.A., Anderson, K., Moore, B., Flannigan, M.D., 2017. cffdrs: an R package for the Canadian Forest Fire Danger Rating System. Ecol. Process. 6. https://doi.org/10.1186/s13717-017-0070-z

Wendler, G., Conner, J., Moore, B., Shulski, M., Stuefer, M., 2011. Climatology of Alaskan wildfires with special emphasis on the extreme year of 2004. Theor. Appl. Climatol. 104, 459–472. https://doi.org/10.1007/s00704-010-0357-9

Wielgolaski, F.E., Goodall, D.W., 1997. Polar and alpine tundra. Elsevier.

Williams, A.P., Seager, R., MacAlady, A.K., Berkelhammer, M., Crimmins, M.A., Swetnam, T.W., Trugman, A.T., Buenning, N., Noone, D., McDowell, N.G., Hryniw, N., Mora, C.I., Rahn, T., 2015. Correlations between components of the water balance and burned area reveal new insights for predicting forest fire area in the southwest United States. Int. J. Wildl. Fire 24, 14–26. https://doi.org/10.1071/WF14023

Wilson, A.B., Bromwich, D.H., Hines, K.M., 2012. Evaluation of polar WRF forecasts on the arctic system reanalysis domain: 2. Atmospheric hydrologic

cycle. J. Geophys. Res. Atmos. 117, 1–18. https://doi.org/10.1029/2011JD016765

Wilson, M.F.J., O'Connell, B., Brown, C., Guinan, J.C., Grehan, A.J., 2007. Multiscale terrain analysis of multibeam bathymetry data for habitat mapping on the continental slope, Marine Geodesy. https://doi.org/10.1080/01490410701295962

Wong, J., Barth, M.C., Noone, D., 2013. Evaluating a lightning parameterization based on cloud-top height for mesoscale numerical model simulations. Geosci. Model Dev 429–443. https://doi.org/10.5194/gmd-6-429-2013

Woo, H., Chung, W., Graham, J.M., Lee, B., 2017. Forest fire risk assessment using point process modelling of fire occurrence and Monte Carlo fire simulation. Int. J. Wildl. Fire 26, 789–805.

Wotton, B.M., Martell, D.L., 2005. A lightning fire occurrence model for Ontario. Can. J. For. Res. 35, 1389–1401. https://doi.org/10.1139/X05-071

Wotton, B.M., Nock, C.A., Flannigan, M.D., 2010. Forest fire occurrence and climate change in Canada. Int. J. Wildl. Fire 19, 253–271. https://doi.org/10.1071/WF09002

Xiao, J., Zhuang, Q., 2007. Drought effects on large fire activity in Canadian and Alaskan forests. Environ. Res. Lett. 2. https://doi.org/10.1088/1748-9326/2/4/044003

Yair, Y., 2008. Charge generation and separation processes. Space Sci. Rev. 137, 119–131. https://doi.org/10.1007/s11214-008-9348-x

Yair, Y., Lynn, B., Price, C., Kotroni, V., Lagouvardos, K., Morin, E., Mugnai, A., Del Carmen Llasat, M., 2010. Predicting the potential for lightning activity in Mediterranean storms based on the Weather Research and Forecasting (WRF) model dynamic and microphysical fields. J. Geophys. Res. Atmos. 115, 1–13. https://doi.org/10.1029/2008JD010868

Yang, J., Weisberg, P.J., Dilts, T.E., Loudermilk, E.L., Scheller, R.M., Stanton, A., Skinner, C., 2015. Predicting wildfire occurrence distribution with spatial point process models and its uncertainty assessment: a case study in the Lake Tahoe Basin, USA. Int. J. Wildl. Fire 24, 380–390. https://doi.org/10.1071/wf14001

Yebra, M., Chuvieco, E., Riaño, D., 2008. Estimation of live fuel moisture content from MODIS images for fire risk assessment. Agric. For. Meteorol. 148, 523–536. https://doi.org/10.1016/j.agrformet.2007.12.005

Yebra, M., Dennison, P.E., Chuvieco, E., Riaño, D., Zylstra, P., Hunt, E.R., Danson, F.M., Qi, Y., Jurdao, S., 2013. A global review of remote sensing of live fuel moisture content for fire danger assessment: Moving towards operational products. Remote Sens. Environ. 136, 455–468. https://doi.org/10.1016/j.rse.2013.05.029

Young, A.M., Higuera, P.E., Duffy, P.A., Hu, F.S., 2017. Climatic thresholds shape northern high-latitude fire regimes and imply vulnerability to future climate

change. Ecography (Cop.). 40, 606–617. https://doi.org/10.1111/ecog.02205

Zepka, G.S., Pinto, O., Saraiva, A.C. V, 2014. Lightning forecasting in southeastern Brazil using the WRF model. Atmos. Res. 135–136, 344–362. https://doi.org/10.1016/j.atmosres.2013.01.008

Zhu, Z., Wang, S., Woodcock, C.E., 2015. Improvement and expansion of the Fmask algorithm: cloud, cloud shadow, and snow detection for Landsats 4–7, 8, and Sentinel 2 images. Remote Sens. Environ. 159, 269–277. https://doi.org/https://doi.org/10.1016/j.rse.2014.12.014